BASIC AND APPLIED STUDIES OF THE RAM ACCELERATOR AS A HYPERVELOCITY PROJECTILE LAUNCHER

AFOSR Grant No. F49620-92-J-0375

Annual Report

1 July 1992 – 30 June 1993

Prepared by:

A.P. Bruckner* and C. Knowlen†

Aerospace and Energetics Research Program
Department of Aeronautics and Astronautics
University of Washington, FL-10
Seattle, WA 98195

December 10, 1993

* Professor; Principal Investigator
† Post-Doctoral Research Associate

REPORT DOCUMENTATION PAGE

Approved for public release; distribution unlimited.

1a. REPORT SECURITY CLASSIFICATION: unclassified	1b. RESTRICTIVE MARKINGS: none
2a. SECURITY CLASSIFICATION AUTHORITY	3. DISTRIBUTION/AVAILABILITY OF REPORT: unlimited
2b. DECLASSIFICATION/DOWNGRADING SCHEDULE	
4. PERFORMING ORGANIZATION REPORT NUMBER(S)	5. MONITORING ORGANIZATION REPORT NUMBER(S): AFOSR-TR- 94 0100
6a. NAME OF PERFORMING ORGANIZATION: Aerospace & Energetics Research Program; 6b. OFFICE SYMBOL (If applicable): FL-10	7a. NAME OF MONITORING ORGANIZATION: Office of Naval Research (ONR)
6c. ADDRESS (City, State and ZIP Code): University of Washington, Grant & Contract Services, JM-24, 3935 University Way NE, Seattle, WA 98195	7b. ADDRESS (City, State and ZIP Code): 1107 NE 45 St., Suite 350 /JD-16, Seattle, WA 98105
8a. NAME OF FUNDING/SPONSORING ORGANIZATION (AFOSR): AFOSR; 8b. OFFICE SYMBOL (If applicable): /NA	9. PROCUREMENT INSTRUMENT IDENTIFICATION NUMBER: F49620-92-J-0375
8c. ADDRESS (City, State and ZIP Code): Building 410, Bolling AFB, DC 20332-6448	10. SOURCE OF FUNDING NOS. — PROGRAM ELEMENT NO.: 6221 7C; PROJECT NO.: 1203; TASK NO.: /05; WORK UNIT NO.:
11. TITLE (Include Security Classification): (unclassified) "Basic and Applied Studies of the Ram Accelerator as a Hypervelocity Projectile Launcher"	
12. PERSONAL AUTHOR(S): BRUCKNER, Adam P. and KNOWLEN, Carl	
13a. TYPE OF REPORT: annual report; 13b. TIME COVERED: FROM 92/7/1 TO 93/6/30; 14. DATE OF REPORT (Yr., Mo., Day): 1993 December 10; 15. PAGE COUNT: 97	
16. SUPPLEMENTARY NOTATION	
17. COSATI CODES — FIELD / GROUP / SUB. GR.	18. SUBJECT TERMS (Continue on reverse if necessary and identify by block number): gas dynamic limits, ram accelerator, in-tube ramjet, detonation propulsion, scramjet

19. ABSTRACT (Continue on reverse if necessary and identify by block number)

The potential of using ram accelerator technology for an impulsive launcher of autonomously guided interceptors, such as the LEAP, has been studied during this contract period. In addition, fundamental investigations on some of the engineering issues which must be addressed for enabling ram accelerator propulsive modes to operate at 4 km/sec have been undertaken. An experimental investigation of the gas dynamic limits of ram accelerator operation has demonstrated the existence of two distinct limiting mechanisms that must be accounted for when designing projectiles for these launchers. Other experiments were conducted to make detailed pressure measurements of the flow fields at the tube walls to study the effects of projectile canting. Results from this LEAP launcher study and the experimental investigations indicate that the ram accelerator technology is well suited for applications as a transportable launcher capable of meeting the needs of theater ballistic missile defense missions.

20. DISTRIBUTION/AVAILABILITY OF ABSTRACT: UNCLASSIFIED/UNLIMITED ☒ SAME AS RPT. ☐ DTIC USERS ☒	21. ABSTRACT SECURITY CLASSIFICATION: unclassified
22a. NAME OF RESPONSIBLE INDIVIDUAL: Donald W. Allen, Director G&C Services	22b. TELEPHONE NUMBER (Include Area Code): 206 543-4043; 22c. OFFICE SYMBOL: JM-24

DD FORM 1473, 83 APR EDITION OF 1 JAN 73 IS OBSOLETE.

BASIC AND APPLIED STUDIES OF THE RAM ACCELERATOR AS A HYPERVELOCITY PROJECTILE LAUNCHER

ABSTRACT

The potential of using ram accelerator technology for an impulsive launcher of autonomously guided interceptors, such as the LEAP, has been studied during this contract period. In addition, fundamental investigations on some of the engineering issues which must be addressed for enabling ram accelerator propulsive modes to operate at 4 km/sec have been undertaken. An experimental investigation of the gas dynamic limits of ram accelerator operation has demonstrated the existence of two distinct limiting mechanisms that must be accounted for when designing projectiles for these launchers. Other experiments were conducted to make detailed pressure measurements of the flow fields at the tube walls to study the effects of projectile canting. Results from this LEAP launcher study and the experimental investigations indicate that the ram accelerator technology is well suited for applications as a transportable launcher capable of meeting the needs of theater ballistic missile defense missions.

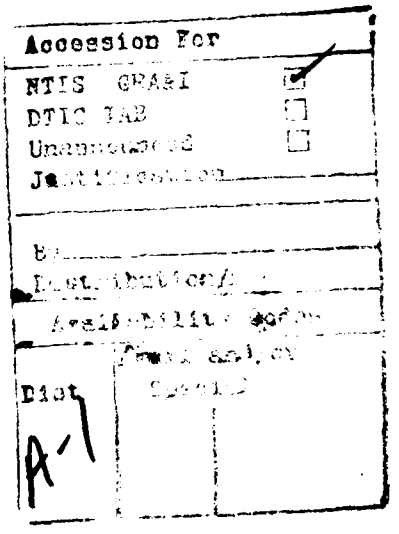

TABLE OF CONTENTS

LIST OF FIGURE CAPTIONS

PREFACE

This research program was conducted by the Aerospace and Energetics Research Program, University of Washington, Seattle Washington 98195, under Grant No. F49620-92-J-0375 with U.S. Air Force Office of Scientific Research (AFOSR), Bolling Air Force Base, Washington, DC 20332. Dr. Julian Tishkoff managed the program for AFOSR. The program was carried out during the contract period from 1 July 1992 to 30 June 1993.

We would like to express our appreciation to E.A. Burnham, G. Chew, A.J. Higgins, and J.B. Hinkey for their invaluable assistance with this research. Malcolm Saynor deserves much credit for his skillful fabrication of the projectiles required for these investigations. We would also like to thank Moeljo Soetrisno and Scott Imlay, both of Amtec Engineering Inc., for helpful discussions about numerical simulations of the ram accelerator.

I. INTRODUCTION

Theater-of-operation defense missions currently constitute a prime motivation for the Ballistic Missile Defense Organization. Ground-based missile defense systems should be flexible, cost-effective, and capable of rapid response following threat detection, to allow engagement as far away as possible from the area to be protected. Autonomously guided interceptors, such as the Lightweight Exo-Atmospheric Projectile (LEAP), could be used to engage high speed warheads at apogee or during the descent phase. To fulfill these mission requirements the prevailing expectation is that the use of rockets with a high boost capability will be necessary; however, an impulsive direct launch system which can deliver interceptors quickly and accurately may be superior, both in effectiveness and cost, particularly in light of recent developments in the technology of the hypervelocity launcher known as the "ram accelerator."[1-27]

The ram accelerator is a device in which a subcaliber projectile, shaped like the centerbody of a supersonic ramjet, is propelled through a stationary tube filled with a combustible gas mixture.[1,2] A mobile LEAP launcher system based on ram accelerator technology has the potential benefits of easy transportation, short setup times, and high barrel slew rates. These operational advantages stem from the absence of the massive and complex recoil systems required by other impulsive launchers, so that pre-arranged concrete and steel emplacements are not necessary. In addition, the fact that the propellant constituents are readily available gases (methane, hydrogen, and air), which have low vulnerability when individually stored, adds to the logistical advantages of the ram accelerator.

Once operational, the objective of this device is to launch an autonomously guided LEAP interceptor, which could be equipped with an upper stage rocket for enhanced range. The high velocity launch provided by the ram accelerator allows rapid atmospheric transit, making it possible to engage incoming warheads exoatmospherically within one minute after launch. Endoatmospheric interceptions are also a possibility. The very low of muzzle blast would reduce the launcher's detectability and significantly reduce the projectile tip-off problems that occur with conventional guns, thus improving trajectory accuracy.

The flexibility and low mass of the ram accelerator system allow it to be considered for installation on other launch platforms, such as ships and even aircraft. A mobile sea-borne defense system could be placed off-shore to provide theater missile defense for land-based assets, as well as protection for a naval fleet. For airborne applications, where launch would occur at altitudes above 10 km, a lightweight ram accelerator capable of LEAP launch could be installed aboard

military transport aircraft, such as the C-141, for both anti-satellite and ballistic missile defense missions.

Ram accelerator technology has been developed at the University of Washington[1-21] and elsewhere[22-27] to the extent where a serious technical evaluation of its potential as an impulsive launcher for autonomously guided projectiles, such as LEAP, can be undertaken. The growing body of pertinent experimental data and operational experience has reached the point that the required launch system parameters can be determined with a high level of confidence. In this report we briefly review the basic operating principles of ram acceleration, present pertinent experimental results, discuss the results of the LEAP system study, and address the engineering issues which must be investigated for successful implementation of the technology in theater defense missions. In addition, a summary of the ram accelerator programs that have been initiated at other research institutions in this country and abroad is presented in Appendix A and a brief description of the "zero velocity start" technique is provided in Appendix B.

II. RAM ACCELERATOR OPERATING PRINCIPLES

The ram accelerator has been under development since 1983 at the University of Washington (UW) for applications as a scalable hypervelocity accelerator capable, in principle, of softly launching projectiles at velocities in excess of 8 km/sec.[1-5] The device is based on an in-bore ramjet concept in which a subcaliber projectile, shaped like the centerbody of a supersonic ramjet (Fig. 1), is accelerated within a stationary tube that contains a pressurized mixture of combustible gases. The projectile itself carries no propellants; the chemical energy required for propulsion is provided by the pressurized propellant gas that is stored in the ram accelerator barrel. This gas is processed by the moving projectile and releases its heat of reaction around and immediately behind the projectile. The result is a high projectile base pressure which continuously thrusts it forward. The peak cycle pressure in the system is always in the vicinity of the projectile, rather than at the breech as in a conventional gun. The projectile thrust is a function of the gas fill pressure and composition, and can thus be readily tailored to provide soft-launch capabilities. Only a small percentage of the propellant gas moves in the direction of the projectile; the bulk of the gaseous combustion products moves backward in the barrel at relatively low velocity. Consequently, the barrel erosion is minimal, the muzzle blast is very small, and there is no recoil. Furthermore, the aerothermodynamic cycle of the ram accelerator is independent of size, so that the device can be directly scaled to any bore diameter.[9]

In order for the ram acceleration process to begin, the projectile must initially be moving above about Mach 2.5 with respect to the propellant gas, which is confined in the tube by means of frangible diaphragms or other suitable closures. To date this initial velocity requirement has been met by means of a light gas gun at the UW and powder guns elsewhere.[22-27] A schematic of a launch system configuration in which a conventional launcher is coupled with the ram accelerator tube is illustrated in Fig. 2. By properly venting the muzzle end of the "starting gun," the recoil induced by the gun and the rearward moving combustion products of the ram accelerator propellant gas can, in principle, be largely counteracted. However, the conventional gun-type initial launcher can be eliminated entirely by implementing a new "zero velocity start" technique patented recently by the authors and their colleagues (see Appendix B).

Since the projectile is aerodynamically unstable in the ram accelerator, some means must be used to keep it centered in the bore. Two approaches are illustrated in Fig. 2: fins on the projectile and rails in the tube. To date fins on the projectile have been in preferred used because of the greater operational flexibility that this approach offers for research purposes and the attendant simplicity of tube fabrication. However, a device with rails on the tube wall has recently become operational at the French-German Research Institute (ISL) in France.[27]

Three distinct ram accelerator propulsive modes, which operate within different velocity regimes centered on the Chapman-Jouguet (CJ) detonation speed (V_{CJ}) of the propellant gas, have been experimentally observed.[6-8] These velocity regimes are arbitrarily designated as subdetonative ($V < 0.9V_{CJ}$), transdetonative ($0.9V_{CJ} < V < 1.1V_{CJ}$), and superdetonative ($V > 1.1V_{CJ}$). Schematics of these three modes are shown in Fig. 3. At subdetonative velocities, subsonic combustion occurs behind the projectile and thermally chokes the flow. As the CJ speed is approached, the nature and location of the ignition process makes a transition to shock-induced combustion which results in heat addition occurring on and behind the projectile. At sufficiently high superdetonative velocities (typically greater than $1.1V_{CJ}$) all of the combustion occurs in the flow between the projectile body and tube walls. The highest velocity achieved to date, 2.7 km/sec, was obtained by partitioning the ram accelerator into several segments, or "stages," each filled with a different methane-based propellant mixture, and accelerating the projectile with the thermally choked propulsive mode. Ram accelerator operation at superdetonative velocities has been demonstrated up to 2.5 km/sec (Mach 8.5) in an ethylene-based propellant mixture having a CJ speed of 1.6 km/sec.[6] More detailed discussions of these modes of propulsion can be found in the cited references.

Conventional Ramjet

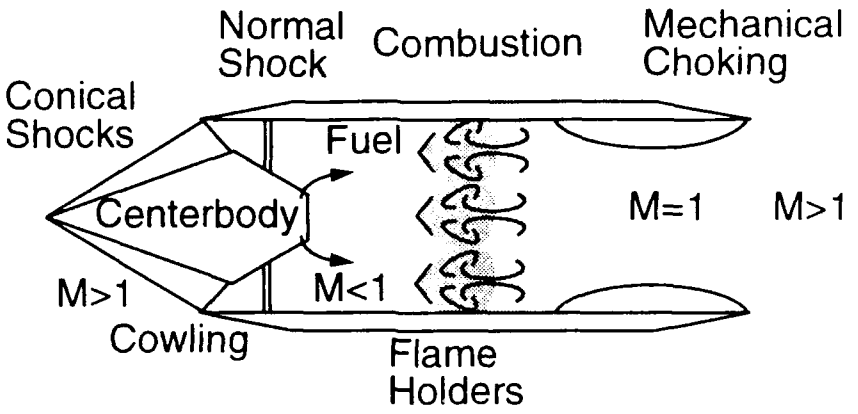

Ram Accelerator

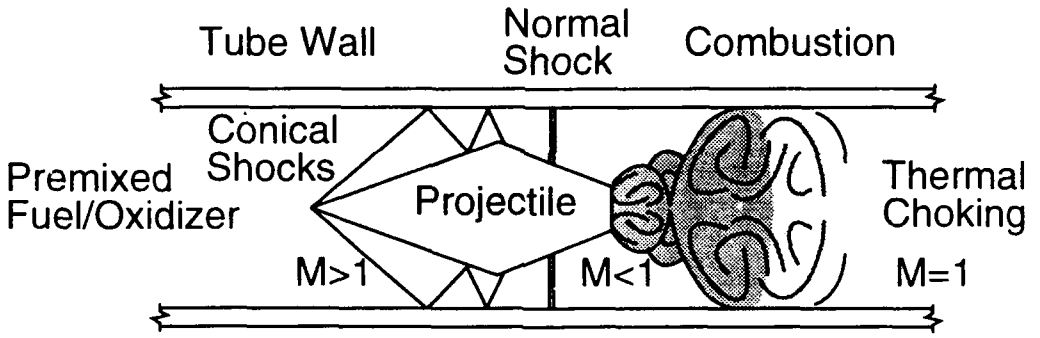

Fig. 1 Schematics of conventional supersonic ramjet and ram accelerator.

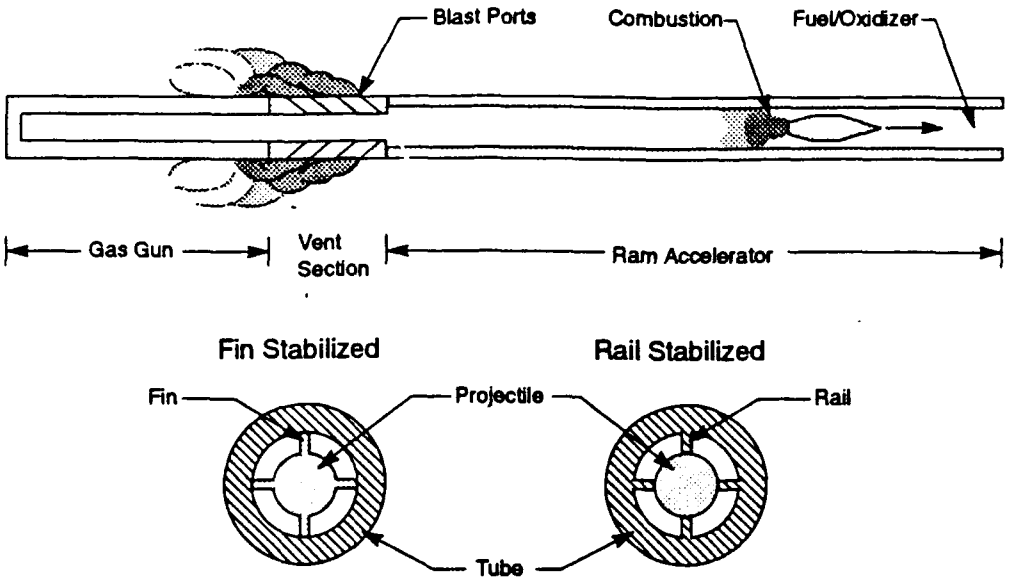

Fig. 2 Ram accelerator with initial launcher. Subcaliber projectile requires fins or rails to center it within the tube.

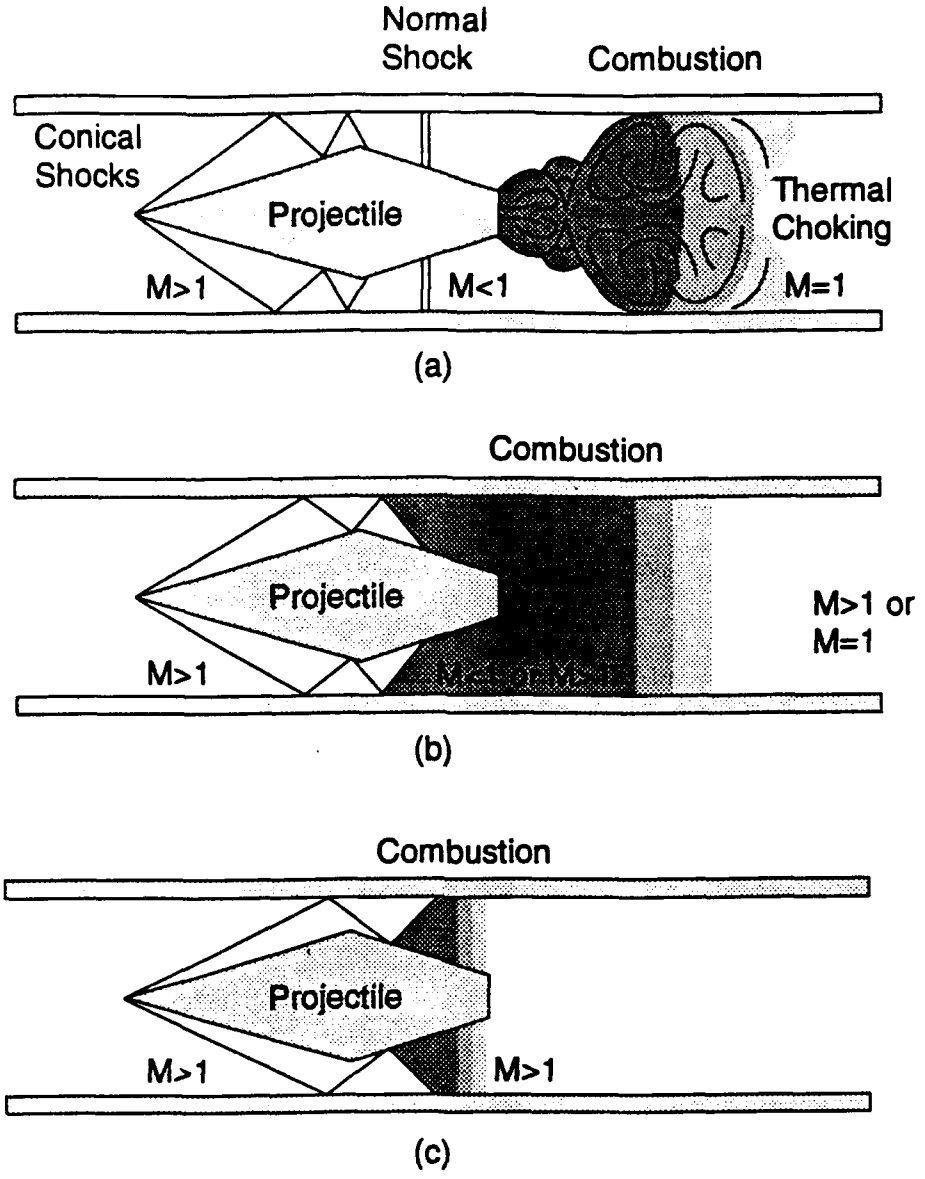

Fig. 3 Ram accelerator propulsive cycles for three different velocity regimes:

a) Subdetonative regime ($V < 0.9V_{CJ}$) with subsonic combustion.
b) Transdetonative regime ($0.9V_{CJ} < V < 1.1V_{CJ}$) with mixed-mode combustion.
c) Superdetonative regime ($V > 1.1V_{CJ}$) with supersonic combustion.

III. UNIVERSITY OF WASHINGTON RAM ACCELERATOR FACILITY

The University of Washington ram accelerator facility, illustrated in Fig. 4, consists of a light gas gun, ram accelerator test section, final dump tank and projectile decelerator. The 38-mm bore, 6-m long, single-stage helium gas gun is capable of accelerating the obturator and projectile combination to a peak velocity of 1.3 km/sec. The ram accelerator test section consists of eight 2 m-long, high-strength steel tubes having a bore of 38 mm and an outer diameter of 102 mm. Detailed descriptions and specifications of the experimental apparatus and accompanying instrumentation can be found in Refs. 13-17.

There are 40 equidistant multiple-port instrumentation stations at 40 cm intervals along the test section of the ram accelerator. To enable more detailed observations of the unsteady wave motions, projectile orientation effects, and three-dimensional flow phenomena, two types of high instrument density tube sections were fabricated; the highly instrumented tube section (HITS) and instrumented inserts,[14-17] both of which are shown in Fig. 5, along with a projectile for scale. The HITS consists of a 17 cm long tube having eight instrument stations with four ports located 2 cm apart.[14] The close spacing of the ports allows 32 transducers to nearly simultaneously monitor the flow field around the projectile with a 45° angular resolution, and to monitor events occurring within half a tube diameter before or after a diaphragm. The instrumented inserts are very short sections of tube which have eight instrument ports separated by 45°. Two inserts can be combined or stacked together to provide an effective angular resolution of 22.5°. Tube couplers (one with a right-hand internal thread and one with a left-hand internal thread) separately thread onto the existing tube segments and provide flanges to which the HITS or inserts are attached.

A schematic of the nominal projectile geometry used in most experimental work to date is shown in Fig. 6. The projectile has been fabricated from both aluminum or magnesium alloys in two hollow pieces – nose cone and body – which thread together at the base of the nose cone. An annular magnet is placed at the cone-body joint to enable accurate tracking of the projectile in the test section by means of wall-mounted electromagnetic (EM) sensors. The hollow design reduces the projectile mass and allows experiments to be conducted at moderate tube fill pressures. Projectile masses have ranged from 45 to 100 g, depending on the material and the structural details. The fins are necessary to center the projectile in the tube.

The experimental capabilities of the UW's facility have steadily improved as the number and variety of sensors have increased and as new diagnostic techniques have been developed. Experiments have been conducted with methane-, ethylene-, and hydrogen-based propellant mixtures at fill pressures ranging from 3 to 50 atm. A wide range of Mach numbers (2.5 to 8.5)

and velocities (0.7 - 2.7 km/sec) has been explored in over 1000 test firings. Operating costs on a per shot basis have proven to be very reasonable for this type of research, thus the experimental part of the research program has been able to provide both significant qualitative and quantitative data on the operating characteristics of the ram accelerator.

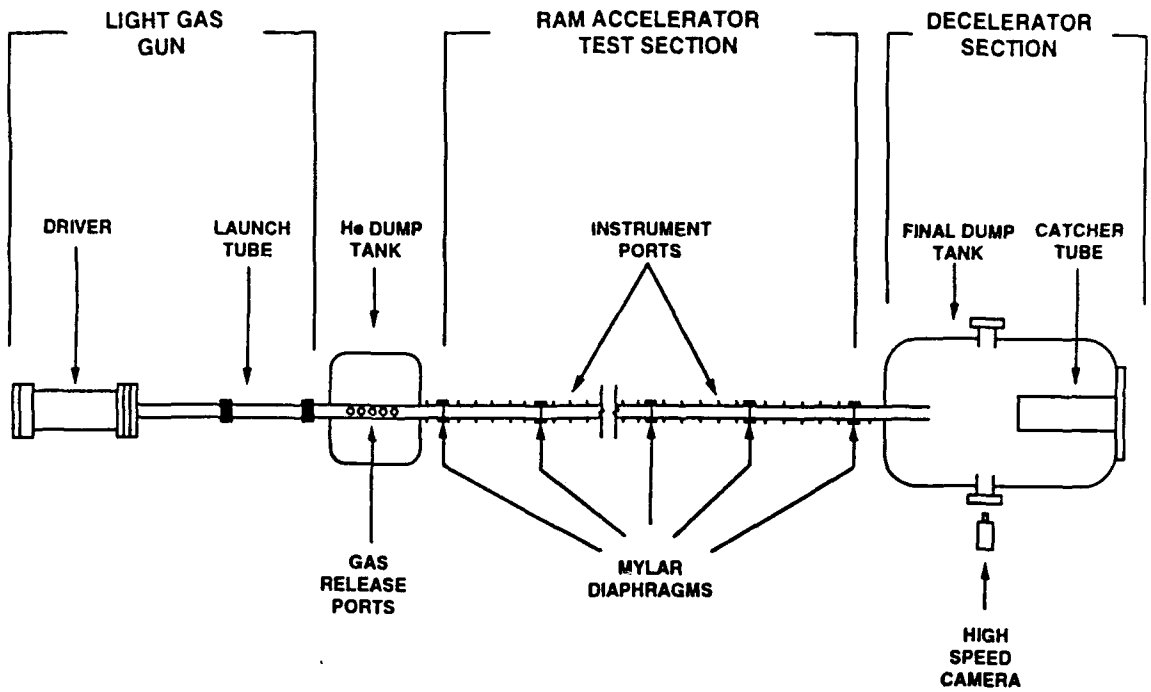

Fig. 4 Ram accelerator experimental facility.

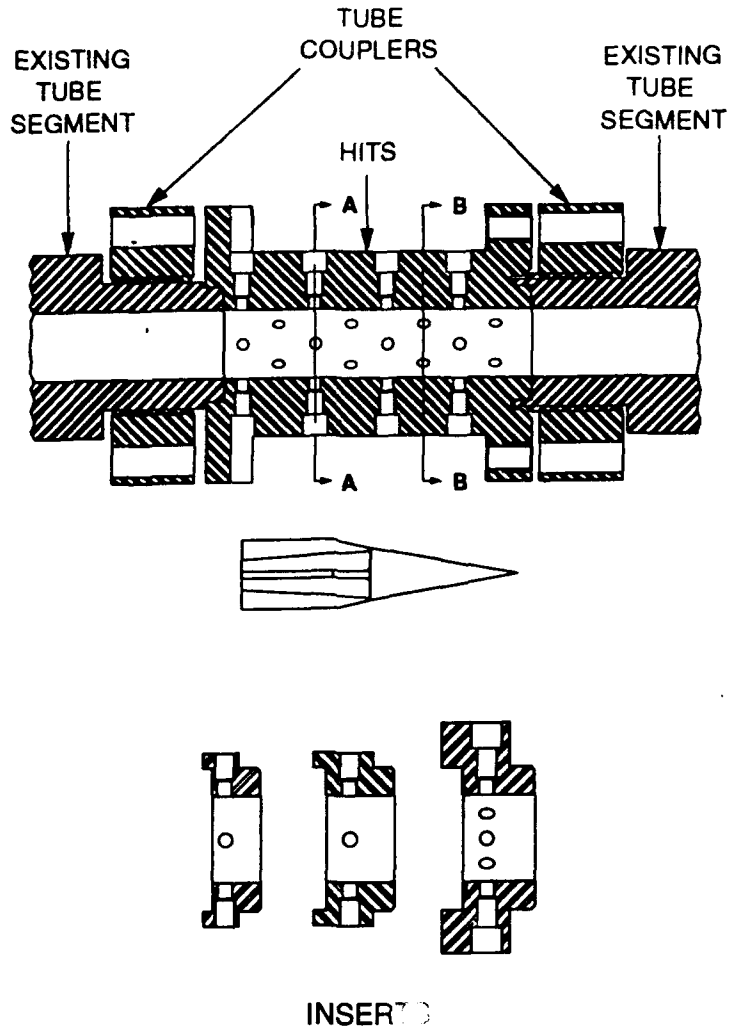

Fig. 5 Highly instrumented tube section and inserts, with projectile shown for scale.

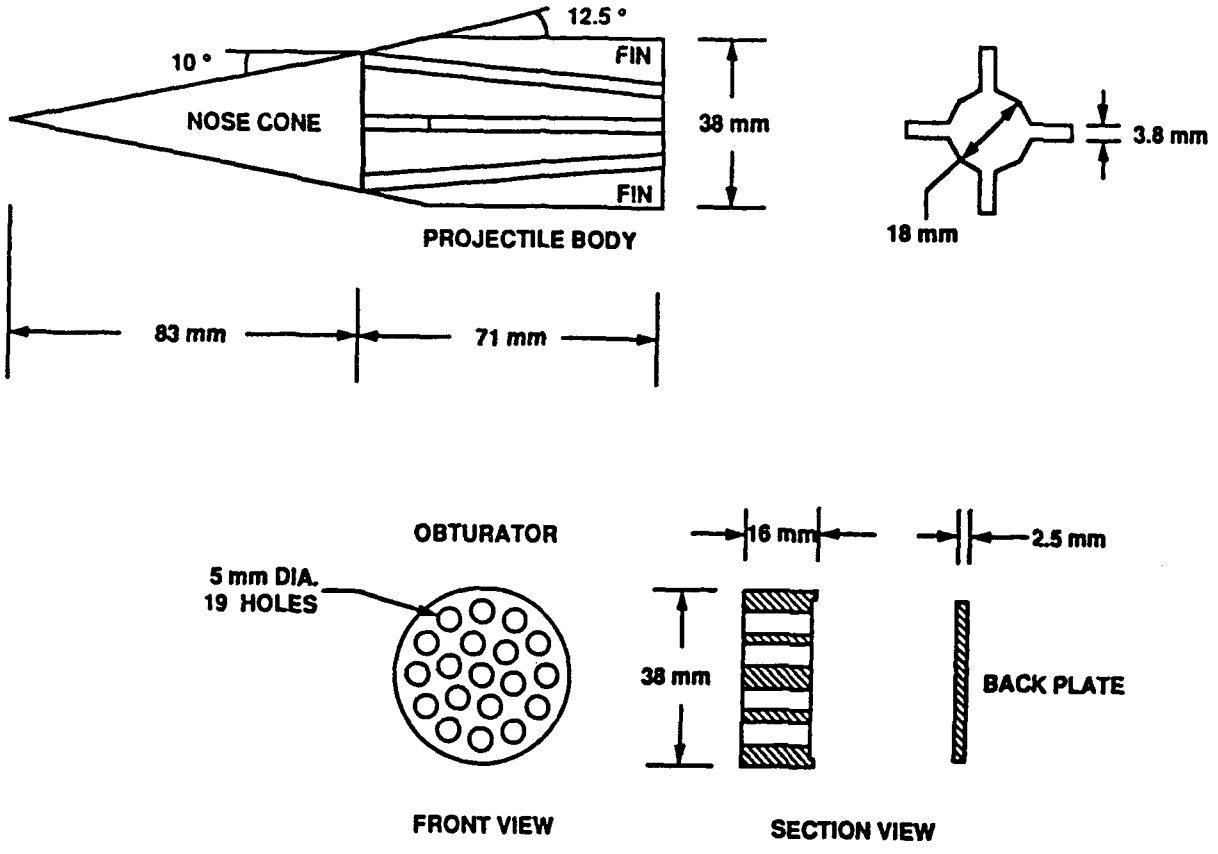

Fig. 6 Projectile configuration used in experiments.

IV. EXPERIMENTAL RESEARCH

During the subject contract period fundamental experimental research has been carried out which is pertinent to evaluating the potential application of the ram accelerator as a LEAP interceptor launcher. This work includes an exploration of the gas dynamic limits to ram accelerator operation and investigations of three-dimensional (3-D) flow effects. The results of these efforts are summarized below.

GAS DYNAMIC LIMITS OF OPERATION

The quasi-steady, one-dimensional "blackbox" model of thermally choked ram accelerator performance[18] that has been widely used by the authors and other researchers produces excellent agreement with experimental implementation of the concept, but says nothing about the regimes of chemistry and Mach number in which the device can operate, since it ignores the details of the flow field. The simplest, one-dimensional, isentropic model of the flow field predicts that the ram accelerator should be able to operate under conditions where the heat release behind the projectile is sufficient to stabilize a normal shock on the body of the projectile.[1-3] A review of experiments, however, shows that the ram accelerator is typically operated in only a fraction of this theoretical operational envelope. To gain an improved understanding of the observed limits, experiments have been performed to explore, for a methane/oxygen/nitrogen based propellant mixture, the regimes of Mach number and chemical heat release in which the ram accelerator can operate.[19] Specifically, the dilution of the mixture was decreased until the combustion wave overtook the projectile and then increased until the combustion wave fell off the projectile. Finally, in an attempt to determine the nature of these observed limits, the ability of the projectile to coast supersonically (i.e., without a combustion wave) through a propellant mixture was examined. The results are suggestive of both the velocity limiting mechanisms and the ultimate potential of the ram accelerator.

Many modes of ram accelerator propulsion have been suggested,[1,2] but the emphasis of experimental work to date has been on the thermally choked propulsive cycle (see Fig. 1). In this mode, a shock system is stabilized on the body by thermal choking via subsonic combustion in the full tube area behind the projectile. The incoming flow is first compressed by a system of oblique and normal shocks, neither of which is strong enough to initiate combustion. Beyond the thermal choke point an unsteady expansion occurs, which is gas dynamically decoupled from the projectile. As the projectile accelerates, the normal shock recedes along the body until it falls off the base of the projectile and occupies the full tube area. For a projectile base which tapers to a

point, the projectile velocity at which the shock falls off and ceases to provide thrust can be shown to equal the Chapman-Jouguet (CJ) detonation speed of the mixture.[3,18]

In practice, however, it has been found that the projectile can accelerate through the CJ detonation speed of a particular mixture.[6-8] This "transdetonative" phenomenon was an unexpected experimental result and is believed to result from partial heat addition occurring on the projectile body. Whether this ignition is caused by shocks, shock-boundary layer interactions, or reactions in the boundary layer, it is believed to result in a "combined cycle" in which some heat is released on the body and some in the recirculation zone behind it.

While considerable effort has been directed at investigating the performance capabilities of the various ram accelerator propulsive modes, little work has been done to determine their operational limits. Moreover, the conditions under which the combustion will overtake the projectile or will fall-off the base are poorly understood. This investigation is motivated by the need for an improved understanding of the gas dynamic phenomena which limit the operation of the ram accelerator, particularly in the subdetonative and transdetonative velocity regimes.

THEORETICAL CONSIDERATIONS

Once the assumption of a thermally choked flow in the full tube area behind the projectile has been made, the thrust on the projectile is uniquely determined by the flow conditions upstream of the projectile and at the thermal choke point. If the flow at the thermal choke point is assumed to be in equilibrium, the conditions can be determined by an equilibrium chemistry combustion routine. This model of the ram accelerator can be thought of as a "blackbox," since it ignores the details of the flow and considers only the conditions at the entrance and exit planes of the projectile control volume.[18] This analysis yields a thrust equation for the ram accelerator which is a function of the projectile Mach number and Q, the non-dimensional heat release of combustion, defined as $\Delta q/c_{p1}T_1$, where Δq is the heat of combustion and the "1" subscript denotes conditions upstream of the projectile.[1,3] Moreover, this relation can be derived as part of a generalized Hugoniot analysis, with the addition of a force component not included in the classical Hugoniot equations.[18,28] The agreement between the theoretical prediction and the observed value of acceleration during operation in the subdetonative velocity regime has been shown to be quite good.[3,10,18,28] Such analysis, therefore, reinforces the idea that the performance of the thermally choked ram accelerator is independent of the details of the internal flow field.

While this "blackbox" model is excellent at predicting performance, it says nothing about the ability of the ram accelerator to operate at a given velocity or in a given mixture. This is to say,

if a ram accelerator projectile successfully stabilizes the combustion process, the model presented above will accurately reproduce its performance, but it will not be able to determine if the projectile can successfully drive at all. To determine the limits to operation, the details of the flow field must be examined.

The simplest model of the thermally choked ram accelerator flow field treats the flow over the projectile as isentropic, except for a single normal shock (Fig. 7).[19] In reality, a single normal shock is unlikely; the flow more closely resembles the complex system of normal and oblique shocks observed in supersonic flow in long ducts.[29] This normal shock is stabilized on the body by the thermal choking of the flow in the full tube area behind the projectile. The combustion behind the projectile is modeled as Rayleigh flow. The normal shock is free to move in response to changing upstream and downstream conditions. As the projectile accelerates, the normal shock recedes until it reaches the base of the projectile. If the projectile base were tapered to a point, the normal shock would recede and reach the full tube area as the projectile is accelerated to the CJ detonation speed. As mentioned earlier, this results in the cessation of thrust, making the CJ speed the maximum theoretical velocity of thermally choked operation.

Such a model imposes three limits on ram accelerator operation. First, the projectile must maintain a certain minimum Mach number (approximately 2.5 for projectile geometries used in the UW facility) to keep the flow supersonic past the throat (station 2 in Fig. 7). Below this Mach number, the flow will choke on the projectile forebody, resulting in an "unstart." Second, a certain maximum is imposed on the heat release of the mixture, beyond which the normal shock is disgorged from the throat, also resulting in an unstart. Finally, a certain minimum heat release is required to keep the shock wave from falling off the projectile base. All three of these limits can be expressed as simple relations of the Mach number of the projectile and the heat release of the propellant mixture (along with the thermodynamic properties of the gaseous mixture, such as the specific heat ratio γ). For a given projectile throat-to-tube and base-to-tube area ratio, these relations define a theoretical region of operation, or operational envelope, for the ram accelerator. This envelope, for the nominal UW geometry, is shown in a plot of heat release vs. projectile Mach number in Fig. 8, along with a curve indicating the dependence of the CJ Mach number on Q. As mentioned before, for a projectile whose base tapers to a point, the shock-at-base condition coincides with the CJ curve. For Fig. 8 the gas was assumed to be calorically perfect, with γ taken as a constant 1.4. Hence, in this example the flow is treated as an inert working fluid with some kind of external heat addition. Modifications can be included in this one-dimensional model to account for losses in the diffuser and across the projectile blunt base, but the changes are minor and do not affect the qualitative nature of the envelope. This envelope bounds a large region of

Mach number and heat release values, indicating that a potentially wide range of operating conditions might be realized.

This model is also a convenient way to examine the influence of various non-ideal flow effects, such as pre-combustion on the projectile. For example, let us arbitrarily prescribe 10% of the total heat release to occur at the projectile throat. The effect this has on the theoretical envelope is shown in Fig. 9. Note that the minimum Mach number for operation at both the sonic-at-throat and shock-at-throat limits has been raised. This is to say, pre-combustion has the effect of driving the flow toward sonic, allowing the area contraction at the throat to more easily choke the flow. Pre-combustion also moves the normal shock forward, allowing it to be disgorged from the throat at lower values of total heat release. The fact that both these unstart mechanisms can be relevant will be of importance later when we attempt to determine the nature of the actual limits to the ram accelerator.

Although these theoretical considerations suggest the ram accelerator has a wide envelope of operation, experimentally it is unable to access most of the operational region that the simple model predicts. Shown in Fig. 10 are the results of two different firings of the UW ram accelerator, which are typical of the experiments performed to date. Velocity-distance data are presented from a single stage experiment (i.e., a single propellant mixture) which exhibited transdetonative operation. The propellant mixture used is indicated in Fig. 10a and the initial fill pressure was 25 atm. The second experiment is an example of staging, where the propellant mixture is tailored down the length of the tube to accelerate the projectile continuously at subdetonative velocities while maintaining high accelerations. In this multistage experiment, the initial fill pressure was 45 atm for all four stages and the propellant mixtures are tabulated in the figure. The projectile masses were 63 and 80 g, respectively. The corresponding theoretical curves (generated by the "blackbox" analysis) are in good agreement with the experimental results while the projectile is operating below ~90% of the CJ speed.

Although the theoretical envelope shown in Fig. 10b shifts slightly for the different thermodynamic properties of each mixture, the changes are too subtle to show in this figure. The fact that the single stage experiment exhibited transdetonative performance, while the multistage experiment remained subdetonative, is easily seen in the Q-M plane. We can see from these plots that, for the most part, the ram accelerator typically operates at Mach numbers beyond which theory predicts a normal shock should move off the projectile.

While attempts have been made to operate in more energetic mixtures, which should exhibit higher acceleration, these experiments often result in an almost immediate "unstart" of the

projectile. An unstart is a very violent phenomenon in which a normal shock is disgorged from the throat of the projectile, often developing into an overdriven detonation wave that propagates down the tube in front of the projectile. This irrevocable phenomenon causes a pronounced deceleration of the projectile and often results in its complete structural collapse. The pressure profiles of such an unstart, normalized by the fill pressure, are shown in Fig. 11. Trace "a" indicates a pressure profile of the flow field while the projectile is in nominal operation at a velocity of 1800 m/sec (Mach 5). A scaled outline of a projectile shows its relative size. The spikes seen near the throat result from the conical bow shock reflecting between the projectile and the tube wall. The elevated pressure region behind the projectile is the result of the heat release from combustion. The remaining traces (b-e) show the progression of an unstart, taken from pressure transducers 0.4 m apart. A very large pressure spike (pressure ratio of ~50) is seen developing at the throat and propagating in front of the projectile, eventually evolving into an overdriven detonation wave. The total time lapse for the records shown in Fig. 11 is ~1 msec.

The actual mechanism of these unstarts, which limit the operation of the ram accelerator, is poorly understood. As mentioned previously, pre-combustion could choke the flow at the throat of the projectile, or the heat release could drive the shock system over the projectile. The observed operational limits and the nature of these limiting mechanisms are the subjects of the investigation presented here. For a single class of propellant mixture, the operational envelope is explored by varying the energetics of the propellant mixture and the entrance Mach number of the projectile.

EXPERIMENTAL PROCEDURE

The theoretical operational envelopes for the thermally choked ram accelerator derived in the previous section are functions exclusively of the projectile Mach number and the heat release. To explore the corresponding experimental operational envelope, the heat release must be varied in a systematic way. Specifying the heat release, however, does not uniquely specify the chemistry of the propellant mixture. For example, a stoichiometric mixture of oxygen and methane (CH_4+2O_2) has a non-dimensional heat release parameter Q of 19.8 if the flow is thermally choked at a projectile Mach number of 4. Suppose we wish to explore a mixture with a Q value of 5.0. We could add excess fuel to dilute the mixture, yielding a mixture of $6.3CH_4+2O_2$, or add an inert gas like nitrogen, giving $CH_4+2O_2+15N_2$. Hence, to uniquely relate a propellant mixture to a value of heat release, we must constrain our choice of mixture in some way.

For this series of experiments, the fuel equivalence ratio was fixed to 2.8 while varying the amount of nitrogen dilution ($2.8CH_4+2O_2+XN_2$). The selection of this chemistry was not made in complete capriciousness. A similar class of mixture ($2.8CH_4+2O_2+5.7N_2$) has proven a reliable

first stage in the operation of our facility and routinely exhibits transdetonative performance (see Fig. 10). In the experiments presented here, the amount of nitrogen dilution was varied from 3 to 12 moles, or 40% to 70% by volume. The heat release parameter Q as a function of this dilution at various projectile Mach numbers is shown in Fig. 12. The heat release decreases with increasing projectile Mach number for a given mixture due to the increased static temperature at the plane of thermal choking, resulting in greater dissociation losses. This loss is visible in plots of experimental data in the Q-M plane as a slight downward slope of the experimental curve, as seen in Fig. 10b. With the aid of Fig. 12, the heat release can be uniquely related to the mixture composition, and vice versa, for any data from this experimental series.

It should be emphasized that the value of Q is the Mach number dependent, non-dimensional heat release for thermally choked flow. Since the flow cannot be thermally choked in the full tube area behind the projectile in transdetonative and superdetonative operation, while producing positive thrust, this value of Q is not the actual heat release. It is, however, believed to be at least qualitatively indicative of the actual heat release and provides a self-consistent measure for comparing the effective heat release of different chemistries under similar flow conditions. Even in experiments where the flow did not ignite, a value of Q is ascribed to the experiment as if it were achieving full chemical equilibrium and thermally choking in the tube behind the projectile.

The process by which the combustion wave is initiated and stabilized on the projectile is an extremely complicated, unsteady interaction between an obturator and projectile occurring upon impact with the first stage of ram accelerator propellant.[15] Since the purpose of these experiments is to determine the limits of ram accelerator operation, as opposed to starting, the experiments must be carefully isolated from the combustion initiation process. To achieve this, a starter stage of the standard propellant mixture described above ($2.8CH_4+2O_2+5.7N_2$) is used. This mixture can consistently initiate and stabilize a combustion process with the projectile. If the entire ram accelerator is filled with this mixture, it will accelerate a magnesium projectile from the entrance speed of 1100 m/sec to 1975±25 m/sec, where an unstart occurs (see Fig. 12). Hence, this mixture forms the "control" in the experiments to follow.

It is believed that within the first meter of the ram accelerator test section the obturator and starting transients are gas dynamically decoupled from the projectile, leaving it in quasi-steady operation.[15] In this series of experiments, the projectile was allowed to travel for a minimum of 2 m in this nominal mixture. The projectile then transitioned into the test mixture, which was a variation of the starter stage with either increased or decreased nitrogen dilution. These two stages were separated by a thin (0.5 mm) Mylar diaphragm. For experiments in which a high Mach

number transition was desired, the starter stage was lengthened to provide a greater velocity gain before the transition. These experimental configurations are shown schematically in Fig. 13.

Although these experiments involved transitions into mixtures with significant changes in energetics and heat release, the sound speed never varied by more than 3%. Hence, there was no sudden shift in Mach number or acoustic impedance for projectiles entering the test mixture. In routine ram accelerator multistage operation, transitions are regularly made resulting in a nearly instantaneous change in Mach number from 4 to 3 (see Fig. 10b). Hence, the current experiments represent a relatively mild gas dynamic transition.

The projectile was tracked down the length of the test section via electromagnetic (EM) probes until an unstart occurred, which could be determined unambiguously from both the pressure traces from the transducers mounted on the tube wall and the sudden projectile deceleration indicated by the EM time-distance data. The propellant fill pressure in all experiments (both starter and test stage) was 25 atm. After an experiment, samples of the propellant mixture drawn from the ram accelerator tube immediately before firing were analyzed via gas chromatography to ensure the correct propellant mixture was used. Although determining the absolute molar ratios to within 5% is difficult with the current gas analysis system, the molar ratios can be accurately varied in a relative and reproducible manner by increments as little at 2%, or about 0.2 mole of N_2 in a $2.8CH_4+2O_2+XN_2$ class of mixture.

EXPERIMENTAL RESULTS

Low Mach Number Transition: The first series of experiments involved transition from the nominal, or starting stage, to the test mixture at a relatively low Mach number of 3.8. The projectile left the light gas gun with a velocity of 1130±25 m/sec. After initiating combustion and accelerating the 2 m length of the starter stage, the projectile reached 1390±20 m/sec at the transition to the test mixture. The remaining 14 m of ram accelerator were filled with the test mixture; although in only one experiment did the projectile continuously accelerate to the end of the test section. The results of these experiments, showing the projectile's velocity as a function of its position in the test section, are shown in Fig. 14a. The velocity-distance profiles are actually higher order (4th-9th) polynomial curve fits to the first-order finite difference of the position-time history of the projectile as given by the EM probes. Note that the acceleration histories of the projectiles in the nominal starting stage were very similar, but upon entrance to the test mixture, the performance varied greatly for the different levels of N_2 dilution, with the more energetic propellants exhibiting higher accelerations. A detailed analysis of the acceleration performance of each propellant mixture and comparison to that predicted by the "blackbox" model of the ram

accelerator is presented in Ref. 28. The primary interest here remains on the gas dynamic phenomena that bound successful operation.

For the two most dilute mixtures (9.0 and $12N_2$), the projectiles actually decelerated. This concurs with the pressure profiles from the tube wall transducers, which showed a clear wave fall-off ~0.5 m after transition into the test mixture. All the other mixtures exhibited at least some acceleration in the test mixture, except for the most energetic, which unstarted within ~0.5 m of the transition.

As a general rule, the less reactive/energetic a mixture, the farther the projectile drove into the test section before unstarting. The ultimate velocity, however, exhibited a maximum with respect to the amount of dilution. This observation becomes clearer when the data are plotted in the *Q-M* plane (Fig. 14b), where examples of theoretical operational envelopes were shown earlier. The curve which begins at Mach 3.1 is the nominal, or starting, mixture. All experiments began on this curve and then transitioned, after 2 m of ram acceleration, to the appropriate test mixture, at which time the projectile was traveling at approximately Mach 3.8.

Experiment 2f in Fig. 14b (corresponding to a propellant mixture of $2.8CH_4+2O_2+4.8N_2$) exhibited the maximum projectile velocity. Although the projectiles in the more diluted mixtures unstarted at a lower Mach number, the reduced energetics of these mixtures compromised the acceleration. Hence, the projectiles actually drove farther into the test section and were accelerated for a greater length of time before failing. This longer history of heat transfer and projectile wear makes it difficult to ascribe these unstarts to pure gas dynamics. For example, the projectiles may have sustained extreme fin erosion, leading to severe canting and eventual unstart,[17] or suffered melting and ablation due to aerodynamic heating.[30] Indeed, it is known that projectiles constructed of different materials will drive farther and to higher final velocities in the nominal mixture, suggesting an unstart mechanism which depends on a structural factor.[11] Hence, the observed limit comprised of the unstarts 2a-f in Fig. 14b is not believed to be pure gas dynamic in nature, despite the fact that the unstarts indicate an envelope which is remarkably self-similar to the CJ detonation curve.

The more energetic mixtures plotted in Fig. 14b, i.e. groups 3 and 4, unstarted earlier in the test section than the maximum velocity firing (2f). The fact that these projectiles unstarted earlier in the experiment, despite their reduced history of heat transfer and fin erosion, strongly suggests that the unstarts were gas dynamic in nature. As the mixture was made more energetic, these unstarts occurred at lower Mach numbers. For the most energetic of mixtures (group 4), the unstarts occurred almost immediately, i.e., within the first meter, after transition into the test

mixture. Hence, the group 4 unstarts indicate the maximum heat release for which the ram accelerator can operate in this class of propellant mixture with this projectile configuration.

The extremely diluted mixtures (1a,b in Fig. 14b) which exhibited combustion fall-off are also believed to be a pure gas dynamic limit to operation, since the fall-off occurred while the projectile retained structural integrity. It is interesting to note that the projectiles exhibited transdetonative performance until the mixture was diluted to a point where wave fall-off occurred.

Our earlier observation that the ram accelerator is not routinely operated in the region predicted by the one-dimensional, quasi-steady model of the flow field is borne out in these experiments. We see from Fig. 14b that almost all of the operation in these experiments occurred under conditions in which a normal shock would have fallen off the base of an ideal projectile or in which no thrust should be available at all, i.e., in the transdetonative regime. Moreover, the observed "hot" limit appears to concur with the conditions under which a normal shock would just barely be supported on the projectile base.

High Mach Number Transition: The lack of an upper bound on heat release for the theoretical envelope in Fig. 8 suggests that the observed "hot" limit in these experiments may only apply when entering the mixture at Mach 3.8. Moreover, the device may be able to operate in more energetic mixtures via a higher Mach number transition. To answer this question, a second series of experiments was performed which used an additional 2 m of the nominal starting mixture before transition to the test mixture, as shown schematically in Fig. 13. The projectile now entered the test mixture at 1540±25 m/sec or Mach 4.2. As mentioned previously, the longer projectile residence times in the test section required to observe an unstart in heavily diluted mixtures make the gas dynamic nature of these unstarts suspect. Hence, the emphasis in this second series is exclusively on the more energetic mixtures, for which the limits are believed to be purely gas dynamic in nature.

The velocity-distance profiles of these experiments are shown in Fig. 15a. Again, the projectiles exhibit similar velocity profiles in the first stage of nominal propellant, then depart following entrance to the test stage. The well-ordered sequence of unstarts as a function of mixture energetics observed in the previous section appears less distinct here. More dilute mixtures did not always drive the projectiles farther into the test section. The dependence of the Mach number range of operation on chemistry becomes clearer by again plotting the data in the Q-M plane (Fig. 15b). The Mach number of unstart did not exhibit a monotonic decrease with decreasing dilution. Two of the group 5 experiments (c and d) failed at anomalously low Mach numbers. Although the 5c-d unstarts occurred ~1 m after transition, by which time the transition transients are believed to have

passed, this result leads to suspicions that high Mach numbers may be less tolerant of transitions to more energetic mixtures. For the most part, however, the observed operational limits appear to concur with those found in the lower Mach number transition experiments. The agreement in observed operational limits between the low and high Mach number transition experiments reinforces the supposition that the limits are pure gas dynamic in nature. The two experiments in which the projectiles unstarted anomalously early, however, suggest that high Mach number transitions might be more susceptible to transition-induced failure, either due to unsteady flow phenomena, or the lengthened history of fin wear and heat transfer arising from a longer residence time in the starter stage.

Limits to Supersonic Coasting: While these experiments have succeeded in mapping out the operational envelope for this particular class of propellant and projectile configuration, they do little to reveal the cause of the limiting mechanism, the unstart. Consideration of the one-dimensional, quasi-steady model of the flow field indicates that there are two potential unstart mechanisms. One may arise from premature combustion on the nose cone leading to a choking of the flow at the throat. Alternatively, the disgorging of the normal shock/combustion wave system may be due to excessive heat release behind the projectile. Ideally, the former mechanism (pre-combustion leading to choking at the throat) is independent of the presence of a combustion wave. If this is the relevant mechanism, it should result in an unstart upon entrance into the test mixture regardless of the character of combustion process behind the projectile. The second unstart mechanism, however, requires that combustion first be initiated behind the projectile.

Of course, viscous flow effects tend to blur this distinction, since the flow field upstream of the shock system is no longer purely hyperbolic in nature, and combustion can be propagated upstream via the boundary layer. Nevertheless, we can attempt to differentiate these two by "stripping" the combustion wave from the projectile before it enters the test mixture. The thermally choked ram accelerator is believed to require the complicated and unsteady interaction with the obturator to initiate operation. Hence, by stripping the combustion wave before entering the test mixture, the projectile should "coast" supersonically through the test mixture, while it steadily decelerates. If the coasting projectile immediately unstarts, then the unstart mechanism is likely some form of pre-combustion leading to thermal choking at the projectile throat. On the other hand, if the projectile coasts uneventfully through a test mixture in which an accelerating projectile would unstart, the unstart mechanism requires the presence of a driving combustion wave.

The combustion strip is accomplished via a 4-m-long inert stage placed between the starter/accelerator stage and the test mixture. This inert mixture consists of a chemistry identical to the test mixture, only with the oxygen swapped for nitrogen. For example, if a test mixture of

$2.8CH_4+2O_2+3N_2$ is used, the inert stage immediately upstream of the test section is $2.8CH_4+5N_2$. This is shown schematically in Fig. 16. Matching the gases in this way ensures the smoothest possible gas dynamic transition. This ability to strip off the combustion wave is a luxury available only with thermally choked operation, since the superdetonative modes of operation, which are capable of inducing combustion via shocks, are initiated by the projectile immediately upon entrance to the propellant mixture.

Only four such experiments were performed, each near the observed "hot" limit determined in the prior experiments. The test mixtures used for these experiments were the most energetic of those used in these sets of experiments, e.g., $2.8CH_4+2O_2+3.0N_2$, which has a heat release parameter value of $Q \approx 6.0$. The results of these experiments are shown, along with the low and high Mach number transition results, in Fig. 17. In all cases, a projectile entering the test mixture after passing through an inert stage was able to coast successfully in the combustible gas.

In the lowest Mach number transition case ($M = 3.5$), the projectile was able to coast th entire 8 m length of the test section uneventfully, while experiment 4b from the low Mach number transition sequence (Fig. 14b) unstarted almost immediately upon transition into to this same mixture. In the three other combustion stripping experiments (those involving transitions above Mach 4), ignition occurred in the wake of the projectile, resulting in a combustion wave which eventually caught up with the projectile and reestablished ram accelerator drive. These projectiles eventually unstarted, similar to the unstarts which occurred when projectiles entered the same mixtures with the combustion wave already attached. The unstarts occurred, however, only after the projectile had coasted ~2 m, a distance significantly longer than the corresponding unstarts observed in experiments where the projectile entered the test section with a stabilized combustion wave. These results, while still under investigation, suggest that the unstart mechanism in this "hot" limit seems to require the presence of the combustion wave and is not a simple choking of the flow due to shock-induced pre-combustion around the nose cone.

SUMMARY OF GAS DYNAMIC OPERATIONAL LIMITS

The operational envelope for an oxygen/methane/nitrogen based propellant mixture with a fuel equivalence ratio of 2.8 has been investigated. By varying the diluent concentration, limiting phenomena were observed from immediate unstart to combustion wave fall-off. The regimes of chemistry in which the projectile can operate are readily discerned by examining the experimental data in the heat release-Mach number (Q-M) plane. A relatively wide range of chemistry ($3.8 < Q < 5$) has been identified which continuously accelerates the projectile through the CJ detonation speed and into the superdetonative regime, where the unstart mechanism is believed to

depend on the projectile's structural integrity. The ability of the ram accelerator to operate at Mach numbers above which one-dimensional theory predicts the normal shock can be stabilized on the body indicates that this model is inadequate for predicting the observed operational limits. The one-dimensional model also fails to account for an observed upper limit ($Q \approx 6$) on the energetics of mixture. This limiting mechanism requires the presence of the combustion wave behind the projectile. These experimental results are indicative of the range of gas dynamic phenomena that must be addressed by analytical and computational flow field models to accurately predict the operational characteristics of the ram accelerator.

HIGH SPATIAL RESOLUTION PRESSURE MEASUREMENTS

An experimental and numerical investigation of the three-dimensional ram accelerator flow fields induced by canting of the projectile is presented. Data obtained by using highly instrumented sections of tube have, in some instances, revealed a flow field that deviates from that expected if the projectile was centered in the tube as it was accelerated.[14,16,17] These deviations of the flow field from previous experiments and previous inviscid, non-reacting three-dimensional simulations have implications with respect to operational performance and velocity limits of the ram accelerator. Three-dimensional, inviscid, non-reacting numerical simulations of a canted axisymmetric projectile are presented and are compared to new and previously published pressure data. Tube wall pressure data from projectiles traveling in non-reacting mixtures at equivalent sub- and superdetonative velocities reveal the structure of the ideal and non-ideal non-reacting three-dimensional flow field. In addition, experimental data from an "unstart" are presented and the possible causes of this phenomenon are speculated upon. The information gained from these experiments and simulations is relevant to enhancing our understanding of the underlying nature of the ram accelerator propulsive regimes.

Recent numerical and experimental studies have investigated the effect of the fins on the three-dimensional flow field around the ram accelerator projectile.[14,16,31,32] These computational studies have modeled the ideal three-dimensional flow field by assuming that the major axis of the projectile was collinear with the tube axis. The experiments reported on here utilized highly instrumented sections of tube to investigate the non-ideal three-dimensional flow field around a ram accelerator projectile due to the phenomenon of projectile canting (i.e., when the projectile axis is not parallel with the tube axis).[17] The interpretation of the experimental data is aided and confirmed by numerical simulations of a canted axisymmetric projectile, using a fully three-dimensional, non-reacting, inviscid, finite volume-based computational fluid dynamics code. In addition, an analytical method is used which, in conjunction with experimental data, is able to estimate the position and orientation of a projectile when it is canted. This experimental study was

undertaken in a single-stage methane-based ($2.7CH_4+2O_2+5.8N_2$) combustible gas mixture with a CJ detonation speed of approximately 1750 m/sec, projectile velocities between 1400 m/sec and 2060 m/sec, initial pressures of 28 to 33 atm, and four-fin projectiles having masses of 74 g.

PROJECTILE CANTING

The phenomenon of projectile canting has been previously reported but no detailed investigations were attempted. The projectile is said to be "canted" when the major axis of the projectile is not parallel with the tube axis, resulting in the nose cone having a non-zero angle of attack, as illustrated in Fig. 18. A projectile with its axis collinear with the tube is shown in Fig. 18a, a projectile with its axis parallel to, but not collinear with the tube axis (translated only) is shown in Fig. 18b, and a canted projectile (a combination of rotation and translation) is shown in Fig. 18c.

The phenomenon of canting manifests itself most noticeably in the variation of the time of arrival at the tube wall of the initial shock wave generated by the projectile nose cone. There is also a variation of the magnitude of the reflection from the tube wall of the initial shock over different azimuthal angles at the tube wall. The differences in arrival time and reflected shock magnitudes are conceptually illustrated by Fig. 19, which shows a canted projectile with the resulting difference in arrival time of the initial shock wave and the difference in the magnitude of the resulting tube wall pressure for opposite sides of the tube. It has been generally observed that the azimuthal position where the initial shock wave arrives the earliest in time is also where the weakest reflected shock occurs, and where the initial shock arrives later in time is where the reflected shock strength is the greatest. Cases which do not exactly exhibit this behavior are thought to be due to the projectile being canted in the tube in a manner which places the plane of symmetry of the flow somewhere between a pair of adjacent pressure transducers.

High resolution pressure measurements were made of a canting projectile while it was traveling at 1560 m/sec (Mach 4.3) or 89% of the CJ detonation speed in a propellant mixture consisting of $2.7CH_4+2O_2+5.8N_2$ at 28 atm. Displayed in Fig. 22 is a series of line plots of the pressure data from eight transducers placed in the HITS, each angularly separated from its adjacent neighbors by 45°. The number of each trace corresponds to the small inset figure that shows the projectile fin orientation with respect to the transducers in the HITS. An outline of one-half of a projectile is placed at the bottom of the line plots to indicate the position of the projectile body and fins relative to the pressure traces. Traces 3 and 7 show the greatest difference in arrival time (approximately 19 μsec) and magnitude of the reflected shock pressure ratio (1.5 to 2 for trace 7 as compared to approximately 6 for trace 3). To aid in recognizing these differences the data of

Fig. 20a are shown in Fig. 20b but with the time scale expanded. The difference in arrival time of the initial shock is accentuated in Fig. 20b, in which lines have been drawn from trace to trace to connect the times at which the initial shock waves arrive. The resulting "s" shape is quite distinct. If a projectile were not canted but simply translated to one side of the tube, this "s" shape would still persist; however, the magnitude of the reflection of the initial shock would remain azimuthally constant. This is obviously not the case with the data from this experiment.

Use of the Taylor-Maccoll Solution: Several experiments have shown the distinct features of canting, and a method has been developed to determine approximately to what degree these projectiles were canted in the tube.[17] Specifically, it is desired to determine the angle of attack of the projectile and its physical position relative to the tube. Through the use of a combination of the Taylor-Maccoll solution for conical flow[33] and experimental data, the approximate angle of attack of the nose cone (and hence the projectile) and the amount by which the nose tip of the projectile is translated from the centerline of the tube can be determined. A brief outline of this procedure is presented in the following, a more detailed discussion can be found in Ref. 17.

The procedure is based on the assumption that the projectile angle of attack is not large and hence the Taylor-Maccoll solution for determining the cone angle for a given shock angle is approximately valid at all azimuthal angles of the cone. It is assumed that the projectile is canted in the tube in such a way that there exists a half-plane of symmetry which includes the axis of the tube, i.e., it is assumed that the projectile is rotated and translated in a single common plane that defines this plane of symmetry. It is also assumed that the gas behaves ideally and is calorically perfect, with the freestream properties evaluated at standard conditions. The method also depends upon accurate reading of the experimental tube wall pressure data and, hence, the accuracy of the pressure transducers.

The method is implemented as follows: First, the difference in arrival time of the shock from the nose cone is measured for each pair of opposing pressure transducers and the maximum value found is used. It is assumed that the transducers which produce the maximum difference in arrival time, together with the tube axis, define the plane in which the projectile is canted. This may not exactly be the case since there is 45° between transducers in the HITS and 22.5° between transducers in the inserts and, hence, the actual maximum difference in arrival time may occur as much as one-half the separation angle from one of the pairs of opposed transducers. Next, from this pair of transducers the pressure ratio of the reflected shock wave is measured for each one. This pressure ratio is the pressure immediately behind the point where the reflected shock is located, since in conical flow the pressure will continue to rise after the shock has reflected from the tube wall. Schematically this is presented in Fig. 21 which depicts a cone traveling

supersonically in a tube at an angle of attack with the nose tip translated and the notation applied for the analysis.

The measured tube wall pressure ratio immediately behind the reflected shock on the side of the cone with the largest effective angle of attack is denoted as P_u (upper wall), while that of the opposite side is denoted by P_l (lower wall in Fig. 21). The corresponding incident and reflected shock wave angles from the upper and lower walls are denoted by θ_{ui}, θ_{ur}, θ_{li}, and θ_{lr}, respectively. The diameter of the tube is denoted by D, the angle of attack of the cone is α, and the amount by which the tip of the nose cone is displaced from the centerline of the tube is Δy. From the measured pressure ratios P_u and P_l, the reflected and incident shock angles for both the upper and lower walls can be determined, as well as the amount by which the tip of the nose cone deviates from the centerline of the tube.

To determine the angle of attack of the cone, α, we must utilize the Taylor-Maccoll solution that relates the cone half-angle to the initial shock angle, θ_{ui} or θ_{li}, for a given freestream Mach number and ratio of specific heat of the gas. Both θ_{ui} and θ_{li} are used in the Taylor-Maccoll solution to determine separate effective cone half-angles. The resulting calculated cone half-angles are then subtracted from the known projectile nose cone half-angle, δ_c, to produce two estimates for the angle of attack of the cone.

It has been found (and will be shown later) that the angle of attack calculated using the upper wall variables (P_u and θ_{ui}) produced a better estimate of the angle of attack. This may be due to the breakdown of the Taylor-Maccoll assumption on the lower part of the cone as a result of viscous effects. Also, the accuracy of the recorded tube wall pressure may be higher at larger pressure ratios. The determination of Δy is more robust, since it relies on the oblique shock relations rather than the Taylor-Maccoll solution and the error is largely dependent upon reading the pressure ratios and arrival times of the initial shock from the experimental data.

EXPERIMENTAL RESULTS AND NUMERICAL SIMULATIONS

Ideal Three-Dimensional Flow Field: Previous studies have presented experimental data and numerical simulations that revealed the three-dimensional character of the flow field around the ram accelerator projectile induced by the presence of the projectile fins.[14,16] A three-dimensional, non-reacting Euler code was developed which revealed the qualitative nature of the ideal (not canted) three-dimensional flow field (including fins) and was instrumental in interpreting the experimental data.

The tube wall pressure distribution of one of these three-dimensional simulations is shown in Fig. 22 and is compared to previously published experimental data. The data are from an experiment which used a combustible gas ($2.7CH_4+2O_2+5.8N_2$) and hence the measured tube wall pressure may have been affected by the presence of combustion. In this figure the pressure distribution on the tube wall generated by the projectile passage is visualized by representing the pressure as the radial distance of a point away from the surface of a cylinder representing the ram accelerator tube wall. The different angular stations in the instrumented inserts correspond to the same angles on the hypothetical tube. The length of the tube represents time in the stationary (lab) reference frame or distance in the projectile (moving) reference frame (assuming steady flow). Another way to explain this visualization is as if the projectile were traveling through an infinitely thin, flexible tube that instantaneously deforms radially outward proportionally to the pressure on the tube wall. Data between angular stations were linearly interpolated. A projectile with the correct fin orientation with respect to the pressure surface is also shown for reference. The surface is cut along the centerline of both a channel (the space between adjacent fins) and a fin in this and all similar figures. The fin and channel shocks are more apparent in this format as compared to simple line plots. In Fig. 22 the major disparity between the numerical simulations and the experiment can be seen in the difference in the maximum pressure near where the fin leading surfaces first contact the tube wall.

Recently, experiments were performed with projectiles traveling in non-reacting mixtures in an attempt to study the non-reacting three-dimensional flow field around and to the rear of the projectile and to quantify the effects of combustion on and near the projectile. The mixtures were chosen to have nearly the same thermodynamic properties as the combustible mixtures. This was accomplished by simply replacing the oxygen directly with nitrogen, resulting in a mixture of $2.7CH_4+7.8N_2$. The projectiles were accelerated using a length of ram accelerator until they achieved the desired speed at a particular position along the facility. Then they made a transition into the equivalent non-reacting mixture, where they then passed through one of the HITS tube sections.

Line plots of the measured tube wall pressure from one such experiment are shown in Fig. 23. This experiment utilized a pair of instrumented tube inserts placed 4 m from the entrance of the ram accelerator. The projectile was accelerated by a 2 m long stage containing combustible gas at 28 atm and then it transitioned into a non-reacting section at the same initial pressure. The projectile passed through the inserts with a velocity of 1410 m/sec (Mach 3.9 or 81% of the CJ detonation speed of the equivalent reacting mixture) with an orientation such that fins passed over transducers 1, 5, 9, and 13. This results in the large pressure peak at the point where the projectile fins first contact the tube wall. Trace 2 is a flat line which resulted from a defective transducer.

Traces 3, 7, 11, and 15 are the tube wall pressure traces along the centers of the channels (the space between two adjacent fins). Shocks in the tube behind the projectile are also recognizable and seem to form a consistent pattern.

Figure 24 represents a visualization using the experimental pressure data of Fig. 23. As in Fig. 22, both the surface shading and radial distance from the tube wall are proportional to the pressure. Figure 24 can be directly compared to the numerical simulation of Fig. 22, since the Mach numbers are quite close. The computed pressure ratios at the leading edge of the fins of the numerical simulation agree well with the experiment which used the non-reacting gas. It can then be concluded that the large pressure ratios found in the experimental data of Fig. 22 are due to combustion at the stagnation point, where the fin first meets the tube wall. This demonstrates that even at low subdetonative velocities there is likely combustion occurring on these parts of the projectile.

At higher velocities the ideal non-reacting flow fields of previous numerical simulations generally exhibit similar structure to those of lower velocities, but with the expected changes due to the increase in projectile Mach number. The experimental data, however, do not follow this same trend. It is routinely observed (at least for single stage experiments using a single gas mixture) that as the projectile increases in Mach number, the effect of the fins on the measured tube wall pressure tends to decrease and the large pressure rise due to the fin leading edge generally completely disappears.[14,16] This is thought to be due to the reduction of the fin height due to frictional wear and/or erosion by hot gas.

Experiments Exhibiting Projectile Canting: The previously described procedure for determining the angle of attack and displacement of the nose cone was applied to the experimental data shown in Fig. 20b. The maximum difference in arrival time of the initial shock at the tube wall was 19 μsec. With a projectile velocity of 1560 m/sec this is equivalent to a difference in arrival position of the initial shock at the tube wall, Δx, of approximately 30 mm. The measured pressure ratios at the tube wall are $5.5 \le P_u \le 6$ and $1.5 \le P_l \le 2$ which give incident shock angles of $20.7^\circ \le \theta_{ui} \le 21.2^\circ$ and $14.8^\circ \le \theta_{li} \le 15.8^\circ$, respectively. These shock angles then give the amount of the nose tip translation as $7.2 \le \Delta y \le 8.5$ mm. The uncertainty in the estimate for Δy is approximately ±0.6 mm. The ranges in uncertainty are derived from the inaccuracies in reading the pressure data and determining exactly when the shock from the nose cone first contacts the tube wall and do not take into account the uncertainty in knowing the plane of canting/translation. The corresponding effective cone half-angles given by the Taylor-Maccoll solution using θ_{ui} and θ_{li} are $14.6^\circ \le \delta_u \le 15.2^\circ$ and $6.7^\circ \le \delta_l \le 8.5^\circ$, respectively. Thus, the corresponding effective cone angles of attack are $4.6^\circ \le \delta_u - \delta_c \le 5.2^\circ$ and $-1.5^\circ \le \delta_l - \delta_c \le -3.3^\circ$, respectively.

There is a considerable difference in the calculated angle of attack of the cone depending on whether P_u or P_l is used in the calculation. The more accurate value is probably P_u, since the amount of error involved in reading it from the experimental data is much less, and viscous effects on the side of the cone with the reduced angle of attack are thought to be significant.

In an effort to study the non-reacting flow field at superdetonative velocities, an experiment was performed with a non-reacting mixture ($2.7CH_4+7.8N_2$) and the projectile was accelerated using 6 m of reacting mixture, both at 33 atm initial pressure. The projectile velocity was 1920 m/sec (Mach 5.3) or 110% of the CJ speed of the equivalent reacting gas as it passed through a pair of inserts. The resulting 16 line plots are shown in Fig. 25a. Figure 25b shows the same data as Fig. 25a, but with the time scale expanded to accentuate the variation in the arrival time of the initial shock wave. It is readily apparent that the projectile is canted in the tube since the arrival time of the shock generated by the nose cone and the magnitude of the reflected shock vary considerably from trace 3 to trace 11. Also, less apparent, is the non-uniformity or lack of symmetry of the shocks behind the projectile, as compared to those which were shown in Fig. 20b. There also are no distinct pressure rises corresponding to the leading edges of the fins. From the azimuthal differences in arrival time and strength of the initial conical shock it was determined that the projectile fins passed over transducers 1 and 4. Hence, the projectile was translated and canted as shown in the orientation diagram of Fig. 25.

The maximum difference in arrival time of the initial shock at the tube wall was measured to be 13 μsec. At a velocity of 1920 m/sec this is equivalent to a Δx of approximately 25 mm. The measured pressure ratios are $6.5 \le P_u \le 7$ and $3 \le P_l \le 3.5$ which give incident shock angles of $17.4^\circ \le \theta_{ui} \le 17.8^\circ$ and $14.1^\circ \le \theta_{li} \le 14.7^\circ$, respectively. These shock angles then indicate a nose tip translation as $4.5 \le \Delta y \le 6.1$ mm. The corresponding effective cone angles given by the Taylor-Maccoll solution using θ_{ui} and θ_{li} are $12.7^\circ \le \delta_u \le 13.1^\circ$ and $8.8^\circ \le \delta_l \le 9.5^\circ$, respectively. We see that the corresponding effective cone angles of attack are $2.7^\circ \le \delta_u - \delta_c \le 3.1^\circ$ and $-0.5^\circ \le \delta_l - \delta_c \le -1.2^\circ$, respectively. Again there is a considerable difference in the calculated angle of attack of the cone depending on whether P_u or P_l is used in the calculation.

Numerical Simulation of Canted Projectiles: The experiments indicate that projectiles may be canted while they are accelerating or "coasting" through the pressurized gases in the tube. To validate the data reduction technique for estimating the projectile orientation and to investigate the flow field of a canted projectile, numerical simulations of the non-ideal (canted) flow fields were carried out.

The numerical simulations were accomplished with a three-dimensional non-reacting, inviscid CFD code based on the finite volume method. It assumes an ideal, calorically perfect gas with no chemical reactions. The integral forms of the Euler equations are solved to find the spatially averaged state of the flow variables at the center of a control volume or computational cell (a cell centered scheme). The Flux Vector Splitting method of Van Leer[34] along with the MUSCL differencing[35] (differencing followed by flux splitting) are used to calculate the fluxes at cell boundaries.

The general geometry used to simulate a canted projectile is shown in Fig. 26 and represents one-half of the flow field for a three-dimensional axisymmetric projectile without fins. No projectile fins are modeled since only the arrival time and magnitude of the initial reflection of the shock generated by the nose cone are desired and not the influence of the fins, which occurs farther to the rear of the projectile. As noted earlier, it is assumed that the projectile is both rotated and translated in a plane of symmetry which contains the axis of the tube. Thus, only one-half of the three-dimensional flow field need be solved (although the code is capable of simulating the full flow field if necessary).

To determine how the pressure ratio of the initial reflected shock wave varies over the tube wall for a canted projectile, two test cases were simulated, whereby the projectile was only simply translated or the projectile was fully canted (translated and rotated about the nose tip). For both cases the gas has the non-reacting thermodynamic properties of the mixture $2.7CH_4+2O_2+5.8N_2$ and a Mach number of 4.0 (1450 m/sec). Figure 27a shows the line plots of the calculated pressure along the upper and lower tube walls (directly opposite each other) for a projectile which is translated by 2 mm toward the bottom of the tube and has a zero angle of attack. A grid consisting of 149x49x49 cells was used (axial, radial, and azimuthal directions). The calculated arrival points of the initial conical shock differ between the upper and lower portions of the tube wall, but the initial magnitude of the reflections are identical, which is not what has been observed in the experiments. The case of a canted projectile is shown in Fig. 27b for a nose cone with an angle of attack of 4° and the nose tip translated by 5 mm from the centerline of the tube. Note the differences in the arrival position of the initial shock and the initial magnitude of the reflected shock. These line plots are qualitatively similar to the experimental data previously thought to be caused by a canted projectile.

With the angle of attack and nose tip translation estimated from the experimental data, the resulting three-dimensional flow field about the projectile nose cone and initial part of the projectile body can be investigated. In order to utilize the finest computational grid possible in the region of interest, only the first two-thirds of an axisymmetric canted projectile is simulated. The general

geometry for the remainder of the calculations is shown in Fig. 28. Some grid clustering is used near the tip of the nose cone to help resolve the conical shock in this region.

The first experimental data numerically simulated were those of Fig. 20b, in which the projectile is traveling at 1560 m/sec (Mach 4.3). It was found that numerical simulations using the angle of attack calculated with P_u gave the best match to the data from the experiment. The values used for the numerical simulation were $\alpha = 4.5^\circ$ and $\Delta y = 7.5$ mm. The line plots of the calculated pressure distributions corresponding to the upper and lower walls are shown in Fig. 29 and are compared to the experimental data. Figure 30 shows the computed tube wall pressure distribution as a three-dimensional surface plot that reveals the variation in the arrival position and magnitude of the reflected shock over the tube wall. The differences in arrival times of the conical shock wave on opposite sides of the tube agree well, while the magnitudes of the pressure pulses are close, but not identical. This is the best simulation possible without a prohibitive number of numerical iterations on the values of α and Δy. It must be remembered that the transducers used in Fig. 20b may not have been exactly in the position where the maximum or minimum reflected shock pressure occurred or where the earliest or latest arrival time of the initial shock occurred (i.e. they may not have been exactly in the plane of symmetry of the canted projectile). In addition there are possible errors in the calibration factors for each probe. It has also been found that there is a dynamic error in the measured pressure which results in overshoots of 10 to 30% when the probes are subjected to a step change in pressure. It is this error that accounts for the bulk of the discrepancy between the simulation and experiment. With these limitations it is surprising how well the simulation matches the experiment.

The second experiment numerically simulated was that of Fig. 25, in which the projectile was traveling at 1920 m/sec (Mach 5.3) in a non-reacting mixture. It was found that the angle of attack calculated using P_u again gave the best match to the data from the experiment. The values used for the numerical simulation were $\alpha = 3^\circ$ and $\Delta y = 6.5$ mm. The line plots of the calculated pressure distributions corresponding to the upper and lower walls are shown in Fig. 31 and are compared to the experimental data. Again, the differences in arrival times agree well, while the magnitudes of the shock waves are not as well simulated, but can be adequately accounted for by the dynamic error in the measured pressure. Figure 32 shows the computed tube wall pressure distribution and reveals the variation in the arrival position and magnitude of the reflected shock on the tube wall.

UNSTART PHENOMENA

The canting of a projectile at subdetonative and transdetonative velocities is expected to reduce its acceleration and its ability to successfully accomplish high velocity mixture transitions. A canted projectile has a higher drag and a lower diffuser efficiency than a centered projectile, although there has been no experimental attempt to establish a correlation between canting and acceleration performance. It also has been found that the incidence of transition failures increases with projectile velocity and may thus be related to the increase in projectile fin wear, which inevitably occurs as the projectile travels through the tube.

At superdetonative velocities the effects of projectile canting are thought to contribute to the unstart phenomenon that limits the projectile velocity to ~120% CJ detonation speed in the present mixture. Axisymmetric Navier-Stokes (N-S) simulations using finite rate kinetics fail to predict an unstart at significantly higher superdetonative velocities,[31] suggesting that centered projectiles may be capable of being accelerated to much higher velocities than are currently achieved in practice. In fact, two-dimensional N-S finite rate kinetics simulations of a 2-D planar projectile will produce an unstart only if the projectile is canted. Fin effects on a canted projectile for reacting flow are not known at this time. For multiple stage experiments, for example, projectiles fail to reliably reach velocities significantly greater than the CJ speed in the stages subsequent to the first, whereas in single stages they routinely exceed the CJ speed.

The unstart phenomenon in a single stage mixture of $2.7CH_4+2O_2+5.8N_2$ was investigated by placing a pair of instrumented tube "inserts" near the point in the test section where a projectile would reach approximately 120% of the CJ detonation speed of the mixture. Several experiments were required, since the exact location where an unstart would take place could not be accurately known *a priori* and had to be iterated upon by adjusting the initial tube fill pressure. Previously published data[16] showing the state of the flow field immediately prior to an unstart (within approximately 0.5 m) indicate that the reflected shock wave is being augmented in magnitude by shock-induced combustion in the bulk flow (as opposed to boundary layer combustion). This shock-induced combustion phenomenon has been reproduced in N-S, finite rate kinetics, axisymmetric calculations[32] and the resulting tube wall pressure profiles compare quite favorably with experiment.

The tube wall pressure distribution during the unstart of the projectile was successfully recorded in one of the experiments. The 16 line plots of the tube wall pressure measured using a pair of tube inserts from this experiment are shown in Fig. 33. The projectile was traveling at 2060 m/sec (Mach 5.7) or 118% of the CJ detonation speed of the mixture. Most noticeable is

the very strong shock located at the throat of the projectile. Also note that the pressure rise from the initial shock generated by the nose cone is still recognizable. The strong shock (probably normal) is moving forward through the diffuser and is therefore traveling at a speed greater than that of the projectile. The pressure decreases immediately behind the shock due to the increase in the velocity of the subsonic flow to a choke point near the projectile throat. It is this choking of the flow somewhere on the projectile body that disgorges the shock ahead of the projectile. The largest observed difference in arrival time of the initial shock was approximately 5 μsec, equivalent to a spatial variation, Δx, of 10 mm.

A line plot of the tube wall pressure from one of the transducers in Fig. 33 is shown with the EM and pressure data from an instrument station 22 cm directly upstream (opposite the direction of projectile motion) in Fig. 34. This comparison gives a sense of the development of the large amplitude shock wave at the projectile throat, since at the upstream station the wave is of smaller amplitude, the initial shock generated by the nose cone is more distinct, and the overall pressure distribution is closer to what would be expected at lower velocities. The EM data locates the projectile relative to the pressure data at the upstream instrument station and thus the projectile's position with respect to the pressure data from the inserts is inferred.

SUMMARY OF PROJECTILE CANTING EFFECTS

The previously described experiments demonstrate that projectile canting occurs at sub- and superdetonative velocities and in reacting and non-reacting mixtures. Projectile canting has in fact been observed in all velocities regimes. The canted projectiles that were first accelerated with a section of reacting gas and then injected into a non-reacting mixture most probably were canted during their acceleration and remained so after transition into the non-reacting gas. It is not known if the projectiles remain canted to one side of the tube during acceleration, ballot from one side to the other or precess about the tube axis.

The phenomena causing projectile canting have not been definitively determined to date, but several mechanisms have been postulated. The projectile is likely to cant as a resuit of its fin geometry being altered by mechanisms such as bending and frictional wear due to large, aerodynamically generated forces and moments and/or melting and erosion by hot gases. In its present design the projectile is aerodynamically unstable while accelerating in the tube, because its center of mass is typically ahead of the center of pressure.* This instability may be the root cause

* It should be noted that the stability criterion under acceleration is exactly the reverse of that for a coasting projectile, which is stable when the center of mass is ahead of the center of pressure.

of canting. There has also been experimental evidence that there may be asymmetric combustion phenomena occurring which contribute to projectile canting by generating excessive side forces.[16]

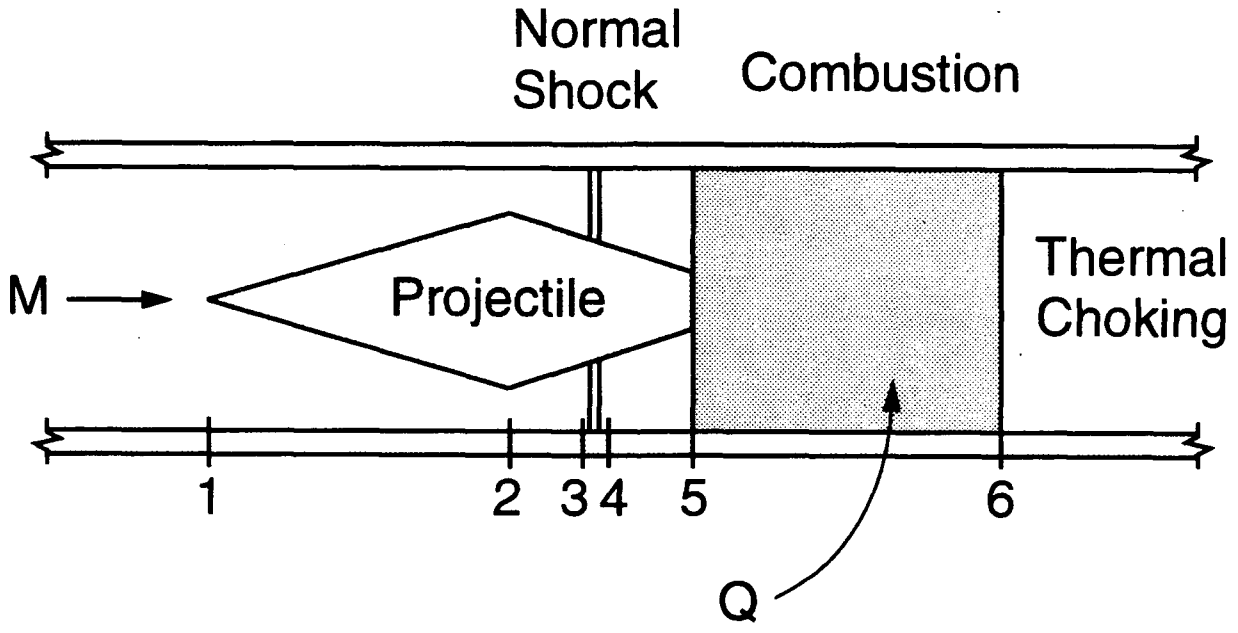

Fig. 7 One-dimensional, quasi-steady model of the thermally choked ram accelerator flow field.

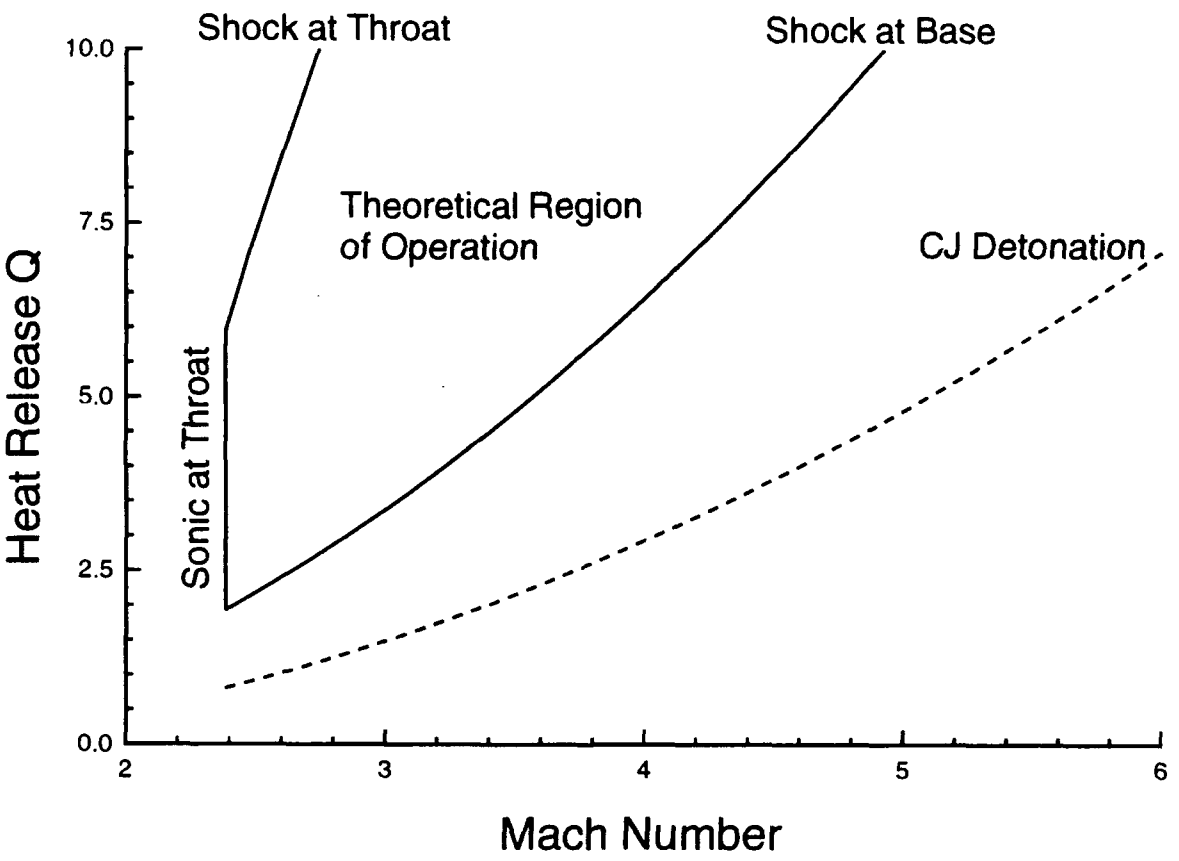

Fig. 8 Operational envelope of the ram accelerator as predicted by one-dimensional theory.

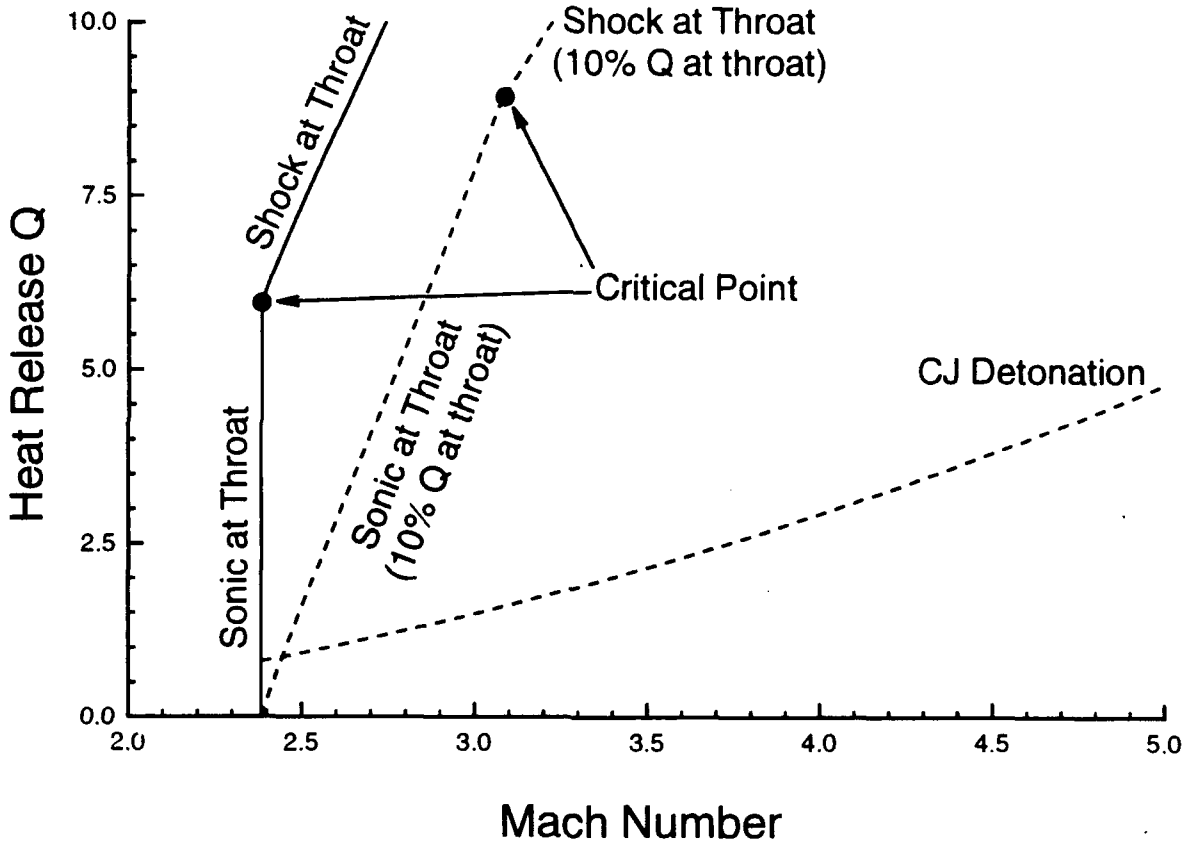

Fig. 9 The effect on the operational envelope of a 10% release of the total Q at the throat. The unstart mechanism changes at the critical point.

(a)

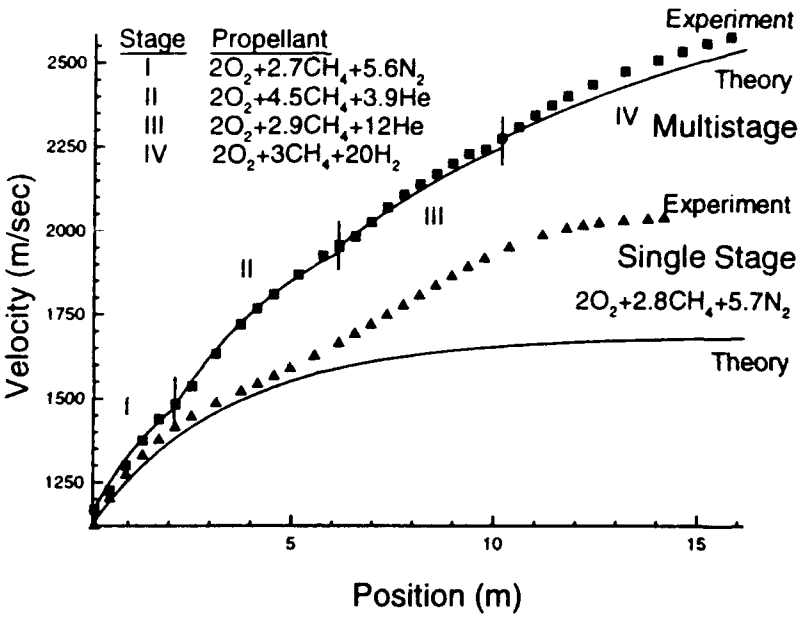

(b)

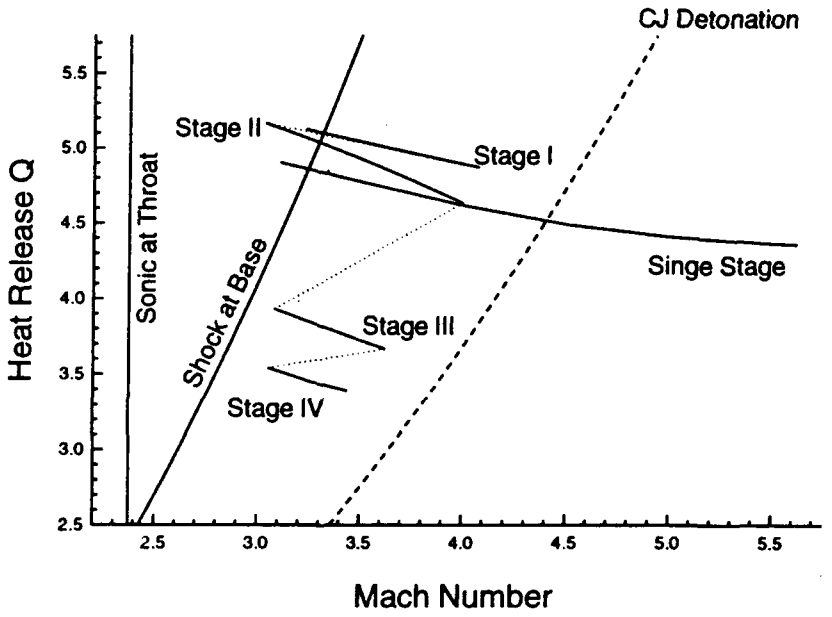

Fig. 10 Two experimental firings of the ram accelerator:

a) Velocity-distance profiles.
b) Comparison of experiments with the theoretical operating limits.

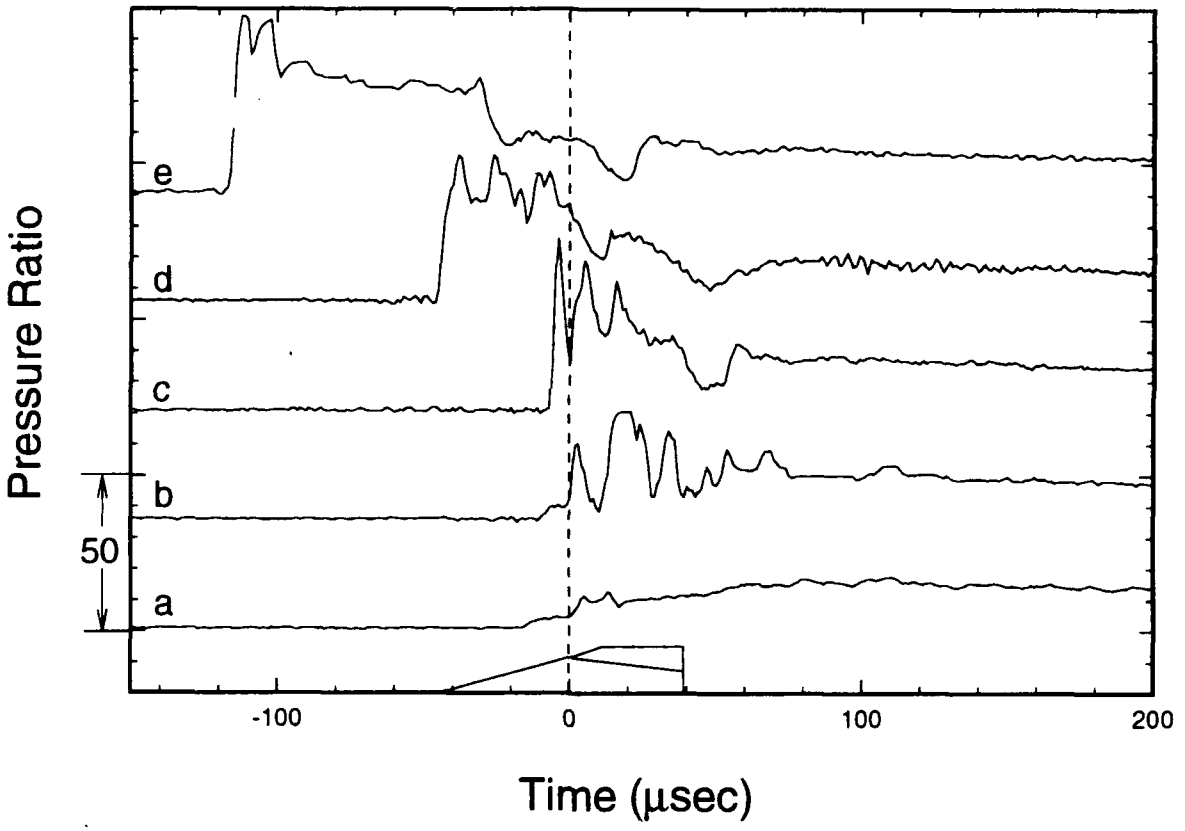

Fig. 11 The evolution of an unstart as seen by tube wall mounted pressure transducers. Time is measured relative to the passing of the projectile throat. Each probe is approximately 40 cm apart. The projectile is traveling at Mach 5.

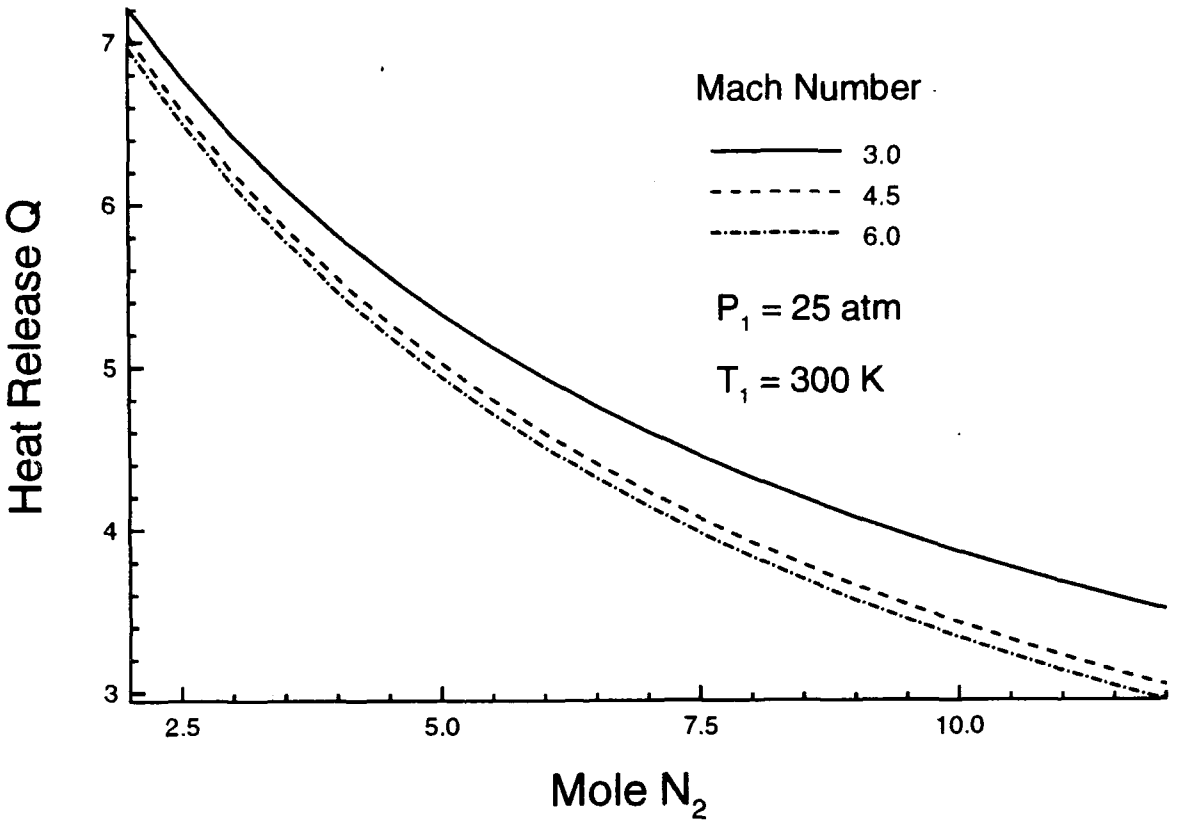

Fig. 12 Thermally choked heat release as a function of nitrogen dilution for $2.8CH_4+2O_2+XN_2$.

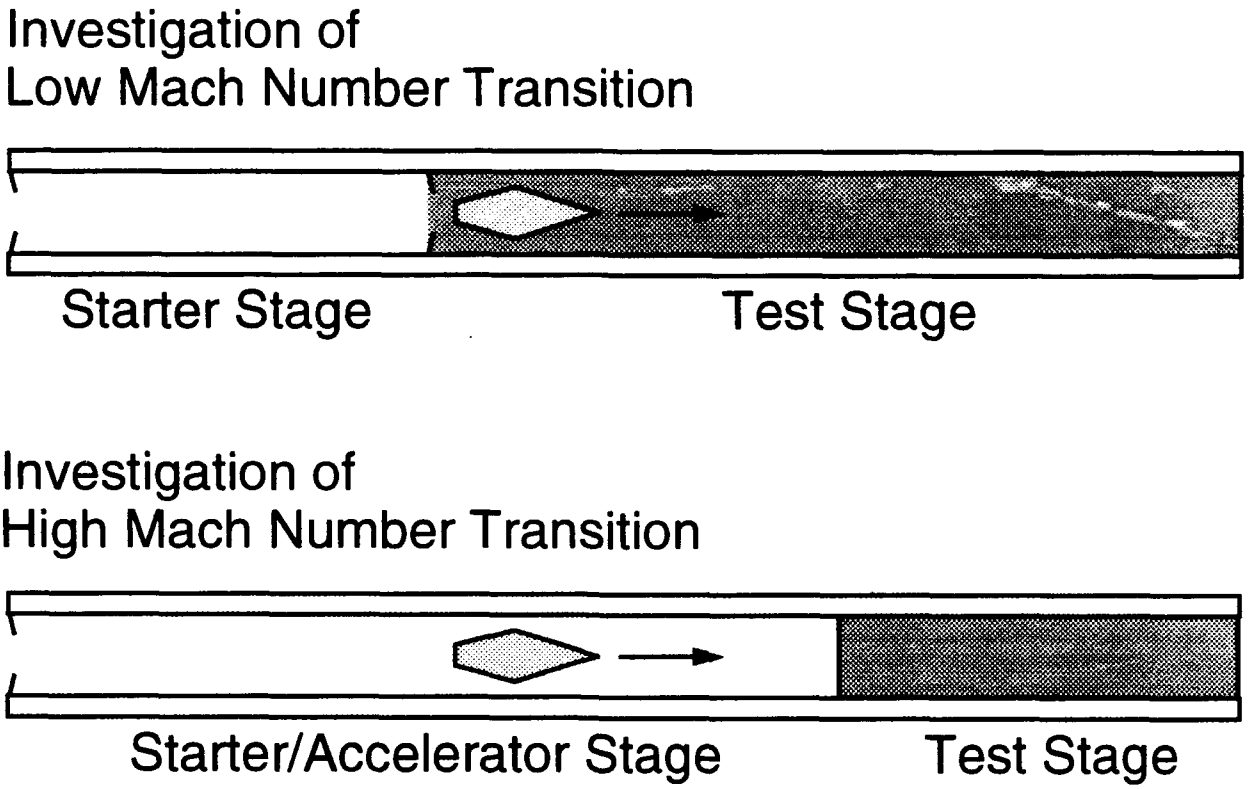

Fig. 13 Experimental configurations used to investigate limits to ram accelerator operation.

(a)

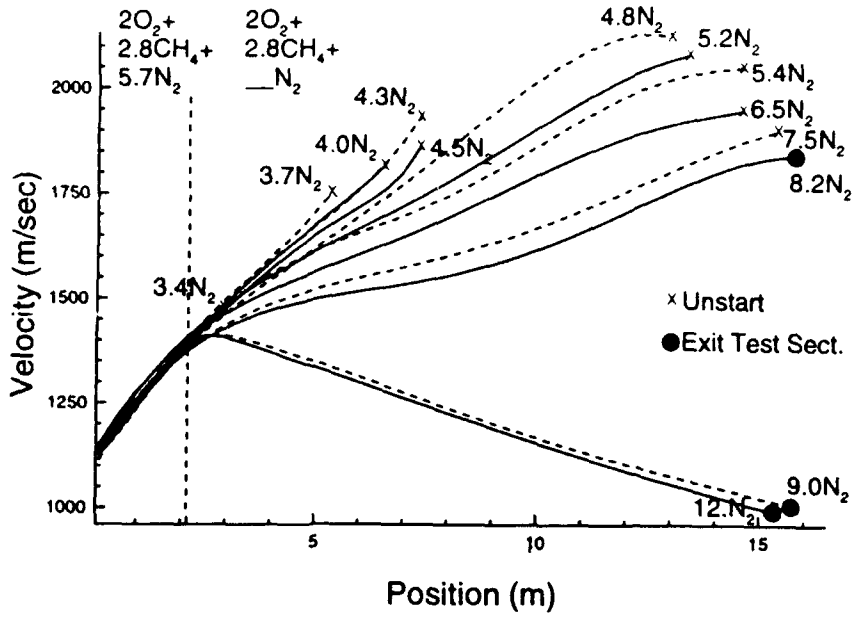

(b)

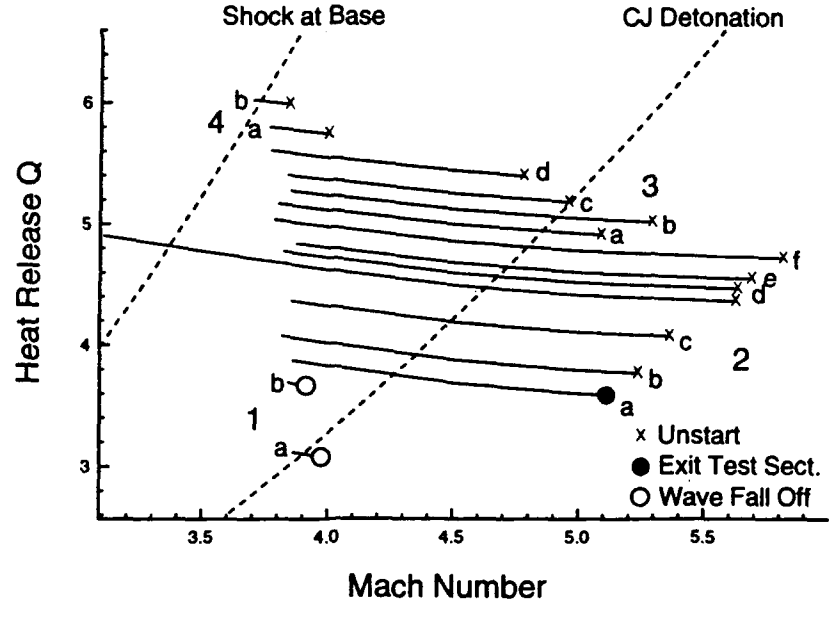

Fig. 14 Low Mach number (M = 3.8) transition experiments:

a) Velocity-distance profiles.
b) Comparison of experiments with the theoretical operating limits.

(a)

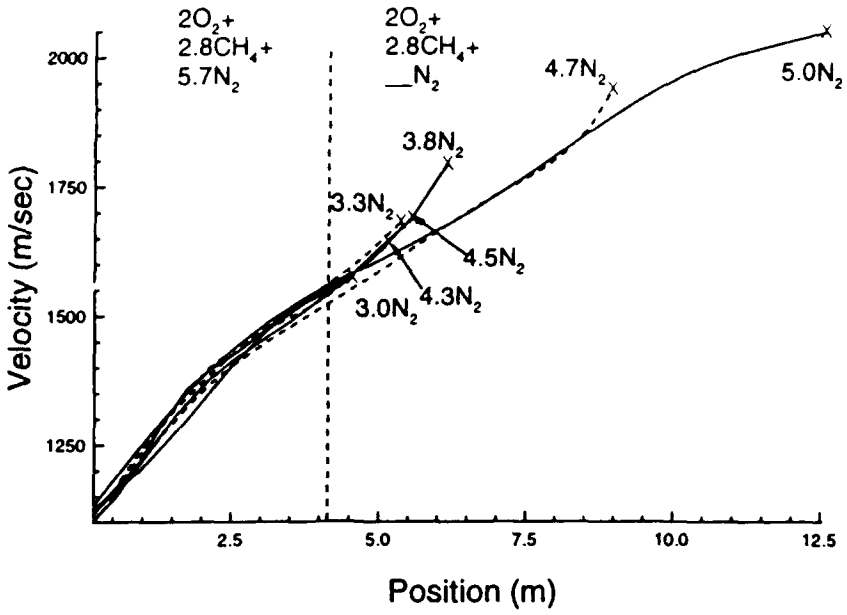

(b)

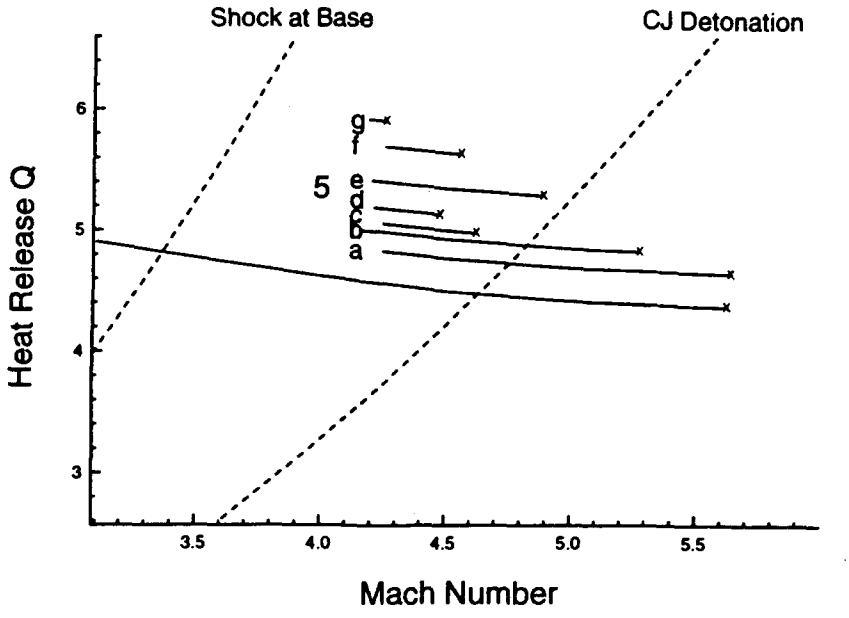

Fig. 15 High Mach number (M = 4.2) transition experiments:

a) Velocity-distance profiles.
b) Comparison of experiments with the theoretical operating limits.

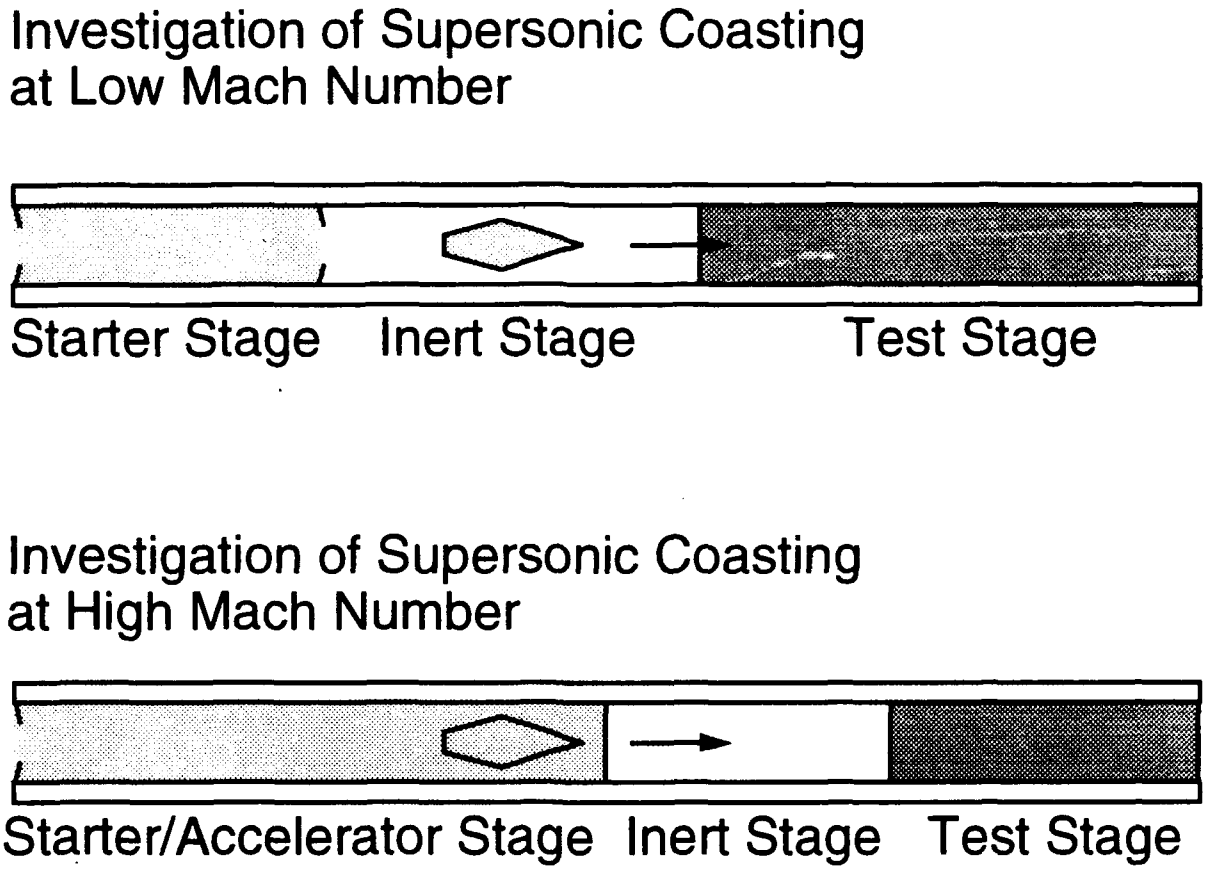

Fig. 16 Schematic of experiments to determine limits to the projectile's ability to supersonically coast through a combustible mixture.

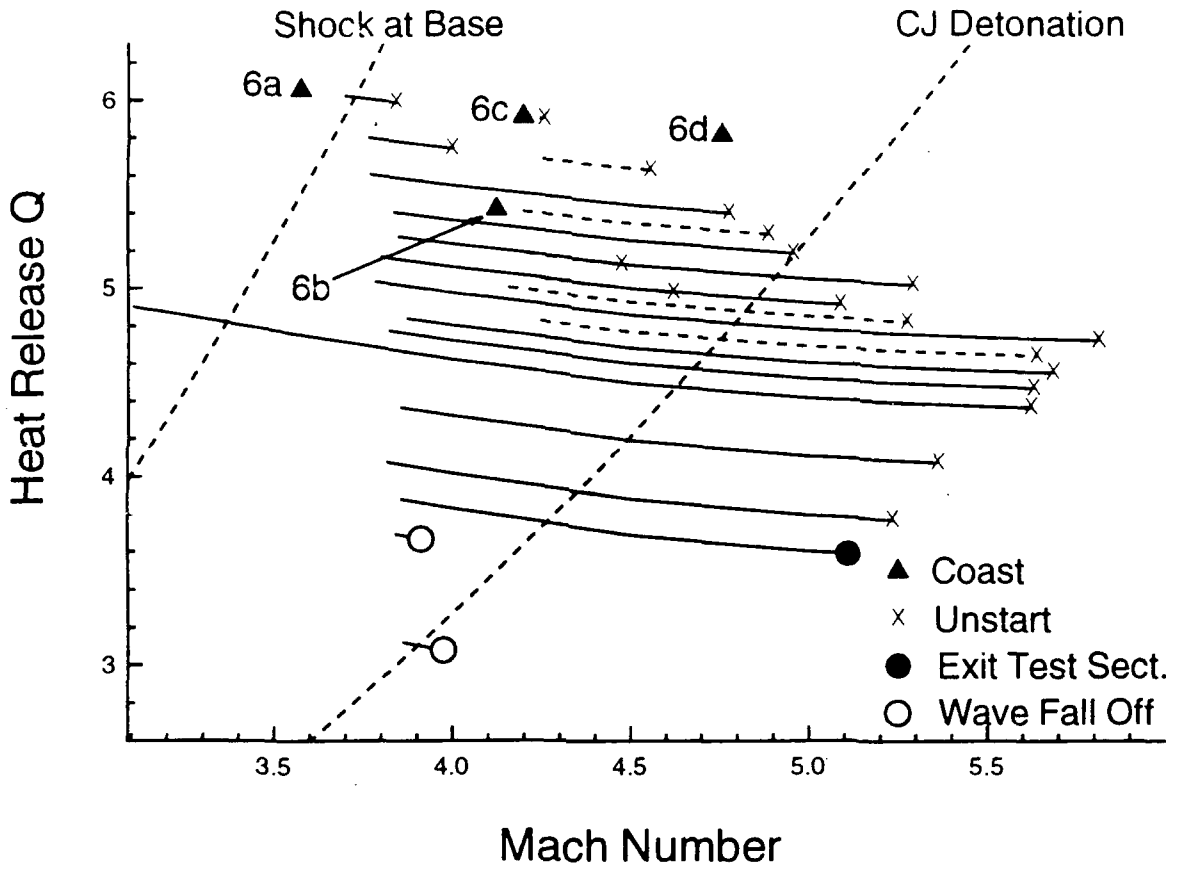

Fig. 17 Observed limits to ram accelerator operation. The triangles indicate experiments in which the projectile successfully coasted several meters in a mixture without unstarting. Dashed lines represent the higher Mach number transition experiments (cf. Fig. 15).

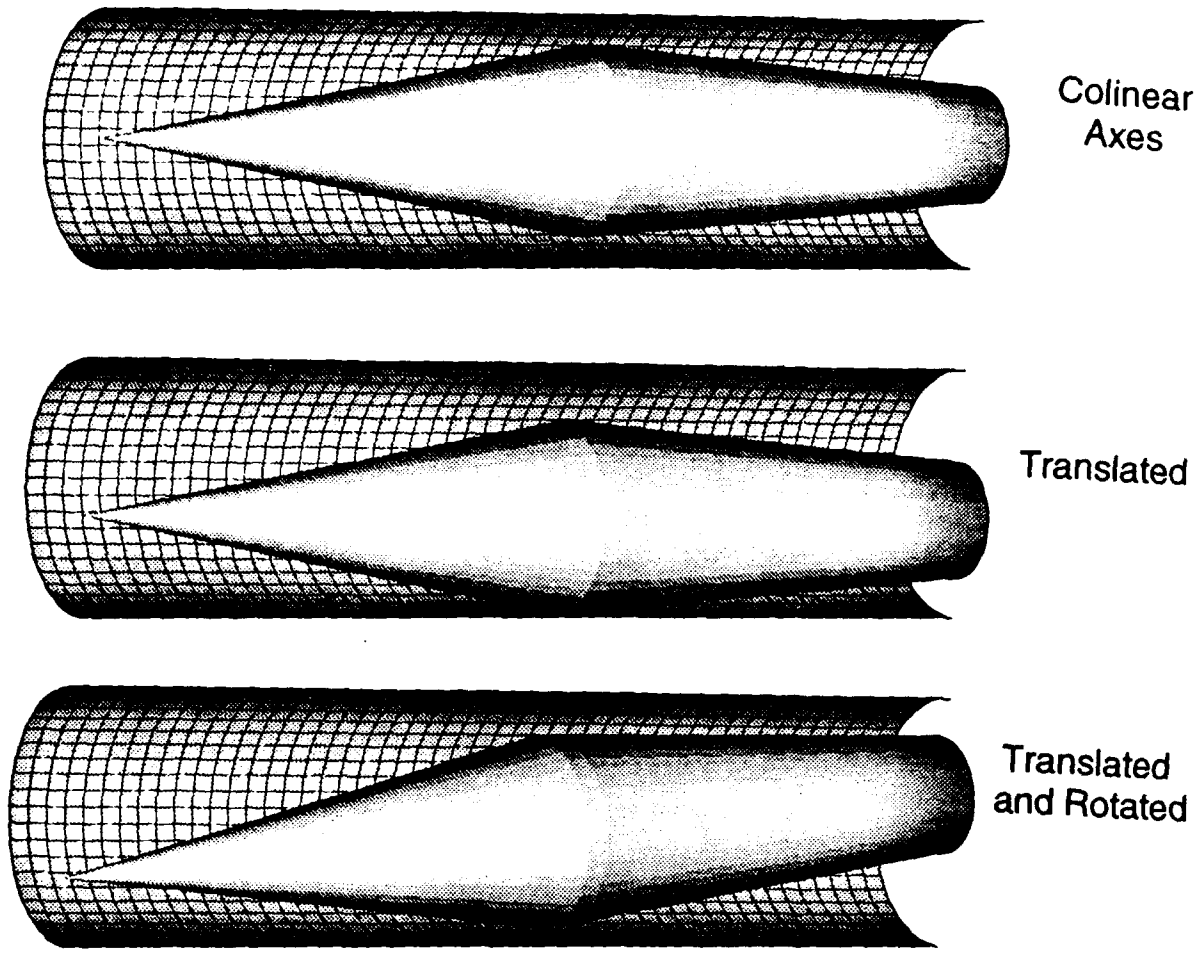

Fig. 18 Three possible positions of a projectile relative to the tube wall.

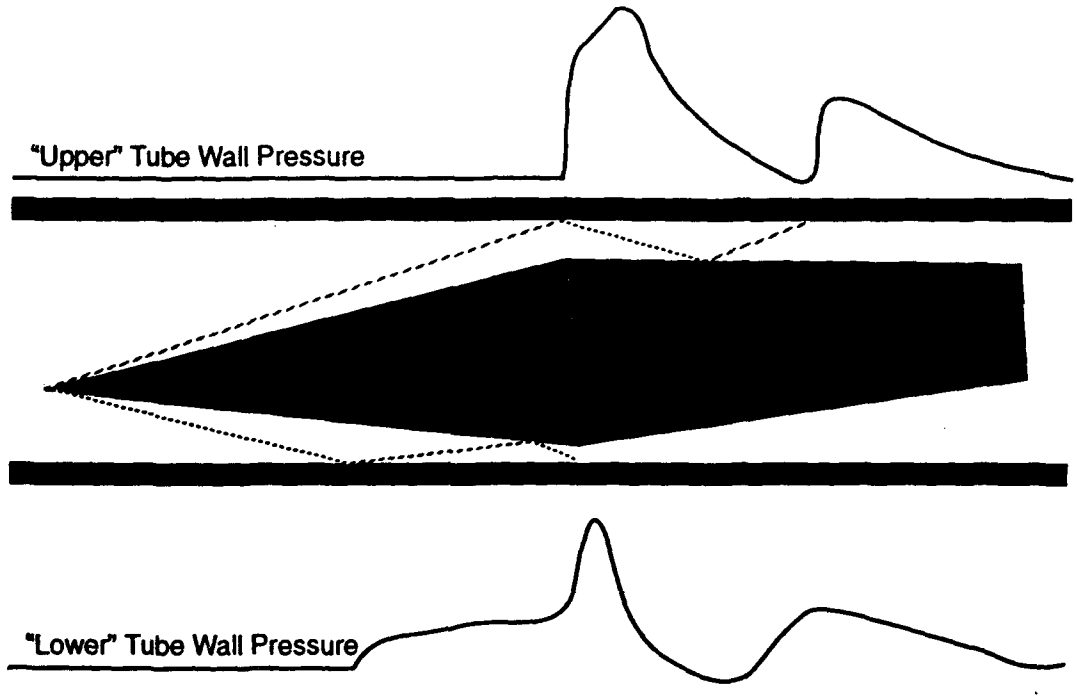

Fig. 19 Illustration of the differences in arrival time of the initial conical shock and the pressure magnitude after its reflection at the opposing sides of a tube for a canted projectile.

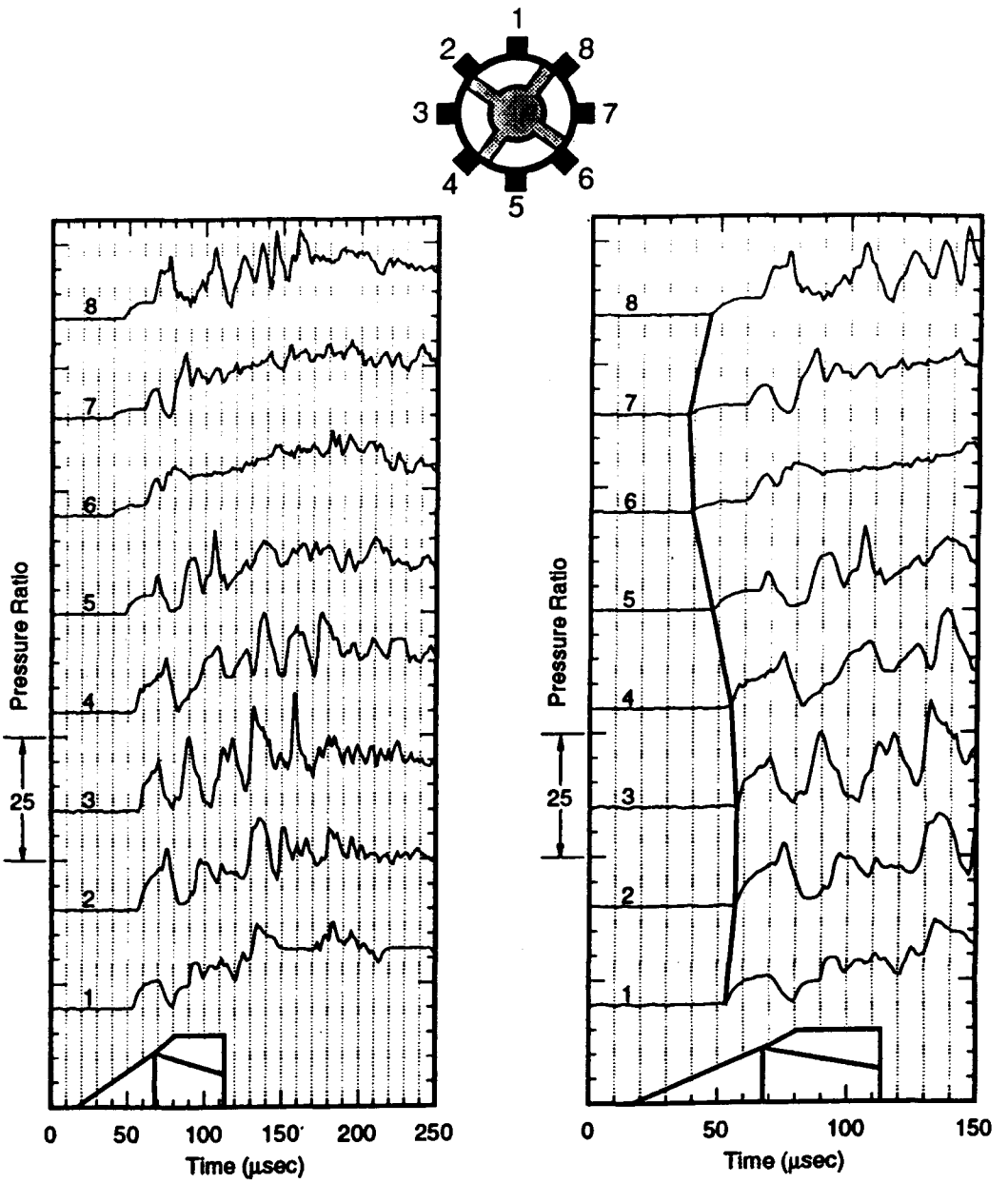

Fig. 20 Tube wall pressure traces from HITS data for a canted projectile traveling at 1560 m/sec (Mach 4.3) or 89% CJ speed. Reacting propellant mixture is $2.7CH_4+2O_2+5.8N_2$.

a) Pressure ratio vs. time for data window corresponding to 2.5 projectile lengths.
b) Expanded time scale to accentuate the difference in arrival time of conical shock.

Taylor-Maccoll Solution:

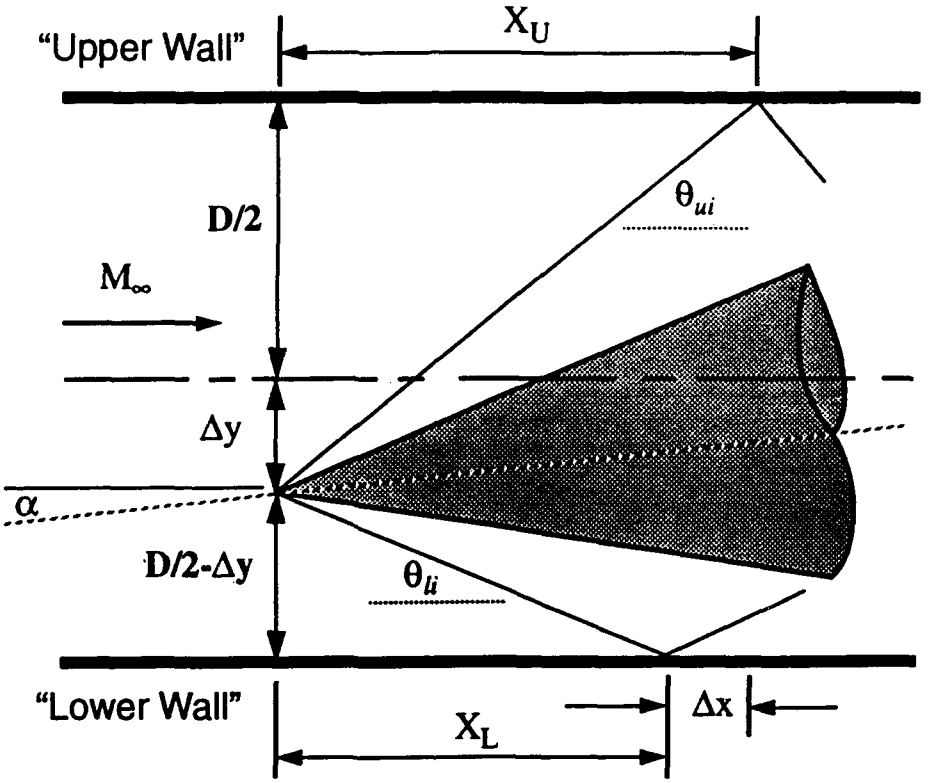

Fig. 21 Notation for determining location of nose tip.

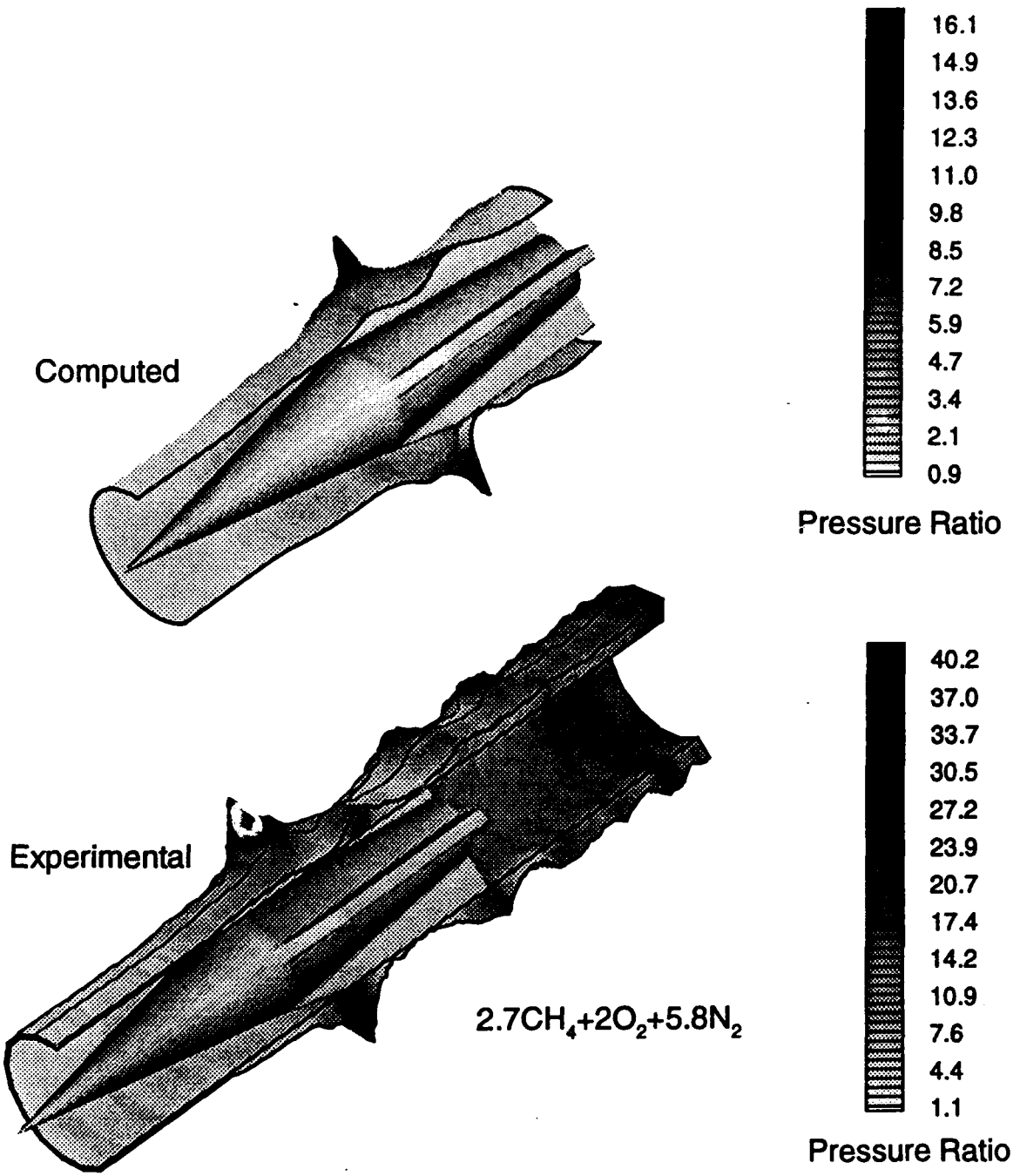

Fig. 22 Comparison of tube wall pressure from experiment (bottom) in reactive mixture to calculated (top) for same gas without reactions. Projectile velocity is 1440 m/sec (Mach 4) or 82% CJ speed. Pressure proportional to both shading and radial distance.

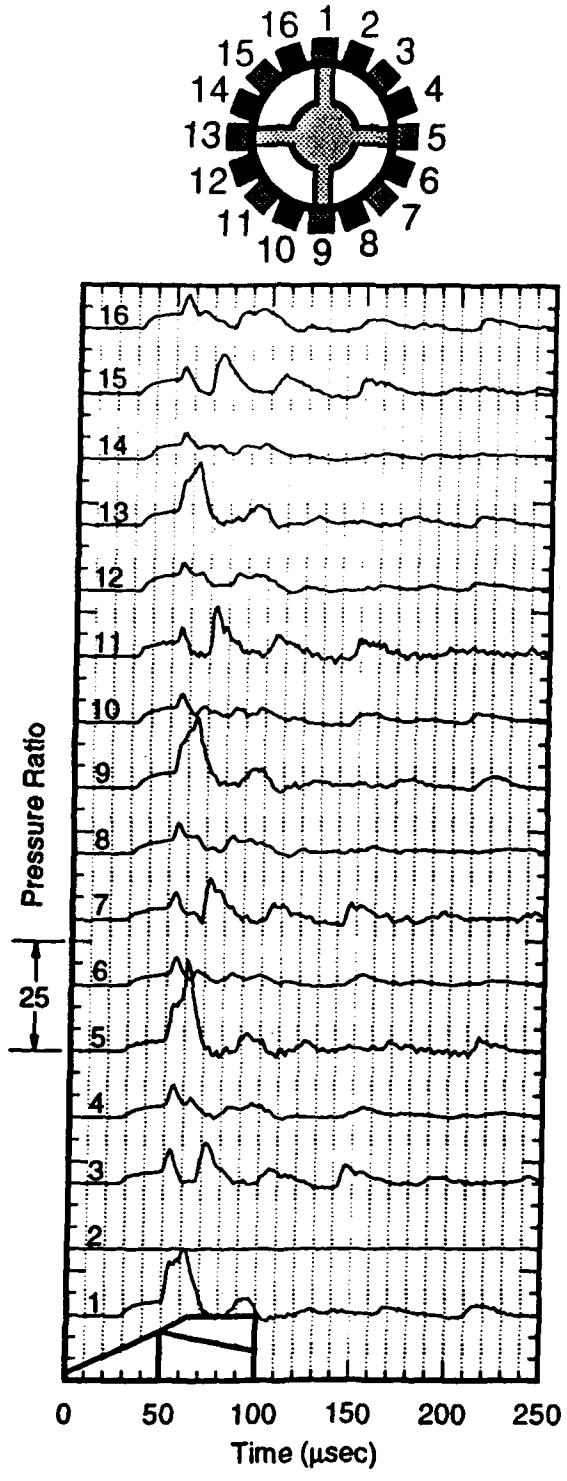

Fig. 23 Tube wall pressure traces from experiment in a non-reacting mixture of $2.7CH_4+7.8N_2$. Projectile velocity is 1410 m/sec (Mach 3.9) or 81% CJ speed of the equivalent reacting mixture.

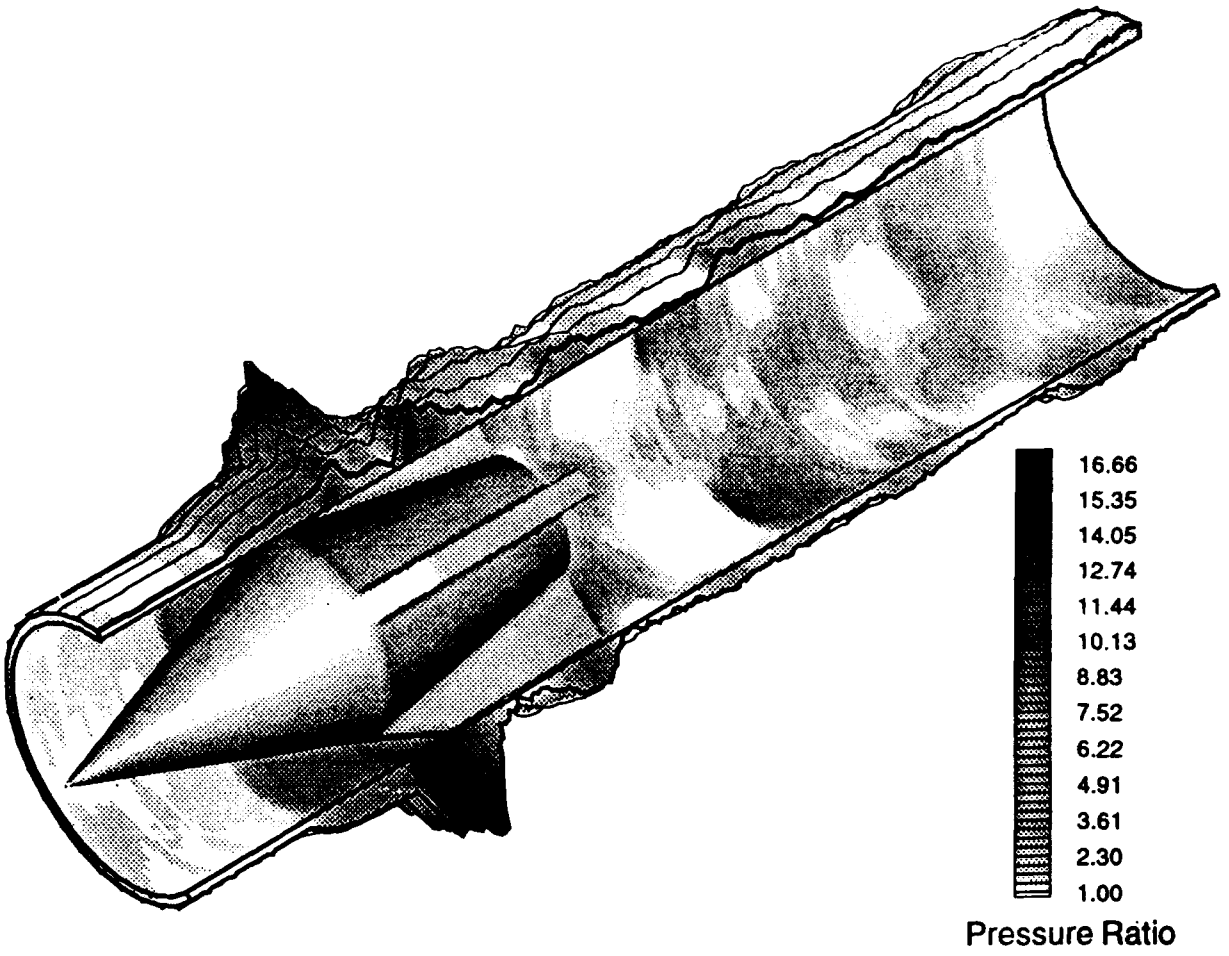

Fig. 24 Representation of tube wall pressure distribution determined from experimental data presented in Fig. 23. Projectile shown for fin orientation and scale.

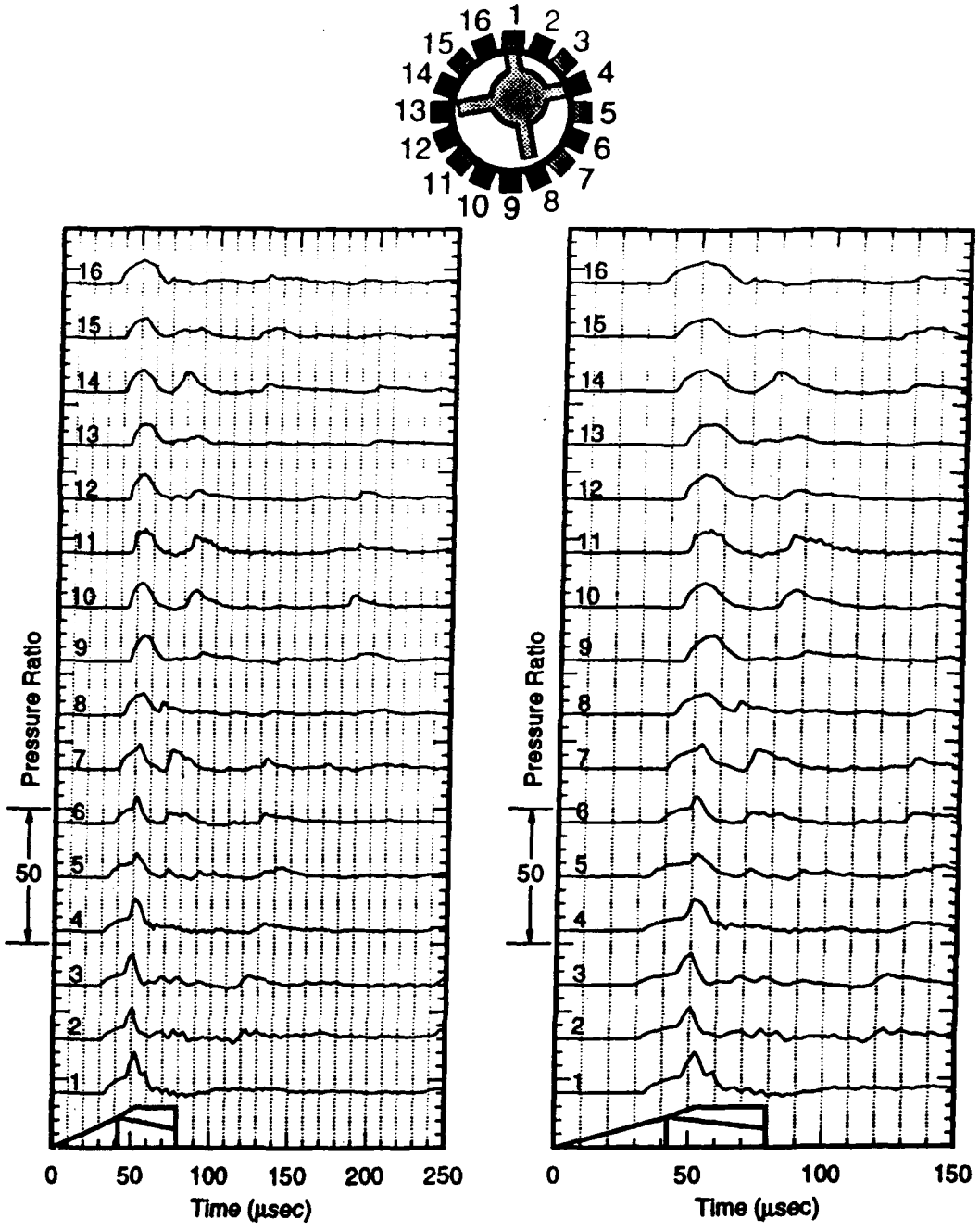

Fig. 25 Tube wall pressure traces from HITS data for a canted projectile traveling at 1920 m/sec (Mach 5.3) or 110% CJ speed. Non-reacting propellant mixture is $2.7CH_4+7.8N_2$.

a) Pressure ratio vs. time for data window corresponding to 3 projectile lengths.
b) Expanded time scale to accentuate the difference in arrival time of conical shock.

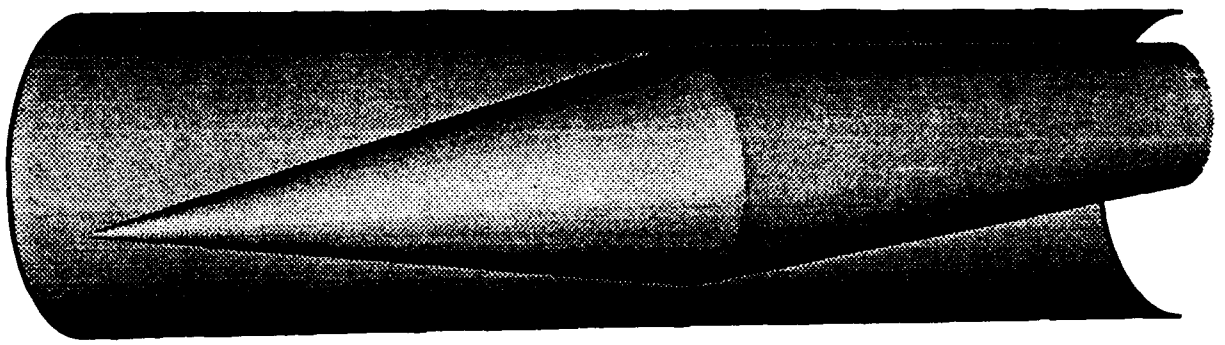

Fig. 26 General geometry of a canted, axisymmetric, three-dimensional projectile used in the numerical simulations. One-half of the full tube is numerically simulated by assuming a plane of symmetry. The computational grid is 150x50x50 in the axial, radial, and azimuthal directions respectively.

(a)

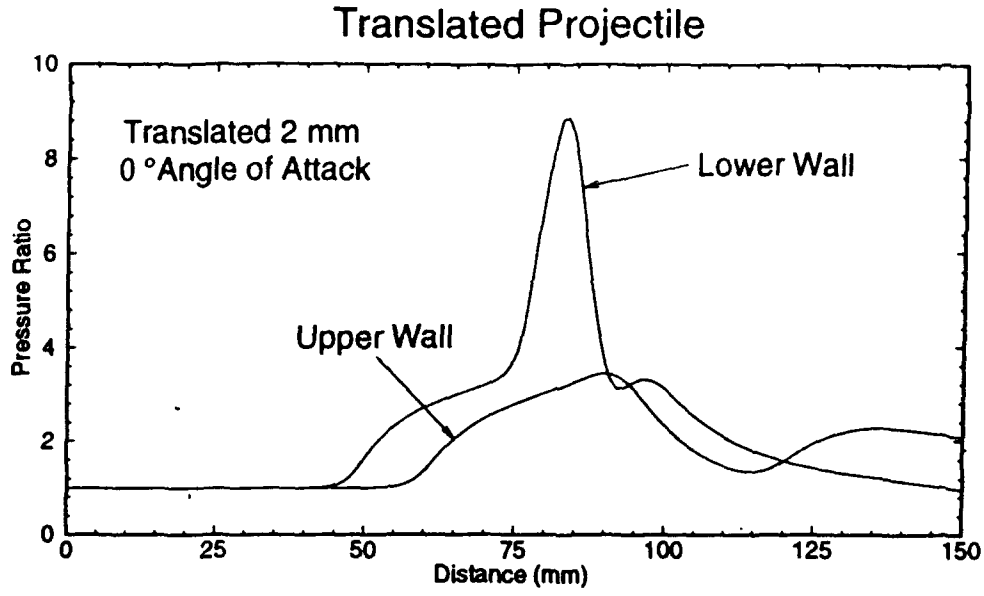

(b)

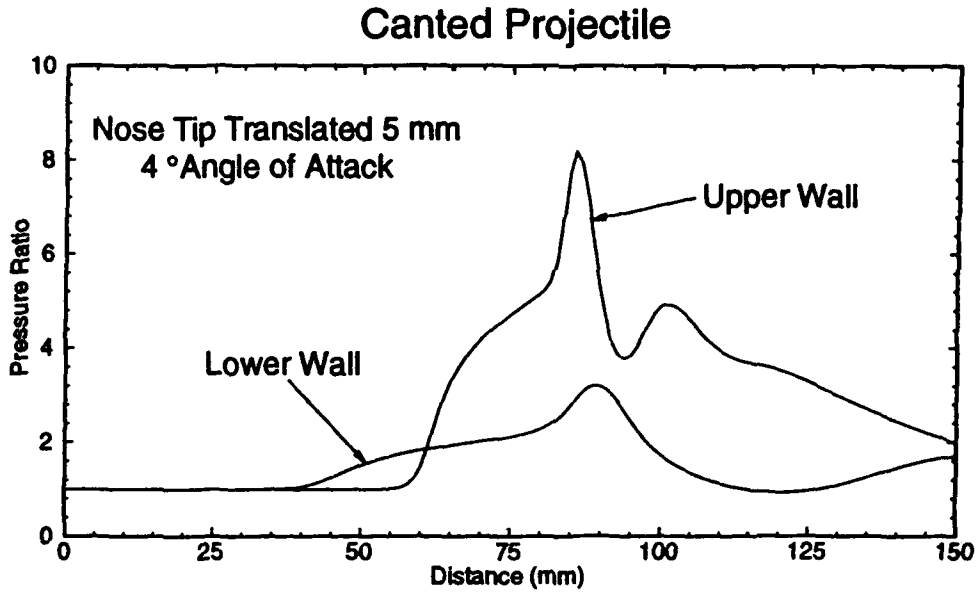

Fig. 27 Non-reacting calculations of upper and lower tube wall pressure ratio for an axisymmetric projectile traveling at 1450 m/sec (Mach 4.0) or 83% CJ speed in $2.7CH_4+2O_2+5.8N_2$.

a) Angle of attack is 0° and projectile is translated by 2 mm toward lower wall. The the magnitudes of the first conical shock reflection are equal all around the tube.
b) Angle of attack is 4° and nose tip is translated by 5 mm toward lower wall. The magnitudes of the first conical shock reflection depend on azimuthal location.

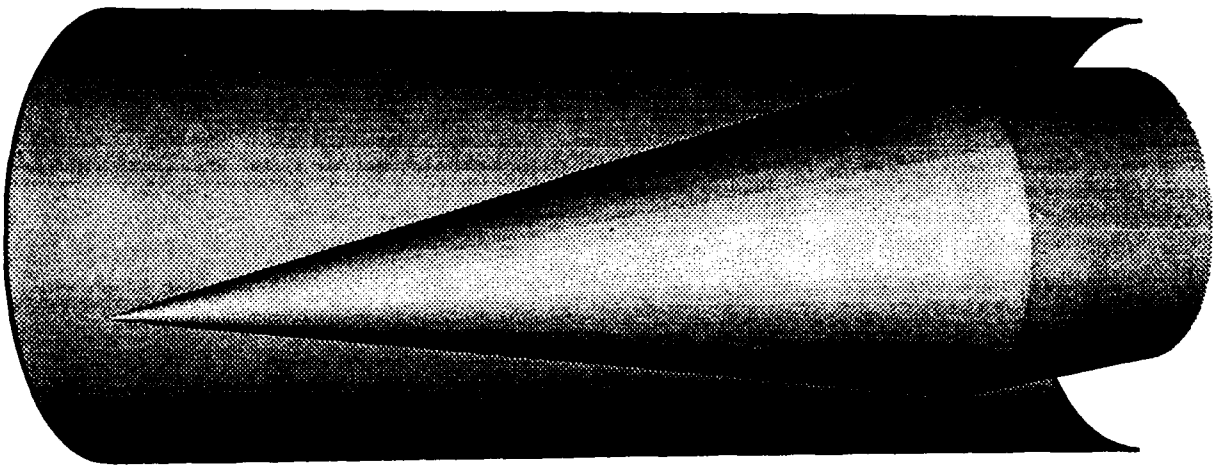

Fig. 28 General geometry of a canted axisymmetric projectile used in the remainder of the numerical simulations. One-half of the full tube is numerically simulated by assuming a plane of symmetry, while only the first 2/3 of the projectile length (102 mm) is simulated. The computational grid is 150x50x50 in the axial, radial, and azimuthal directions respectively.

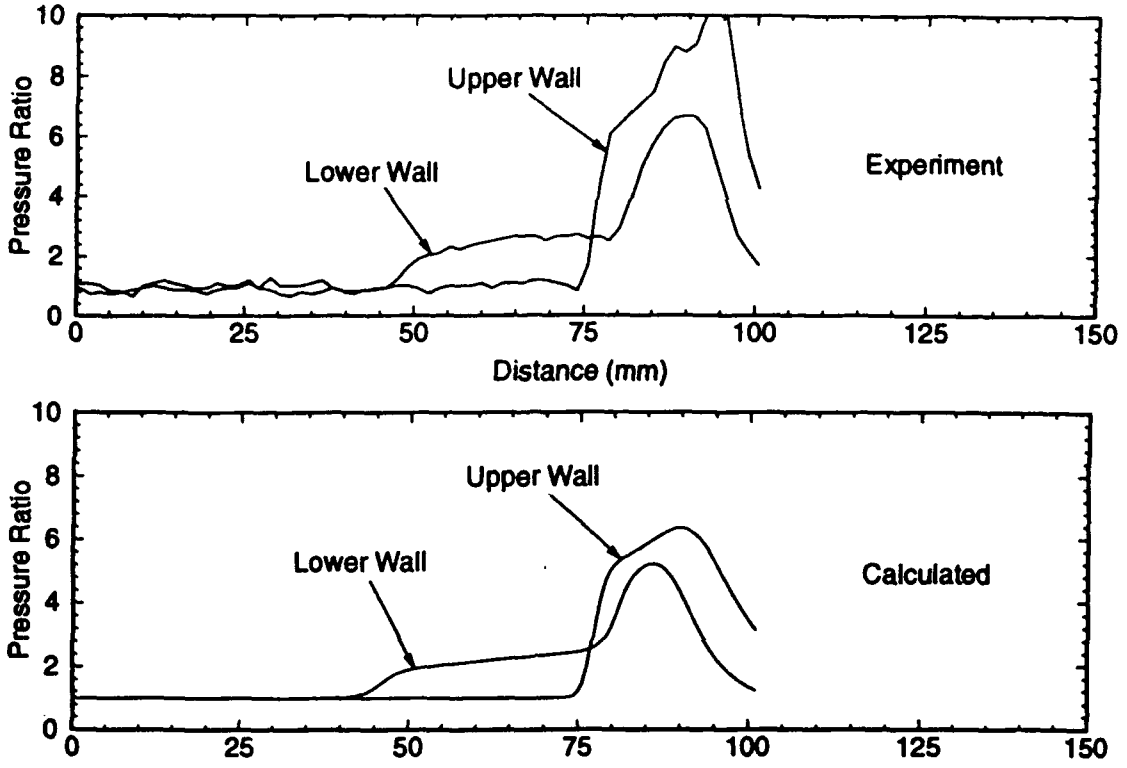

Fig. 29 Comparison of calculated (bottom) to experimental (top) tube wall pressure profiles from a canted projectile with estimated angle of attack of 4.5° and a nose tip translation of 7.5 mm. Subdetonative velocity regime, 1560 m/sec (Mach 4.3) or 89% CJ speed.

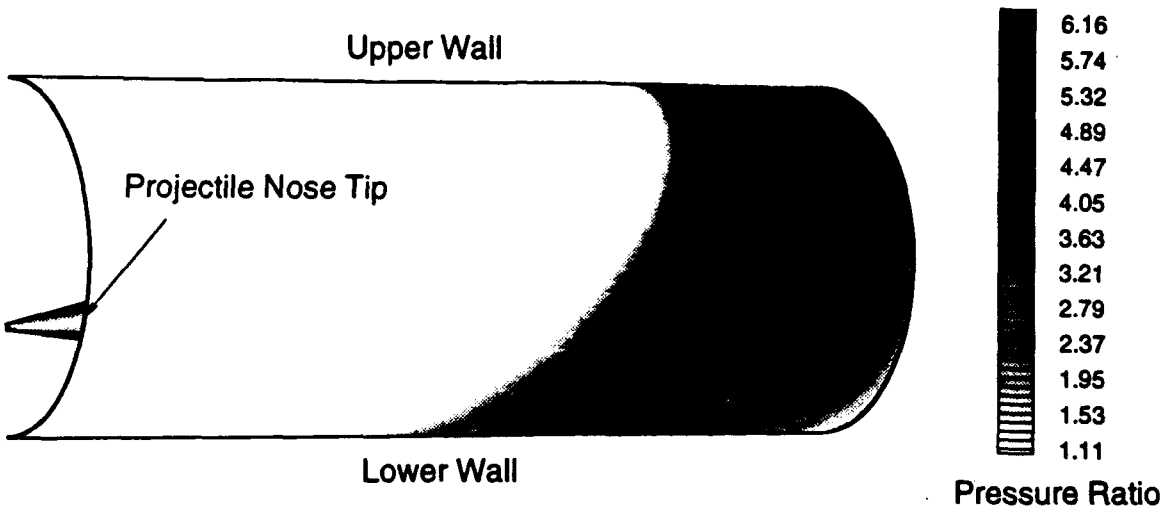

Fig. 30 Three-dimensional surface plot of the calculated tube wall pressure distribution resulting from projectile having an angle of attack of 4.5° and a nose tip translation of 7.5 mm. Subdetonative velocity regime, 1560 m/sec (Mach 4.3) or 89% of the CJ speed. Surface shading is proportional to pressure.

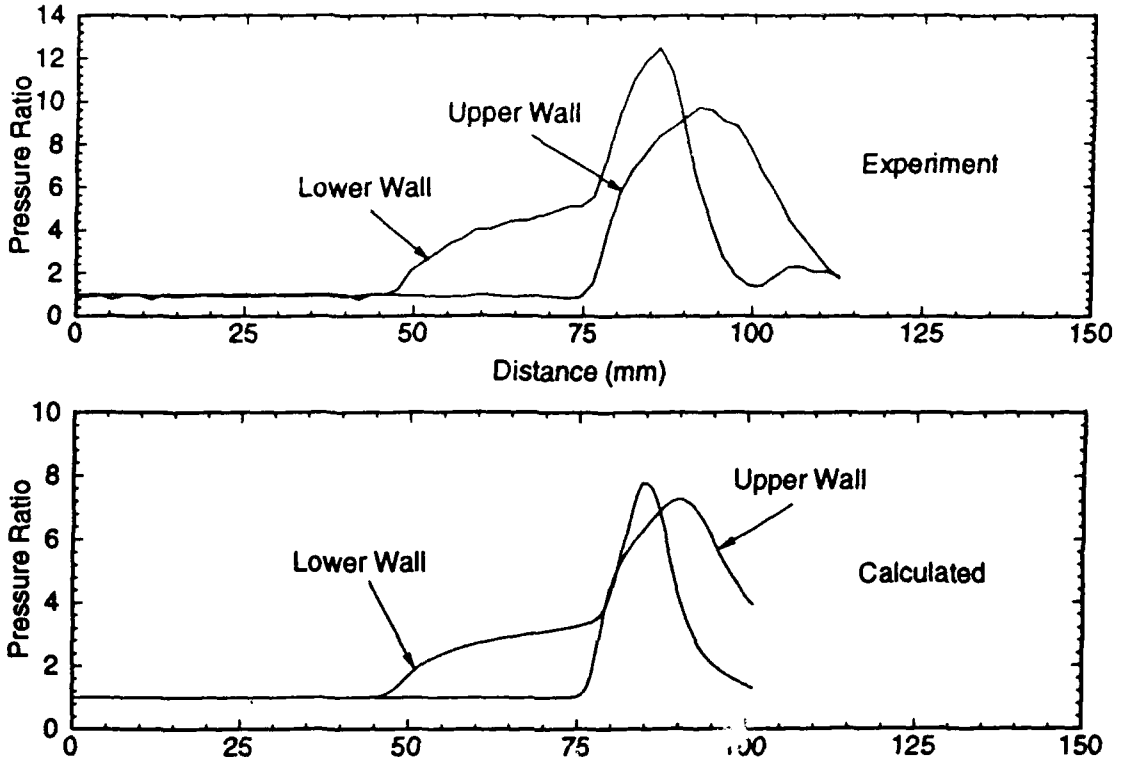

Fig. 31 Comparison of calculated (bottom) and experimental (top) tube wall pressure traces from a canted projectile with estimated angle of attack of 3° and a nose tip translation of 6.5 mm. Superdetonative velocity regime, 1920 m/sec (Mach 5.3) or 110% of the CJ speed. Non-reacting mixture of $2.7CH_4+7.8N_2$.

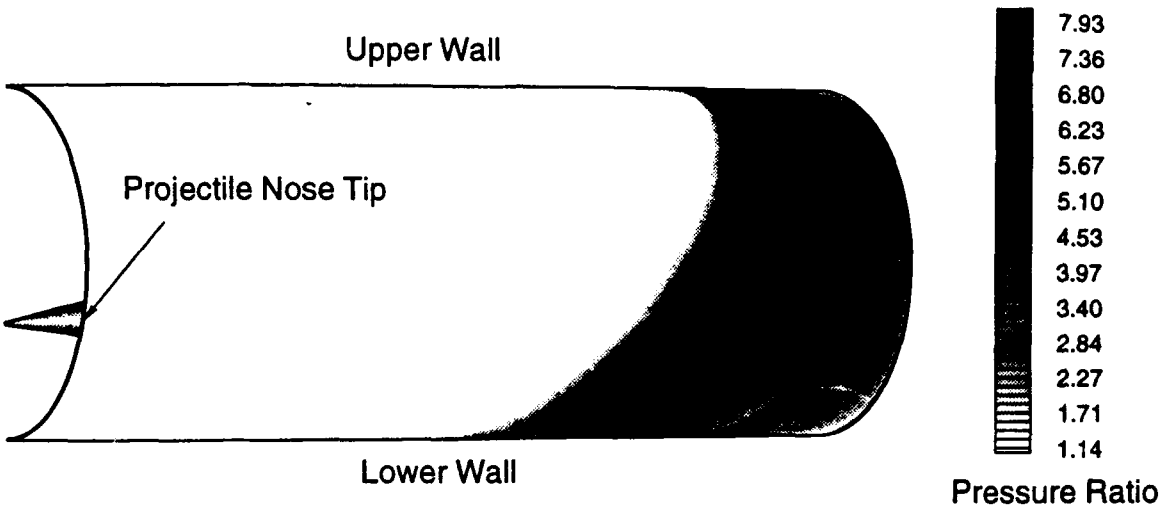

Fig. 32 Three-dimensional surface plot of the calculated tube wall pressure distribution resulting from canting at an angle of attack of 3° and having a nose tip translation of 6.5 mm. Superdetonative velocity regime, 1920 m/sec (Mach 5.3) or 110% of the CJ speed. Surface shading is proportional to pressure. Non-reacting mixture of $2.7CH_4+7.8N_2$.

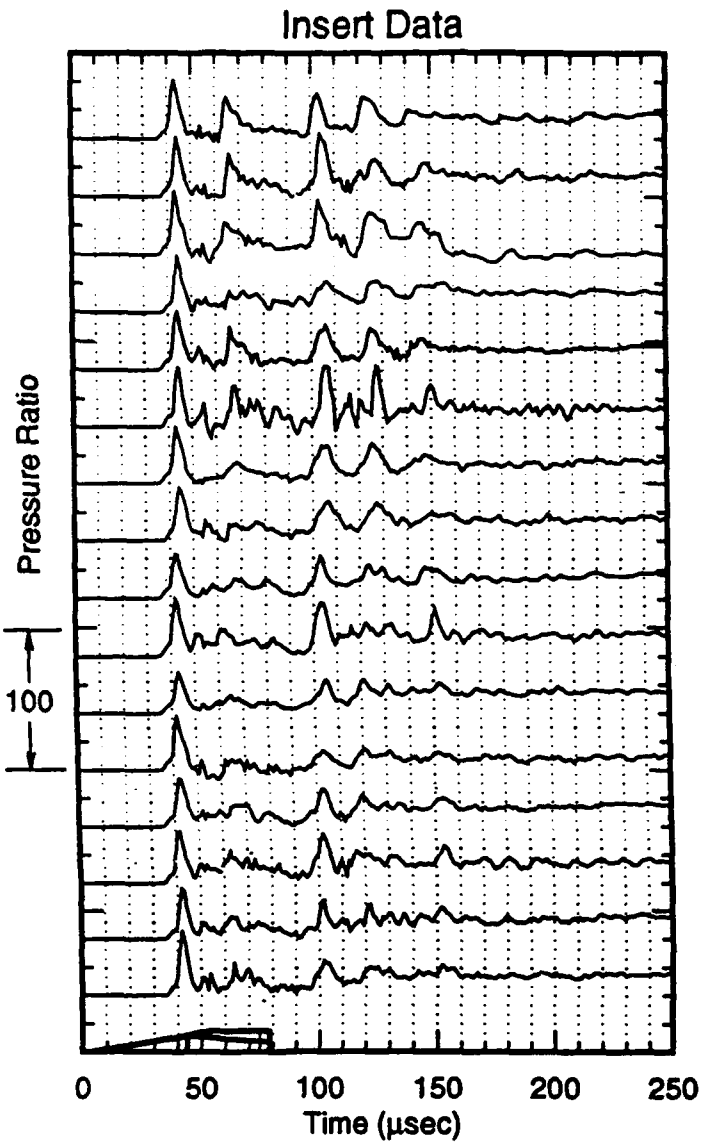

Fig. 33 Tube wall pressure traces from an unstart. Projectile velocity is 2060 m/sec (Mach 5.7) or 118% CJ speed. Note the large amplitude shock wave and the remains of the initial conical shock generated by the projectile nose cone. Reacting propellant mixture is $2.7CH_4+2O_2+5.8N_2$.

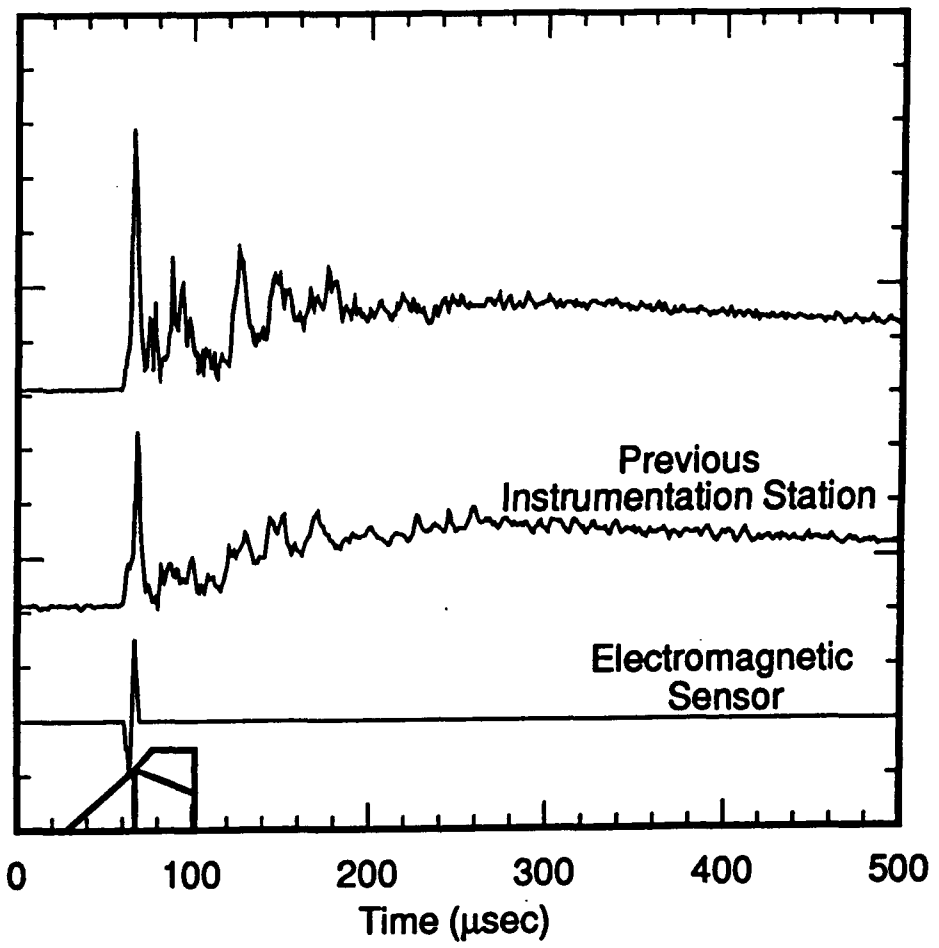

Fig. 34 Comparison of data from trace 1 of Fig. 33 to that of an instrumentation station approximately 22 cm upstream (opposite in direction of projectile motion) with the same azimuthal orientation. Magnetic sensor data correlate projectile position with the pressure traces. Note difference in shock pressure peak amplitude.

V. LEAP LAUNCH CASE STUDY

SYSTEM DESIGN

The ram accelerator offers several major advantages over other impulsive launchers, such as gas guns and electromagnetic railguns, for launching LEAP-type interceptors: 1) It is capable of being easily scaled up in bore size; 2) It has the ability to launch relatively massive projectiles to hypervelocities without subjecting them to extreme variations in acceleration; 3) It generates very little muzzle blast and has no recoil; 4) Its operating conditions can readily be adjusted to provide a wide range of muzzle velocities; 5) The propellants consist of common, inexpensive gases that can be obtained or produced in the field; 6) It is relatively lightweight and can be easily carried by conventional surface vehicles.

The parameters for the launcher design presented here are based on our experimental results and have been made for a ram accelerator scaled for launching a LEAP payload having the same general dimensions as the one proposed by the Boeing Company (see Fig. 35). A simplified schematic of the proposed launcher is shown in Fig. 36 and the parameters of this device for accelerating a 10-kg, 14-cm dia., 59-cm-long saboted LEAP payload to velocities of 2.5, 3, 3.5, and 4 km/sec, are shown in Table 1. The launcher's length is governed by the desired muzzle velocity and the maximum allowable internal pressure in the accelerator barrel. The average density of the payload plus sabot is 1.0 g/cm^3. The propellant fill pressure was set at 340 atm (5,000 psi) to limit the peak cycle pressure to 6,800 atm (100,000 psi). This results in a maximum acceleration of 37,000 *g* and an average acceleration which ranges between 18,500 and 24,400 *g*, depending on the desired muzzle velocity. The "zero velocity start" section comprises 9.9 m of the barrel length in all cases and accelerates the projectile to an initial velocity of 1 km/sec, with average and peak accelerations of 13,500 *g* and 21,600 *g*, respectively.

Note that the projectile's external geometry is dictated by the aerothermodynamics of the ram accelerator, thus the LEAP payload must be encased in a sabot of the appropriate shape, as shown schematically in Fig. 37. (For simplicity, no internal structural details are shown in this schematic). The sabot was assumed to be made of 3-D carbon-carbon composite having a density of 1.4 g/cm^3. This material will provide the necessary thermal protection against aerodynamic heating both in the launch tube and during atmospheric transit. The estimates for the barrel masses are based on 4340 alloy steel (ultimate strength is 18,700 atm (275,000 psi)) and a wall thickness sufficient to limit the peak internal stress to 9,180 atm (135,000 psi) in static loading. This results in a ratio of outer to inner barrel diameter of 2 and provides a safety factor slightly greater

Table 1 Physical parameters for ram accelerator launchers.

Barrel I.D.:	30 cm	LEAP Dimensions:	14 cm O.D. x 59 cm
Barrel O.D.:	60 cm	LEAP Mass:	10 kg
Barrel Material:	4340 steel	Sabot Material:	Carbon Composite
Fill Pressure:	5000 psi	Sabot Dimensions:	23 cm O.D. x 125 cm
Max. Gas Pressure:	100,000 psi	Sabot Mass:	17.8 kg
Max. Barrel Stress:	135,000 psi	Total Projectile Mass:	27.8 kg

Launch Velocity (km/sec)	2.5	3	3.5	4
Average Acceleration (g)	18,500	21,750	24,400	24,400
Peak Acceleration (g)	37,000	37,000	37,000	37,000
Barrel Length* (m)	17.2	21.1	25.6	33.4
Barrel Mass* (tonne)	28	35	42	58

* Includes initial accelerator

than 2. (This is a conservative estimate based on an assumed peak gasdynamic pressure ratio of 20 for the propulsive modes. The experimentally observed pressure ratios are typically 12-15).

The accelerators are partitioned into up to three different sections: the initial launcher, thermally choked stages, and transdetonative stages. A zero velocity start ram accelerator section was assumed as the initial launcher, and its length was determined from theoretical performance predictions for attaining 1 km/sec with a fill pressure of 340 atm (see Appendix B). Each of the subsequent phases of ram acceleration involves a propellant mixture whose composition is tailored to maintain the necessary in-tube Mach number for the desired thrust level as the projectile velocity increases. Thermally choked propulsion is assumed in the velocity range of 1 to 3.5 km/sec and transdetonative propulsion from 3.5 up to 4 km/sec. Superdetonative propulsion was not invoked but is available if higher velocities are desired.

Since all of the stages are assumed to be filled to the same pressure, the partitions between stages are opened shortly before launching to allow some mixing at the stage transitions to minimize sudden in-tube Mach number changes and the corresponding acceleration jumps.[10] These partitions could resemble fast-acting hydraulically actuated gate valves. Given that the ram accelerator barrel would typically be aimed at a relatively steep upward angle, the adjacent stage gases would mix by diffusion alone because the molecular weights of the fill gases decrease towards the muzzle. In fact, this opens the possibility of filling the barrel with a smoothly graded

mixture composition for optimum performance throughout the acceleration process. This option will be investigated in the future, as part of our continuing studies. The entrance and exit seals, which are assumed to be replaceable frangible diaphragms, would be burst just before projectile impact to reduce potential damage to the nose cone.

An inherent benefit of the ram accelerator launcher is that its recoil is non-existent and its muzzle blast is very small compared to that issuing from an equivalent gun launch. This is a consequence of the fact that in a ram accelerator the bulk of the burnt propellant gas moves in the rearward direction. Recent work at the Army Research Laboratory (ARL) has shown that a relatively small, non-luminous puff of soot issues from the muzzle of their 120 mm ram accelerator after the projectile exits.[24] Even though the propellant mixtures in use are fuel-rich, no combustion of the excess methane outside the muzzle has been observed.

MISSION ANALYSIS

In this analysis it is assumed that the ram accelerator launched LEAP will be capable of surviving a peak of ~37,000 *g* and will be able to operate effectively at altitudes greater than 50 km. After the LEAP-carrying sabot leaves the muzzle of the ram accelerator, its tail cone is discarded and several fins (or a small base skirt) are deployed to aerodynamically stabilize the projectile during its atmospheric transit. The LEAP is released from the sabot at either a predetermined altitude or after a fixed delay time, and continues to coast until its terminal propulsion and guidance systems are activated to direct it to its target. The sabot stripping procedure must be operational in both a vacuum and the upper atmosphere to provide the most effective defensive capability. The envelope of engagement of the LEAP after its release from the sabot has not been included here because of a lack of data on the projected propulsion capabilities of a *g*-hardened LEAP. Nevertheless, the potential defensive capabilities of an impulsively launched, self-guiding interceptor can be seen by examining its ballistic trajectories.

Shown in Fig. 38a are the ballistic trajectories of the LEAP projectile, for four different launch velocities at an elevation angle of 80°. Time contours are also shown to indicate how quickly the payload can reach a given target space. The atmosphere model is a two-exponential curve fit to the 1976 Standard Atmosphere. The ballistic coefficient used in our computations is based on a projectile having a mass of 27.8 kg, an outside diameter of 23 cm, and a drag coefficient of 0.1. It can be seen that an altitude of 50 km can be reached in less than 60 sec with a muzzle velocity of only 2.5 km/sec. With a launch velocity of 3.5 km/sec, the projectile will reach 80 km altitude in 60 sec, which is above the planned minimum operational altitude of the LEAP configurations currently under development.

The effects of launch elevation angle on a 4 km/sec projectile are shown in Fig. 38b. This launch velocity would enable the projectile to attain nearly 60 km in 30 sec, enabling a quick response to any short-range missile threat. The projectile will reach 100 km altitude in about 60 sec and its peak apogee will be nearly 190 km. (Note also that the horizontal range of this 27.8 kg projectile is over 250 km at 60° launch elevation angle, indicating significant potential for ram accelerator launchers to be used in long range bombardment). Additional vertical range and shorter time-to-target could be achieved by adding a small *g*-hardened booster rocket to the LEAP. This rocket would be fired after an initial coasting period of 15-20 sec, at which time the projectile would be above most of the atmosphere. The large envelope of coverage and quick response capability of a ram accelerator LEAP system indicate that it can achieve the goals of theater missile defense very effectively.

ENGINEERING CONSIDERATIONS

The consideration of a new technology, such as the ram accelerator, for impulsively launching exoatmospheric projectiles of the LEAP type naturally gives rise to numerous questions about its engineering feasibility, operational limits, and other critical issues. Several of the most frequently raised issues are discussed in what follows, with particular reference to the system described above.

VELOCITY LIMITS

In the University of Washington ram accelerator facility the maximum velocity achieved to date is 2.7 km/sec, and ultimately about 3 km/sec is expected to be attainable. This particular limit is governed by factors associated with the length of the laboratory which houses the facility and by the issue of operating safely within a university environment. Ideal inviscid flow computations indicate that the propulsive cycles of the ram accelerator should be capable of accelerating projectiles to velocities above 10 km/sec.[2] However, more recent theoretical work at the UW and elsewhere indicate that several phenomena may limit the peak velocity of ram accelerator operation to a somewhat lower value.[27,30,36-38] Discussions of some potential velocity limiting phenomena are provided in the following.

Doomed Propellant Fraction: Preignition of the propellant mixture in the region behind the bow shock at the nose tip of the projectile has been investigated to determine its effect on the peak velocity of ram accelerator operation.[36] The projectile nose tip must have a finite radius determined by the maximum allowable heat transfer rate (which is proportional to the inverse square root of the tip radius). The bow wave is therefore detached from the nose and is approximately normal to the flow up to a radius roughly equal to the tip radius. At projectile

speeds exceeding the CJ detonation speed of the undisturbed gas this portion of the bow shock becomes an overdriven detonation wave which ignites the gas that flows through it. Thus there exists a cylindrical pencil of propellant mixture, the "doomed propellant fraction" (DPF), which will necessarily be consumed on the projectile forebody prior to being ingested at the throat, thereby reducing the amount of propellant available to provide thrust.

The DPF is a function of the projectile Mach number, the nose half-angle, θ_c, the propellant heat release, Q, and the ratio of tube radius, r_t, to nose radius, r_n. At sufficiently high velocities in excess of the CJ speed, this premature combustion consumes a large enough fraction of the propellant to choke the flow at the throat, resulting in a diffuser unstart and complete loss of thrust. The ultimate speed limit is defined by the condition where the DPF approaches unity, i.e., the entire curved bow shock wave is an overdriven detonation. For a projectile with the geometry envisioned for the LEAP launch scenario, i.e., $r_t/r_n = 20$ and $\theta_c = 12.5°$, the velocity limit is approximately three times the detonation speed of the gas. For the methane-based mixture commonly used in our experiments, $2.7CH_4+2O_2+ 5.8N_2$, which has a detonation speed of 1.7 km/sec, the speed limit computed on this basis would be 5.1 km/sec, whereas for a mixture consisting of $8H_2+O_2$, with a detonation speed of 3.53 km/sec, the speed limit would be more than 10 km/sec. Both values are well above the range of velocities of interest here.

Boundary Layer Combustion: Another, more stringent velocity limiting phenomenon of gas dynamic origin is the precombustion of the propellant in the hot boundary layer on the nose cone. This problem was investigated theoretically recently for a stoichiometric mixture of hydrogen and air (acoustic speed = 403 m/sec) for superdetonative operation at Mach numbers up to 8 of a projectile with dimensions similar to those used in our experimental work.[37] At in-tube Mach numbers greater than ~7 combustion within the nose cone boundary layer is found to begin spontaneously just ahead of the nose-body shoulder. At $M = 8$ boundary layer combustion occurs all along the nosecone but does not involve a significant fraction of the total flow, and thus has only a relatively minor effect on the thrust. A more important phenomenon is the shock/boundary layer interaction at the point where the first reflected shock from the tube wall impinges on the projectile body. This gives rise to a sizable separation bubble and a complex shock and combustion zone geometry at Mach numbers approaching 8. However, this theoretical work indicates that significant thrust is generated up to at least Mach 8, equivalent to a speed of 3.2 km/sec for the H_2/Air mixture. This is consistent with our own experimental findings in ethylene-based propellant mixtures, in which operation up to $M = 8.5$ has been observed to date. If we conservatively assume a Mach number limit of 8.5 and the above results to be valid for a mixture of $8H_2+O_2$ (acoustic speed = 810 m/sec), the ram accelerator should be able to operate up to a velocity of at least 6.8 km/sec without being limited by boundary layer combustion.

In-Tube Aerodynamic Heating: Aerodynamic heating is a significant concern for a projectile traveling at high Mach numbers through the pressurized gas environment of the ram accelerator.[27,30] Computations were performed by our group on the effects of heat transfer to a projectile being ram accelerated to velocities of 4-12 km/sec by means of an oblique detonation propulsive mode in a propellant mixture consisting of $2H_2+O_2+4He$ at a fill pressure of 70 atm and with a peak cycle pressure of 5000 atm.[38] The heat transfer at the nose tip and on the body in the region of maximum pressure was investigated, and the ablated mass loss and dimensional change which would occur with a carbon-carbon composite projectile material were calculated. The results for velocities up to 6 km/sec indicate that the mass loss and dimensional change at the nose are virtually negligible. The ablation on the projectile body at the maximum pressure region is greater, resulting in approximately a 2% reduction in radius and a 4% mass loss at 6 km/sec. At 8 km/sec the ablation loss is more severe (nearly 15% change in radius at the maximum pressure point) and at 11 km/sec the heating is severe enough to destroy the projectile. Since the aerodynamic heat flux varies as the cube of the projectile velocity, in-bore aerodynamic heating does not present serious problems in the velocity range of 2.5–4 km/sec considered here. Provided that an appropriate carbon-carbon composite ablative heat shield is used, projectile survival can be assured. (In the section below, the problem of in-tube heating is discussed further, with respect to projectile material issues and experimental observations.)

PROJECTILE GEOMETRY AND MATERIAL

The basic projectile geometry that is currently used in experiments at the UW has not changed significantly since the beginning of our experimental program. Indeed, the 90 mm facility at ISL in France and the 120 mm facility at ARL in this country are also using identical, scaled-up projectile geometries[22,25] (see also Appendix A). The 30 mm device at ISL, on the other hand, uses a finless geometry because the projectile is centered by means of rails on the tube wall.[27] Various finned projectile configurations have been investigated at the UW from time to time. Presently, the most promising change to the conventional body geometry appears to be the use of five or more fins rather than four, for both structural and aerothermodynamic reasons.[14]

It is clear that the geometric features which provide potential for high speed reliability and propulsive mode optimization need to be systematically quantified. Examples of geometric parameters that are being investigated include the throat-to-tube and base-to-tube area ratios, projectile length, nose cone angle and contour, and body taper angle. For the case of finned projectiles, the number of fins, fin thickness profile, and fin leading edge shape and rake angle are parameters being studied experimentally at the UW. Fin damage can occur at any velocity, due to improper operational procedures, inadequate fin design, and unsuitable material selection.

Unfinned, rail-centered projectiles present different problems, such as the appropriate length-to-diameter ratio of the straight portion of the projectile body which bears against the rails, the geometry of the rail cross-section, and the nature of the wear between the rails and the projectile.

The use of magnesium and aluminum alloys by all researchers to date has been an expedient, motivated by cost considerations. These materials (especially the 7075-T6 aluminum alloy) offer high strength-to-weight ratio at low cost, and have performed satisfactorily at velocities up to 2.7 km/sec. It is clear, however, that these materials are far from optimum for higher velocity applications, especially at the larger scale necessary for the LEAP.

The possibilities of composite materials for ultrahigh velocity applications need to be explored. A composite projectile can mean either of two options: 1) the use of advanced composite materials, such as carbon-carbon or metal-matrix composites for the entire projectile; 2) the use of different materials for the various parts of the projectile, e.g., copper-clad titanium or composite nose cone, titanium body and fins; or, perhaps, titanium fins with composite bearing surfaces. Currently, limited experimentation with the use of different projectile materials and with various protective metallic and non-metallic coatings is under way at the UW.

An interesting experimental finding has been that projectiles with magnesium bodies and aluminum nose cones consistently reach higher velocities than all-aluminum projectiles. An investigation of the material properties of these alloys has revealed that the aluminum's strength decreases at a faster rate with increasing temperature than that of the magnesium, such that above 480 K (400° F) the magnesium alloy is actually stronger than the aluminum alloy.[40] At this temperature the yield strength of both alloys is only 1,090 atm (16,000 psi). This indicates that thermal degradation of the projectile material may be a primary cause of fin wear and, perhaps, early structural failure of the projectile in the accelerator tube. It follows that the rapid decrease of strength of both these materials with increasing temperature strongly dictates against their use for anything but research purposes at relatively low velocities.

A study of the aerodynamic heating of projectiles having the same geometry and structural details as ours was carried out by United Technologies Chemical Systems (UTCS).[41] Several different materials were considered under operating conditions similar to those observed in our laboratory. Sample results for heating of the nose are shown in Fig. 39. It should be noted that after 10 msec of ram acceleration an aluminum nose reaches its melting point at its outer surface and becomes sufficiently hot at its inner surface to lose most of its strength. (Recent work at ISL, France, has corroborated these results.[27,30]) Titanium, carbon-phenolic composite, and, in particular, 3-D carbon-carbon composite behave much better in this regard, approaching neither

their melting or sublimation temperatures, as the case may be. The results for heating of the fins show similar trends.

We are currently engaged in our own in-house investigation of projectile heating as it relates to material selection. A coupled CFD and heat transfer model of the problem is being formulated. Early results indicate that for the operating conditions observed in our 38 mm ram accelerator, the integrated heat flux to an aluminum alloy nose is sufficient to cause significant structural weakening by the time the projectile has accelerated for about 10 msec, again confirming the earlier work of UTCS.

Although the launcher proposed here assumes the use of rails on the barrel, rather than fins on the projectile, the phenomena which lead to fin wear are expected to be similar to those which will govern the sliding interfaces at the rail surfaces. The work in progress at the 30 mm ram accelerator facility at ISL should shed light on this problem.

BARREL DESIGN

Barrel design for a LEAP launcher is not expected to present unusual problems, since the fabrication of long-barreled guns of similar and larger sizes is a well-developed technology. The UW ram accelerator barrel is fabricated from 4150 steel alloy. Barrel heating and erosion have not been significant, due to the relatively low gas velocities (hence low heat transfer rates) generated by the ram accelerator propulsion cycles. The first barrel was used for 647 shots before being replaced for reasons having to do with instrument port size and spacing, original bore diameter profile, and other factors unrelated to barrel wear. Although many shots up to 2.5 km/sec were performed in the old barrel sections, they suffered very little wear. The current barrel has supported more than 420 shots, many at the high end of the velocity range, i.e., 2.2–2.7 km/sec. Again, barrel wear has not been significant, even in the highest speed sections, and it is expected that this barrel will continue to be used for many more shots.

The issue of large scale barrels, specifically for application to ram accelerator mass launchers, has received preliminary attention.[42-44] Both conventional high-strength steel alloys (such as 4340 steel) and composite materials could be used. One possibility would be to fabricate the barrel from 3-D carbon-carbon or Kevlar composite and use a replaceable hardened steel liner which carries the rails. Such a design would be of very low weight compared to an all-steel barrel. The aspect of barrel design that differs from that of conventional gun-type launchers is that the ram accelerator propulsive modes generate a traveling pressure pulse, rather than a distributed pressure load that peaks at the breech. Thus, the dynamics of the acceleration process will have to be considered when optimizing the design of the barrel.

The barrel of the ram accelerator presented here, including its zero-velocity-start section, has a constant outside diameter of 60 cm and an overall length of ranging from 17.2 to 33.4 m (57 to 111 calibers), depending on the desired muzzle velocity. A barrel with this range of aspect ratios will need to be externally stiffened to permit it to be elevated and rotated to its desired firing position. This could be accomplished in a variety of ways. An appropriate example is the 36.5-m-long (86 caliber), 42.4 cm bore gun of Project HARP, designed and used by Bull *et al.* in Barbados in the 1960's (Fig. 40),[45] which is of a scale somewhat larger than that of the 4 km/sec ram accelerator proposed here. The HARP gun consisted of two smooth-bored 16 inch naval guns joined end-to-end, and braced with longitudinal and radial ribs and two sets of four longitudinal "straightening" rods, as shown in Fig. 40b. Although this gun was located in a fixed emplacement that was not capable of azimuthal rotation, it did have the capability to be elevated from a horizontal loading position to a near-vertical firing position.

A similar stiffening structure is proposed for the ram accelerator. The design would be less massive because all the options considered here have shorter and lighter barrels than the HARP gun and they do not generate any recoil. The latter fact alone will make the design of the accelerator mount much simpler than that of a conventional, large-bore gun.

GAS HANDLING SYSTEM

The propellant gas handling system will be relatively straightforward in design and will be fully automated. In existing ram accelerators several different fill systems are in use or under development. At the UW we use a manually operated system in which the fuel, oxidizer, and diluent gases are separately but simultaneously metered by means of adjustable sonic orifices (i.e., micrometer needle valves) and mixed in a long feed line on the way to the ram accelerator. Each stage of a multi-stage experiment is filled sequentially. Typically, a four-stage configuration is filled in less than 10 minutes, but by automating the procedure and filling all stages simultaneously, a large-bore ram accelerator could be filled and fired in less than 10 seconds.

The 120 mm ram accelerator at ARL uses a partial pressure fill technique, whereby each individual gas is fed into the barrel separately through several gas ports arrayed along the barrel.[23] The fuel is loaded first, followed by the appropriate diluent, and then by the oxygen. Several minutes are then allowed for the gases to mix in the barrel. Proper mixture ratios are obtained by setting the appropriate partial pressures of the gases. At ISL semi-automated fill systems are used which meter the gases by means of flow meters and then mix them in a small chamber before routing to the ram accelerator.[26] Their *modus operandi* is thus somewhat similar to ours.

At the UW we have recently begun to explore the possibility of a feedback controlled gas mixing and fill system.[46] Preliminary experiments have been successfully performed using nitrogen to fill a shock tube having dimensions similar to one of the eight tube sections which comprise our ram accelerator. Further experimentation on this technique is under way and will involve a variety of gases, individually and in different combinations.[47]

Additional conceptual work has also been done both at the UW and, independently, at Veritay Technologies Inc.[48] on rapid gasdynamic techniques that would be capable of filling the ram accelerator barrel with the desired propellant mixture in a time of the order 10 msec. No experimental verification of these concepts has yet been attempted.

DIAPHRAGMS AND CLOSURES

The pressurized propellant gases in existing experimental ram accelerator facilities have been contained in the accelerator tubes by means of Mylar or PVC diaphragms up to 13 mm thick. No projectile damage has been observed to result from the puncturing of diaphragms by the projectiles. As the ram accelerator is scaled up, so must the thickness of the diaphragms increase. At a scale of 30 cm bore the use of passive diaphragms may not be practical or feasible, therefore some other type of closure may need to be used. Various possibilities exist, such as fast-acting mechanical closures similar to ball valves or gate valves, as noted earlier, or thin metallic diaphragms equipped with shaped charges to effect rapid opening.[49]

INITIAL LAUNCHER

In order for the ram acceleration process to begin, the projectile must be moving above Mach 2.5 with respect to the propellant gas, as noted earlier. To date this requirement has been met by means of a light gas gun launcher (UW) or a powder gun launcher (ISL and ARL). Attaining 1 km/sec muzzle velocity with a large-bore gun while maintaining "soft" launch capabilities is a challenging task, but will not be necessary. The authors and their colleagues have devised a means of initiating the ram acceleration process with the projectile at rest (see Appendix B). This entails configuring the initial section of ram accelerator as a backward pointing expansion tube. To start the process the first diaphragm or mechanical closure is suddenly opened, releasing propellant gas in a free expansion towards the stationary projectile (which is backed by an appropriate obturator). The gas velocity meeting the projectile is supersonic and the flow interaction with the obturator ignites the gas at the projectile base. Thrust is generated and the projectile begins to accelerate until it overtakes the forward moving expansion front in the ram accelerator. Ram acceleration then continues in its normal, quasi-steady manner in the stationary propellant.

This so-called "zero velocity start" technique has not yet been experimentally demonstrated at the UW but planning is underway to do so, particularly in light of recent reports that researchers at ISL are actively engaged in developing the concept.[50] The "zero velocity start" technique offers the possibility of launching a projectile by means of a ram accelerator process from beginning to end, thus eliminating the usual problems attendant to guns, such as excessive and non-uniform acceleration levels, excessive muzzle blast, and potential problems associated with interfacing a gun-type pre-launcher with the ram accelerator at the scale necessary for launching the LEAP.

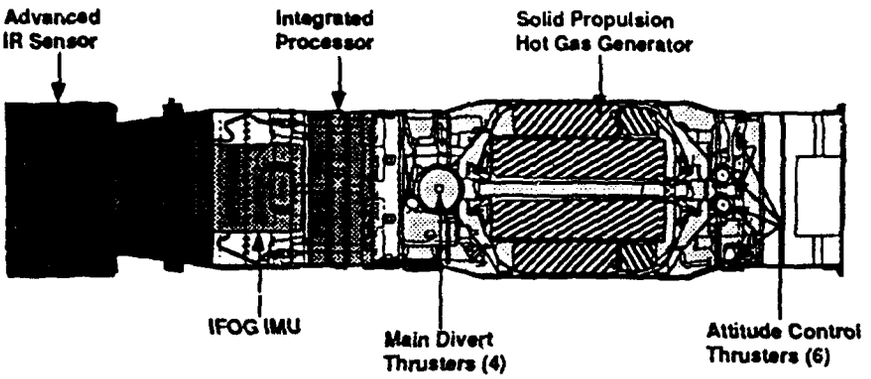

BOEING
Defense & Space Group
P.O. Box 3999
Seattle, WA 98124-2499

Vehicle Dimensions		
Length	23 in	58.5 cm
Diameter	5.5 in	14 cm
Weight	13.2 lbs	6 kg

Fig. 35 Schematic of LEAP configuration proposed by the Boeing Company for rocket launch.

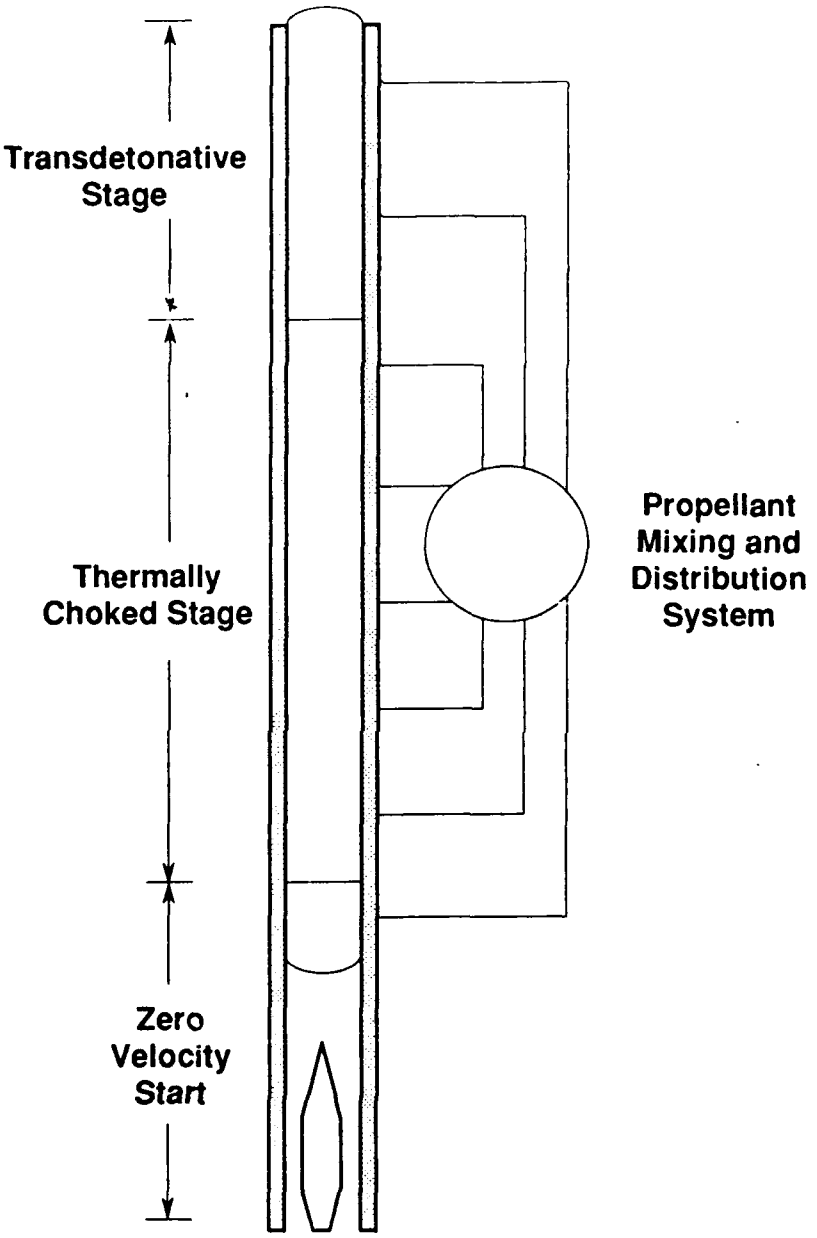

Fig. 36 Schematic of ram accelerator system for launching the LEAP.

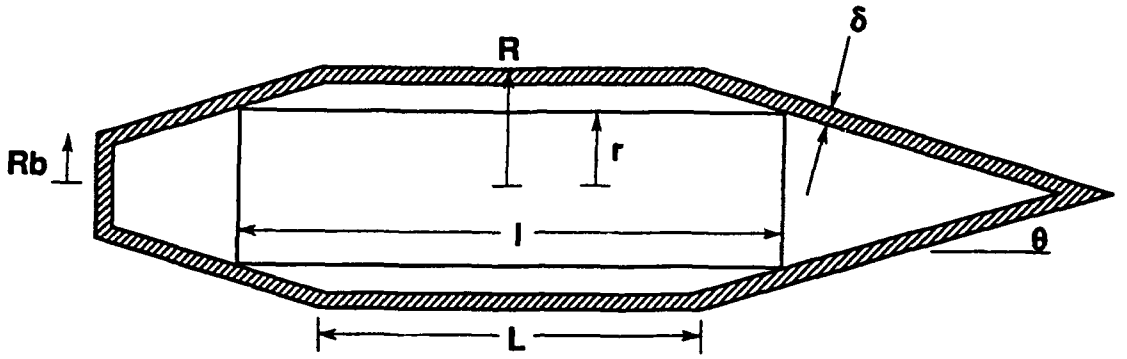

R	11.4 cm	Rtube	15 cm
θ	12.5°	L	45 cm
δ	2 cm	l	58.5 cm
r	7 cm	Rb	9 cm

Fig. 37 Ram accelerator sabot containing the LEAP.

(a)

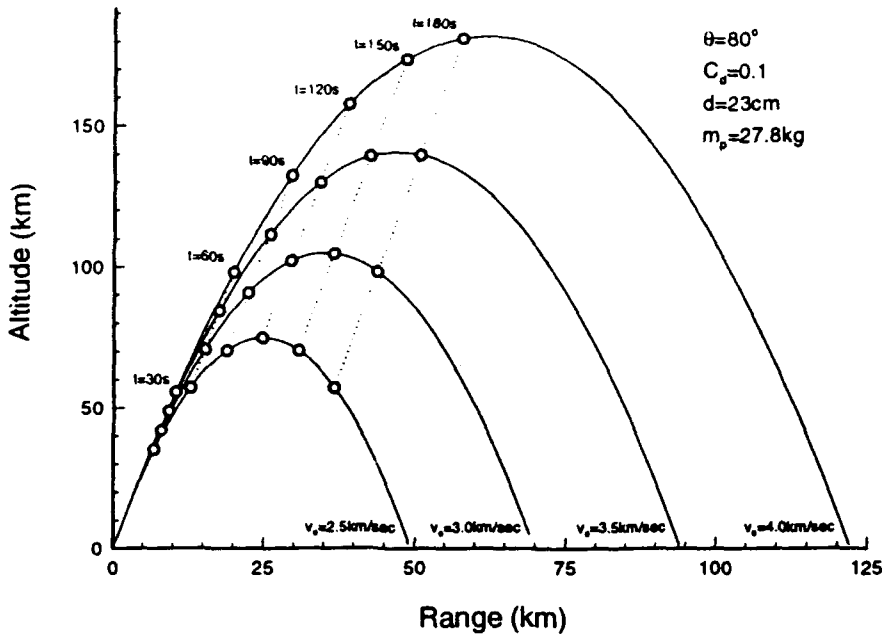

(b)

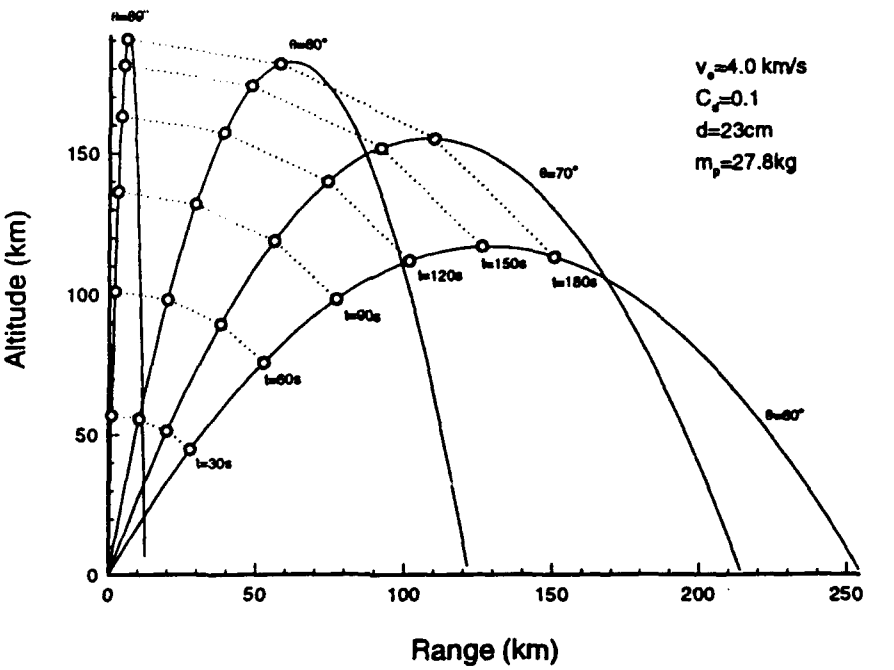

Fig. 38 Trajectories for 30-cm bore ram accelerator launching system:

a) Fixed launch angle of 80° using various launch velocities.
b) Fixed launch velocity of 4 km/sec using various launch angles.

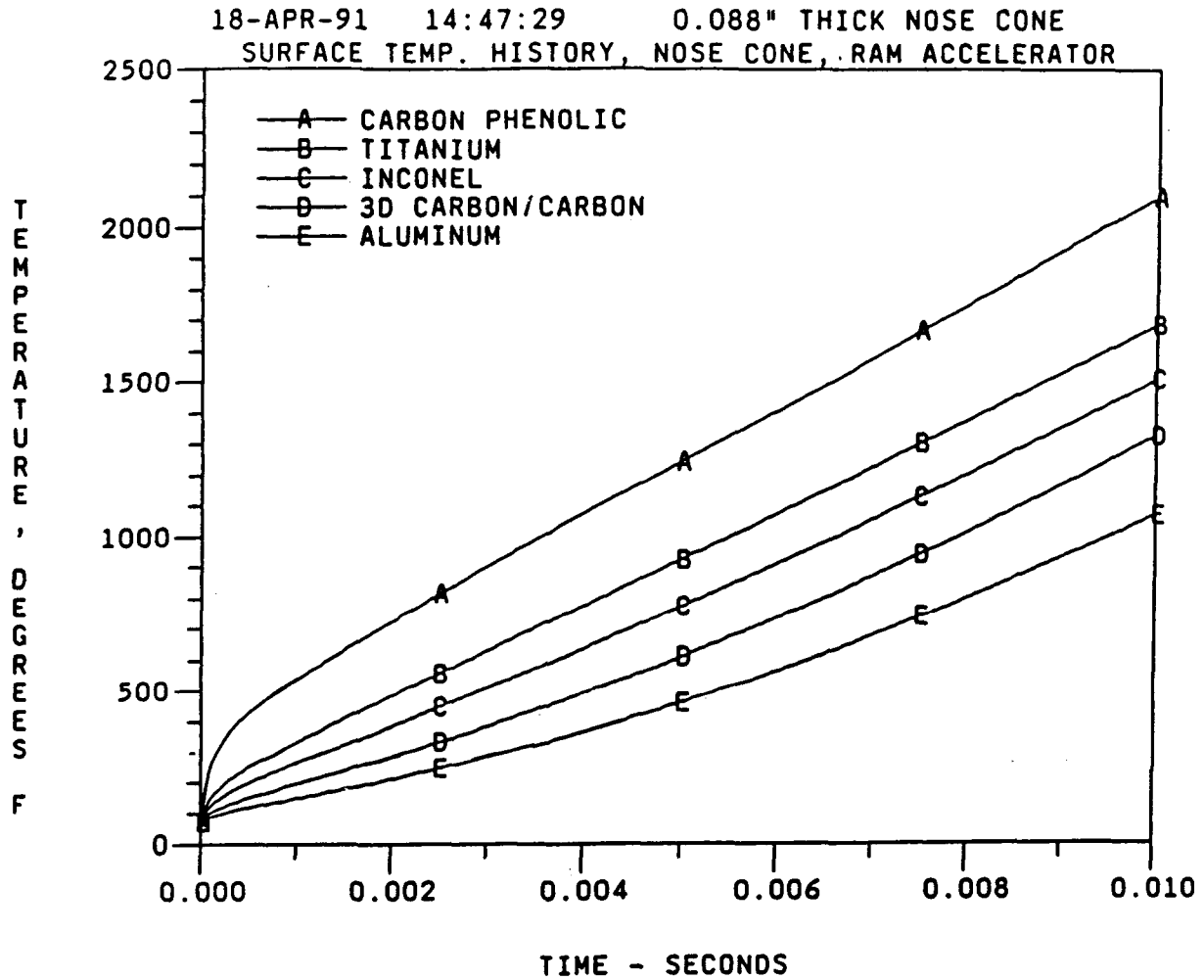

Fig. 39 Surface temperature history of 12.5° half-angle nose cone accelerated in a 33 atm propellant mixture from Mach 2.4 to Mach 7.

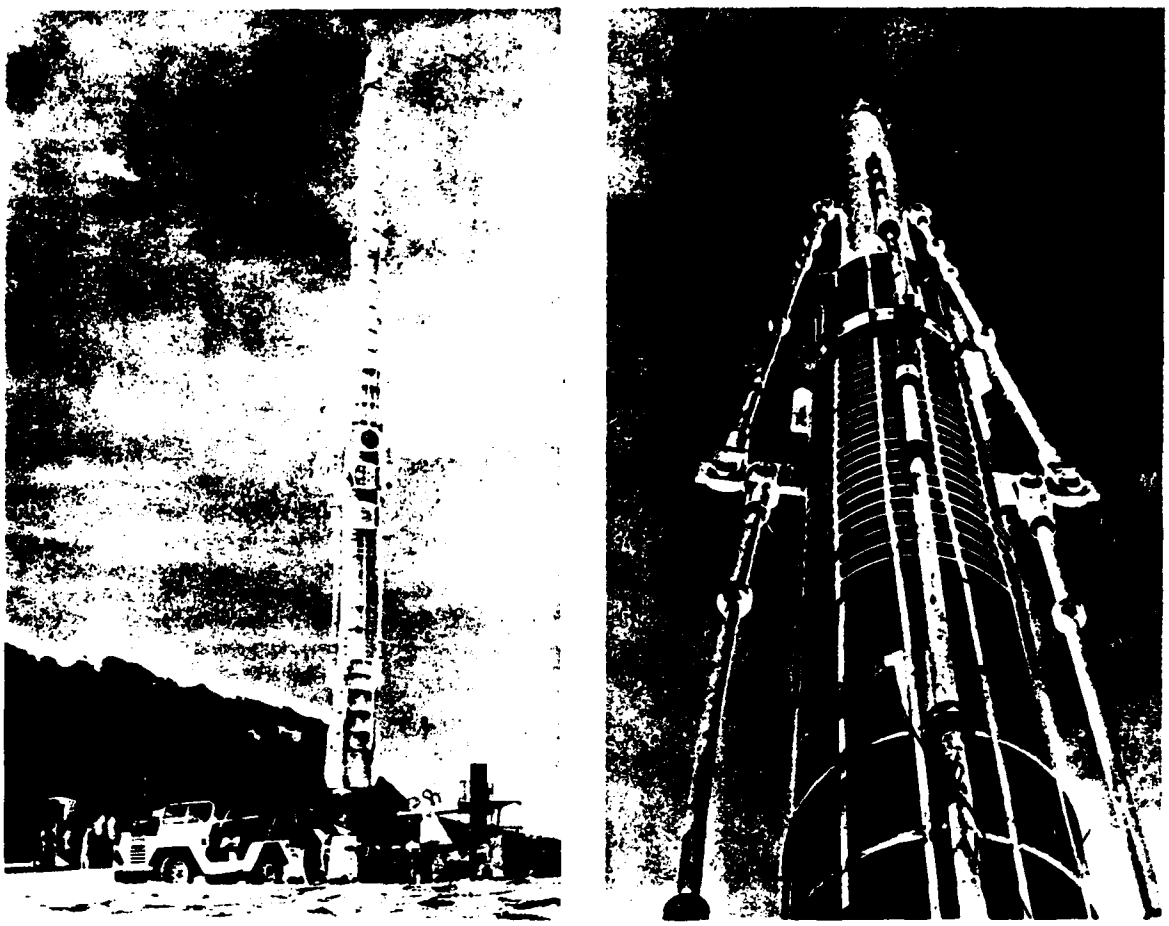

(a) (b)

Fig. 40 The 42.4 cm-bore, 36.5 m-long HARP Barbados gun:

a) Gun in firing position.
b) Barrel stiffening structure.

VI. CONCLUSIONS

The development of ram accelerator technology at the University of Washington and elsewhere has given rise to the possibility of "soft"-launching LEAP-type interceptors in a practical and cost-effective manner. Ram accelerator operation has been demonstrated with 30, 38, 90, and 120 mm bores, supporting the proposition that this launcher concept can be scaled up to large bore diameters. Although projectile acceleration at velocities above 2.7 km/sec has yet to be experimentally demonstrated, the technical and material problems expected for the attainment velocities up to 4 km/sec appear to be surmountable without requiring sophisticated projectile designs or exotic materials. The work presented here has addressed both experimental and systems design issues.

The operational envelope of an oxygen/methane/nitrogen based propellant mixture has been experimentally investigated to provided important data on phenomena limiting the peak velocity capabilities of the ram accelerator. By varying the diluent concentration, limiting phenomena were observed from immediate unstart to combustion wave fall-off. A range of propellant energetics ($3.8 < Q < 5$) has been identified which continuously accelerates the projectile through the CJ detonation speed and into the superdetonative regime, where the unstart mechanism is believed to depend on the projectile's structural integrity. These experimental results are indicative of the range of gas dynamic phenomena that must be addressed by analytical and computational flow field models to accurately predict the operational characteristics of the ram accelerator.

The extent of projectile canting under some operating conditions has been determined through the combined use of experimental data, an analytical method, and numerical simulations. Numerical simulations of the tube wall pressure distribution induced by canted axisymmetric projectiles agree well with the experimental data from sub- and superdetonative regimes in reacting and non-reacting mixtures respectively. Projectile canting has been observed in all propulsive regimes. Data from an "unstart" have been presented and have been linked to the phenomenon of projectile canting. To increase the upper velocity limits of the ram accelerator, projectile canting must be eliminated or minimized.

In the systems study the parameters of ram accelerator systems capable of launching the LEAP at velocities ranging from 2.5 – 4 km/sec have been determined. The barrel masses are very low compared to equivalent-length conventional guns having much lower muzzle velocity capability. The virtual absence of muzzle blast and flash, and the lack of recoil are additional benefits of ram accelerator technology that lead to significant logistical and operational advantages. For example, it appears feasible to mount a 4 km/sec LEAP launch system, including the

supporting propellant gas handling equipment, onto a conventional truck. Naval vessels and large aircraft are also potential platforms for this launch system. The ballistic trajectories of ground-launched LEAP interceptors indicate that targets can be engaged at over 100 km altitude in as little as 60 seconds. The high altitude, quick response time, and rapid firing rate capabilities of the ram accelerator launcher give it the potential to accomplish both theater and hard-point defense missions very effectively.

REFERENCES

1. Hertzberg, A., Bruckner, A.P., and Bogdanoff, D.W., "Ram Accelerator: A New Chemical Method for Accelerating Projectiles to Ultrahigh Velocities," *AIAA Journal*, Vol. 26, 1988, pp. 195-203.

2. Knowlen, C., Bogdanoff, D.W., Bruckner, A.P., and Hertzberg, A., "Performance Capabilities of the Ram Accelerator," AIAA Paper 87-2152, June 1987.

3. Bruckner, A.P., Knowlen, C., Hertzberg, A., and Bogdanoff, D.W., "Operational Characteristics of the Thermally Choked Ram Accelerator," *J. Propulsion and Power*, Vol. 7, 1991, pp. 828-836.

4. Yungster, S., Eberhardt, S., and Bruckner, A.P., "Numerical Simulation of Hypervelocity Projectiles in Detonable Gases," *AIAA Journal*, Vol. 29, February 1991, pp. 187-199.

5. Yungster, S. and Bruckner, A.P., "Computational Studies of a Superdetonative Ram Accelerator Mode," *J. Propulsion and Power*, Vol. 8, 1992, pp. 457-463.

6. Kull, A.E., Burnham, E.A., Knowlen, C., Bruckner, A.P., and Hertzberg, A., "Experimental Studies of Superdetonative Ram Accelerator Modes," AIAA Paper 89-2632, AIAA/SAE/ASME/ASEE 25th Joint Propulsion Conference, Monterey, CA, July 10-12, 1989.

7. Burnham, E.A., Kull, A.E., Knowlen, C., Bruckner, A.P. and Hertzberg, A., "Operation of the Ram Accelerator in the Transdetonative Velocity Regime," AIAA Paper 90-1985, AIAA/SAE/ASME/ASEE 26th Joint Propulsion Conference, Orlando, FL, July 16-18, 1990.

8. Hertzberg, A., Bruckner, A.P., and Knowlen, C., "Experimental Investigation of Ram Accelerator Propulsion Modes," *Shock Waves*, Vol. 1, 1991, pp. 17-25.

9. Bruckner, A.P., Knowlen, C., and Hertzberg, A., "Applications of the Ram Accelerator to Hypersonic Aerothermodynamic Testing," AIAA Paper 92-3949, 17th Aerodynamic Ground Testing Conference, Nashville, TN, July 6-8, 1992.

10. Knowlen, C., Bruckner, A.P., and Hertzberg, A., "Internal Ballistics of the Ram Accelerator," 13th International Symposium on Ballistics, Stockholm Sweden, June 1-3, 1992.

11. Auzias de Turenne, J., "An Analysis of Ram Accelerator Projectile Materials," AIAA Paper 92-0262, 30th AIAA Aerospace Sciences Meeting and Exhibit, Reno, NV, January 6-8, 1992.

12. Auzias de Turenne, J., Chew, G., and Bruckner, A.P., "Recent Progress in Ram Accelerator Technology," AIAA Paper 92-3782, AIAA/SAE/ASME/ASEE 28th Joint Propulsion Conference, Nashville, TN, July 6-8, 1992.

13. Knowlen, C., Li, J.G., Hinkey, J., and Dunmire, B., "University of Washington Ram Accelerator Facility," 42nd Meeting of the Aeroballistic Range Association, Adelaide, Australia, October 22-25, 1991.

14. Hinkey, J., Burnham, E., and Bruckner, A.P., "High Spatial Resolution Measurements of Ram Accelerator Gas Dynamic Phenomena," AIAA Paper, 92-3244, AIAA/SAE/ASME/ASEE 28th Joint Propulsion Conference, Nashville, TN, July 6-8, 1992.

15. Burnham E.A., Hinkey, J., and Bruckner, A.P., "Investigation of Starting Transients in the Thermally Choked Ram Accelerator," 29th JANNAF Combustion Subcommittee Meeting, NASA Langley Research Center, Hampton, VA, Oct. 19-23, 1992.

16. Hinkey, J.B., Burnham, E.A., and Bruckner, A.P., "High Spatial Resolution Measurements In A Single Stage Ram Accelerator," 29th JANNAF Combustion Subcommittee Meeting, Langley Research Center, Hampton, Virginia, October 19-23, 1992.

17. Hinkey, J.B., Burnham, E.A., and Bruckner, A.P., "Investigation of Ram Accelerator Flow Fields Induced by Canted Projectiles," AIAA Paper 93-2186, AIAA/ASME/SAE/ASEE 29th Joint Propulsion Conference, Monterey, CA, June 28-30, 1993.

18. Knowlen, C. and Bruckner, A.P., "A Hugoniot Analysis of the Ram Accelerator," *Shock Waves*, edited by K. Takayama, Springer-Verlag, Berlin, 1992, pp. 617-622.

19. Higgins, A.J., Knowlen, C., and Bruckner, A.P., "An Investigation of Ram Accelerator Gas Dynamic Limits," AIAA Paper 93-2181, AIAA/ASME/SAE/ASEE 29th Joint Propulsion Conference, Monterey, CA, June 28-30, 1993..

20. Bruckner, A.P. and Knowlen, C., "Ram Accelerator Launched LEAP Interceptor," Interim Report, AFOSR Grant No. F49620-92-J-0375, March 1,1993.

21. Hertzberg, A., Bruckner, A.P., Knowlen, C., and McFall, K., "A Method and Apparatus for Zero-Velocity Start of Ram Accelerator Projectiles," U.S. Patent No. 5,097,743, March 24, 1992.

22. Kruczynski, D.L., "Analysis of Ram Accelerator for High Velocity Applications," AIAA Paper No. 91-2488, AIAA/SAE/ASME/ASEE 27th Joint Propulsion Conference, Sacramento, CA, June 24-27, 1992.

23. Kruczynski, D.L. and Nusca, M.J., "Experimental and Computational Investigation of Scaling Phenomena in a Large Caliber Ram Accelerator," AIAA Paper 92-3245, AIAA/SAE/ASME/ASEE 28th Joint Propulsion Conference, Nashville, TN, July 6-8, 1992.

24. Kruczynski, D.L., "Experimental Demonstration of a 120 mm Ram Accelerator," 29th JANNAF Combustion Subcommittee Meeting, NASA Langley Research Center, Hampton, VA, Oct. 19-23, 1992.

25. Giraud, M., Legendre, J.F., Simon, G., and Catoire, L., "Ram Accelerator in 90 mm Caliber: First Results Concerning the Scale Effect in Thermally Choked Propulsion Mode," 13th International Symposium on Ballistics, Stockholm, Sweden, June 1-3, 1992.

26. Giraud, M., Legendre, J.F., and Simon, G., "Ram Accelerator Studies in 90 mm Caliber," 43rd Meeting of the Aeroballistic Range Association, Columbus, OH, September 28-October 2, 1992.

27. Seiler, F. and Naumann, K.W., "Bow Shock Wave Heating and Ablation of a Sharp-Nosed Projectile Flying at Supersonic Velocity inside of a Ram Accelerator," 19th International Symposium on Shock Waves, Université de Provence, Marseille, France, July 26-30, 1993.

28. Knowlen, C., and Bruckner, A.P., "Investigation of Propellant Dilution on Ram Accelerator Performance," 30th JANNAF Combustion Subcommittee Meeting, Monterey, California, November 15-19, 1993.

29. Shapiro, A.H., *The Dynamics and Thermodynamics of Compressible Fluid Flow*, Vol. I, John Wiley and Sons, NY, 1953, Ch. 5.

30. Naumann, K.W., "Heating and Ablation of Projectiles During Acceleration in a Ram Accelerator Tube," AIAA Paper 93-2184, AIAA/SAE/ASME/ASEE 29th Joint Propulsion Conference, June 1993.

31. Soetrisno, M., Imlay, S.T., and Roberts, D.W., "Numerical Simulations of the Superdetonative Ram Accelerator Combusting Flow Field," AIAA Paper 93-2185, AIAA/SAE/ASME/ASEE 29th Joint Propulsion Conference, Monterey, CA, June 28-30, 1993.

32. Soetrisno, M., Imlay, S.T., and Roberts, D.W., "Numerical Simulations of the Transdetonative Ram Accelerator Combusting Flow Field on a Parallel Computer," AIAA Paper 92-3249, AIAA/SAE/ASME/ASEE 28th Joint Propulsion Conference, Nashville, TN, July 6-8, 1992.

33. Taylor, G.I. and Maccoll, J.W., "The Air Pressure on a Cone Moving at High Speeds," Proceedings of the Royal Society of London, Series A, Vol. 159, pp. 459-472, 1937.

34. Anderson, W.K, Thomas, J.L., and Van Leer, B., "Comparison of Finite Volume Flux Vector Splittings for the Euler Equations," AIAA Journal, Vol. 24, 1986, pp. 1453-1460.

35. Mulder, W.A. and Van Leer, B., "Implicit Upwind Methods for the Euler Equations," AIAA Paper 83-1930, July 1983.

36. Ghorbanian, K. and Pratt, D.T, "Doomed Propellant Fraction for a Superdetonative Ram Accelerator," AIAA Paper No. 93-0359, 31st AIAA Aerospace Sciences Meeting and Exhibit, Reno, NV, January 11-14, 1993.

37. Yungster, S., "Numerical Study of Shock-Wave/Boundary-Layer Interactions in Premixed Combustible Gases," *AIAA Journal*, Vol. 30, 1992, pp. 2379-2387.

38. Hertzberg, A., Bruckner, A., Mattick, A.T., and Bogdanoff, D.W., *A Chemical Method for Achieving Acceleration of Macroparticles to Ultrahigh Velocities*, Progress Report No. 1, DOE Grant No. DE FG06 85ER13386, Aerospace and Energetics Research Program, University of Washington, Seattle, WA, February 1986.

39. Hertzberg, A., Bruckner, A.P., and Bogdanoff, D.W., *An Exploratory Study of Ram Accelerator Principles*, Final Report, AFATL-TR-88-94, Air Force Armament Laboratory,, Eglin AFB, FL, Oct. 1988.

40. Lynch, C.T., ed., *Handbook of Materials Science*, Vol. II, CRC Press, Cleveland, OH, 1975, pp. 175 and 203.

41. Lizardo, I. and Melia, P., "Material Comparison, Ram Accelerator," Internal Memorandum No. IJL-12-91E, United Technologies Chemical Systems, April 19, 1991. (Submitted to the University of Washington ram accelerator program).

42. Bruckner, A.P. and Hertzberg, A., "Ram Accelerator Direct Launch System for Space Cargo," Paper No. IAF-87-211, 38th Congress of the International Astronautical Federation, Brighton, England, October 10-17, 1987.

43. Kaloupis, P. and Bruckner, A.P., "The Ram Accelerator: A Chemically Driven Mass Launcher," AIAA Paper 88-2968, AIAA/SAE/ASME/ASEE 24th Joint Propulsion Conference, Boston, MA, July 11-13, 1988.

44. Bogdanoff, D.W., "Ram Accelerator Direct Space Launch System: New Concepts," *J. Propulsion and Power*, Vol. 8, 1992, pp. 481-490.

45. Bull, G.V. and Murphy, C.H., *Paris Kanonen - the Paris Guns (Wilhelmgeschutze) and Project Harp*, Verlag E.S. Mittler & Sohn GmbH, Herford and Bonn, Germany, 1988, pp. 144-238.

46. Jardin, M., "A Feedback Controlled Gas Mixing System for the Ram Accelerator," MSAA Thesis, Department of Aeronautics and Astronautics, University of Washington, Seattle, WA, December 1992.

47. Koch, A.L., "Analysis of a Gas Mixing System Flowing a Non-Ideal Gas," 43rd AIAA Region VI Student Conference, Tucson, AZ, April 1-3, 1993.

48. Fisher, E., "Millisecond Gas Fill System for the Ram Accelerator," oral presentation, Ram Accelerator Workshop, 29th JANNAF Combustion Subcommittee Meeting, Hampton, VA, Oct. 19-23, 1992.

49. Harvey, A., et al., "Ram Accelerator Hypervelocity Launcher Technology," Briefing Report, No. RRC 88-H-1244, Olin/Rocket Research Co., Redmond, WA, Nov. 1988. (Submitted to U.S. Air Force Armaments Technology Laboratory, Eglin AFB, FL).

50. Kruczynski, D., U.S. Army Research Laboratory, Aberdeen Proving Ground, MD, private communication, February 1993.

APPENDIX A:

OTHER FACILITIES AND RESEARCH PROGRAMS

The potential of the ram accelerator as a hypervelocity launcher uniquely suited for a variety of applications has led several groups in this country and abroad to become involved in research on this new concept.[A1] The U.S. Army Research Laboratory (ARL) has constructed a 120 mm bore, two stage, 9.4 m-long ram accelerator to investigate the scaling and other aspects of this technology,[A2] and has been successfully operating it since September 1992.[A3] Experiments with propellant fill pressures ranging from 50 to 100 atm have been conducted with velocities around 1.5 km/sec having been attained to date.[A4] The ARL researchers have demonstrated the feasibility of tracking the projectile with down-bore radar and using high-speed photography to record the phenomena associated with accelerating projectiles in transparent tubes. Another 4.7 m long ram accelerator stage is nearing completion and will be installed in January 1994 to enable operation with three different propellant mixtures.

A 93-mm bore facility is currently under construction by the U.S. Air Force at Eglin A.F.B., with intentions to be fully operational in early 1994.[A5] At NASA Langley Research Center studies have been performed to assess the potential of the ram accelerator as a launcher for the Advanced Hypervelocity Aerophysics Facility (AHAF).[A6] Computational fluid dynamic studies of the chemically reactive flow in the device are being conducted at NASA Lewis Research Center,[A7] the Naval Research Laboratory,[A8] and SAIC.[A9] Related work is being carried out by Amtec Engineering, Inc., which is modeling ram accelerator flow fields to demonstrate the capabilities of its CFD codes,[A10] and by Advanced Projects Research, Inc. (APRI) which has also conducted exploratory experiments in a 38-mm bore test facility under SBIR funding.[A11]

In France, researchers at the French-German Research Institute (ISL) in Saint -Louis are operating a 90-mm-bore, 9-m-long ram accelerator which was first fired successfully in March 1992.[A12] This facility has routinely attained velocities up to 1.6 km/sec and is currently undergoing modifications to increase its length to 30 m, in order to reach velocities above 3 km/sec. In addition, researchers at ISL have completed a 30-mm, 6-m-long device having in-bore rails that mate with a conventional 30-mm powder gun initial launcher.[A13] This ram accelerator was designed specifically to study the superdetonative propulsion mode in the velocity range of 2 to 4 km/sec. Preliminary tests are currently under way, and successful operation at superdetonative velocities in excess of 2.0 km/sec has been demonstrated recently.

Researchers in Japan are also beginning to develop the ram accelerator. The Institute of Fluid Science at Tohoku University in Sendai is in the process of constructing a 25 mm bore,

16-m-long facility for propulsion and impact research at hypersonic speeds,[A14] and plans are underway to build a similar facility at Hiroshima University. In addition, Japan's National Aeronautical Laboratory (NAL) is considering the ram accelerator as a scalable launcher for a major new hypersonic ballistic range facility, and several major aerospace companies have shown interest in the concept not only for hypersonic testing but also for impulsive launch to orbit.[A14]

The importance of the experimental work at ARL and ISL lies in the fact that the predicted straightforward scaling ability of the ram accelerator has been confirmed. (It should be noted that the ARL device's bore of 120 mm (4.72 in) is larger than that of the SHARP Project gas gun at the Lawrence Livermore Laboratory).[A15,A16] Indeed, there is no apparent upper limit to the scaling ability of the ram accelerator and bore diameters as large as a meter or more should be feasible.

REFERENCES

A1. Henderson, B.W., "Ram Accelerator Demonstrates Potential for Hypervelocity Research, Light Launch," *Aviation Week & Space Technology*, Vol. 135, Sept. 30, 1991, pp. 50-51.

A2. Kruczynski, D.L. and Nusca, M.J., "Experimental and Computational Investigation of Scaling Phenomena in a Large Caliber Ram Accelerator," AIAA Paper 92-3245, July 1992.

A3. Kruczynski, D.L., "Experimental Demonstration of a 120 mm Ram Accelerator," 29th JANNAF Combustion Subcommittee Meeting, NASA Langley Research Center, Hampton, VA, Oct. 19-23, 1992, 1992.

A4. Kruczynski, D.L., "Proceeding Toward Hypervelocities in Ram Accelerators," 30th JANNAF Combustion Subcommittee Meeting, Monterey, CA, November 15-19, 1993.

A5. Drabczuk, R.P., Littrell, D.M., and Rolader, G.E., "Eglin Air Force Base Ram Accelerator Research Facility," 30th JANNAF Combustion Subcommittee Meeting, Monterey, CA, November 15-19, 1993.

A6. Witcofski, R.D., Scallion, W.I., Carter, D.J., and Courter, R.W., "An Advanced Hypervelocity Aerophysics Facility: A Ground-Based Flight Test Range," AIAA Paper 91-0296, January 1991.

A7. Yungster, S., "Navier Stokes Simulation of the Supersonic Combustion Flowfield in a Ram Accelerator," AIAA Paper No. 91-1916, June 1991.

A8. Li, C., Landsberg, A.M., Kailasanath, K., Oran, E.S., and Boris, J.P., "Numerical Simulations of Reactive Flows in Ram Accelerators," 29th JANNAF Combustion Subcommittee Meeting, NASA Langley Research Center, Hampton, VA, Oct. 19-23, 1992, 1992.

A9. Sinha, N., York, B.J., Dash, S.M., Drabczuk, R., and Rolader, G.E., "Transient Simulation of Ram Accelerator Flow fields," 29th JANNAF Combustion Subcommittee Meeting, NASA Langley Research Center, Hampton, VA, Oct. 19-23, 1992, 1992.

A10. Soetrisno, M., Imlay, S.T., and Roberts, D., "Numerical Simulation of the Transdetonative Ram Accelerator Combusting Flowfield on a Parallel Computer," AIAA Paper No. 92-3249, July 1992.

A11. Sobota, T.H., and Humphrey, J.W., "Analysis and Demonstration of a Scramaccelerator System," AIAA Paper 93-2183, AIAA/SAE/ASME/ASEE 29th Joint Propulsion Conference, Monterey, CA, June 28-30, 1993.

A12. Giraud, M., Legendre, J.F., Simon, G., and Catoire, L., "Ram Accelerator in 90 mm Caliber: First Results Concerning the Scale Effect in Thermally Choked Propulsion Mode," 13th International Symposium on Ballistics, Stockholm, Sweden, June 1-3, 1992.

A13. Seiler, F. Patz, G., Smeets, J., and Srulijes, J., "Status of ISL's RAMAC 30 with Rail Stabilized Projectiles, First International Workshop on Ram Accelerator, French-German Research Institute (ISL), Saint-Louis, France, September 7-10, 1993.

A14. Takayama, K. and Sasoh, A., Institute of Fluid Sciences, Tohoku University, Sendai, Japan, private communication, January and August 1993.

A15. Henderson, B.W., "World's Largest Light Gas Gun Nears Completion at Livermore," *Aviation Week & Space Technology*, Vol. 137, August 1992, pp. 57-59.

A16. Kuznic, F., "Battle of the Big Shots," *Air & Space*, Vol. 8, August/September 1993, pp. 55-61.

APPENDIX B

THE ZERO VELOCITY START TECHNIQUE

In an effort to eliminate the need for a gun pre-launcher, the authors and their colleagues have devised and patented a means of initiating the ram acceleration process with the projectile at rest.[B1] This "zero velocity start" technique offers the possibility of true soft launch via a ram accelerator process from beginning to end, and the consequent elimination of the potential problems associated with a gun-type pre-launcher, namely the large quantities of gun exhaust and the recoil. In addition, it offers the possibility of reducing the overall length of the launcher facility.

The key to starting the ram accelerator process with a stationary projectile is to configure the initial section of ram accelerator as a backward pointing expansion tube, as shown in Fig. B-1. The projectile is stationary in a section of the tube which is at a very low pressure relative to the sections of the accelerator upstream of the first diaphragm which contain the combustible mixtures. These propellant gases are separated from each other by thin diaphragms also. Behind the projectile a moveable obturator (i.e., a plug) is used to temporarily seal the tube. To start the launch process the diaphragm closest to the projectile is burst, releasing propellant gas in a free expansion towards the stationary projectile as shown in Fig. B-2. The expanding gases flow over the projectile at a Mach number sufficient to ensure supersonic flow over the entire projectile. When the flow meets the obturator it stagnates, generating a reflected shock wave which moves back toward the projectile. The interaction of the flow with the obturator also raises the gas temperature sufficiently to initiate combustion in the region between the obturator and the projectile. The pressure waves generated by the combustion merge with the reflected shock. When this shock reaches the projectile, the high post-shock pressure acting on its base begins to accelerate the projectile into the expanding gas mixture. Under the proper conditions the shock stabilizes on the projectile and the latter continues to accelerate. Eventually, the projectile overtakes the forward moving expansion front in the ram accelerator and normal quasi-steady ram acceleration ensues. Additional details of the process are discussed in the patent.

REFERENCES

B1. Hertzberg, A., Bruckner, A.P., Knowlen, C., and McFall, K., "A Method and Apparatus for Zero-Velocity Start of Ram Accelerator Projectiles," U.S. Patent No. 5,097,743, March 24, 1992.

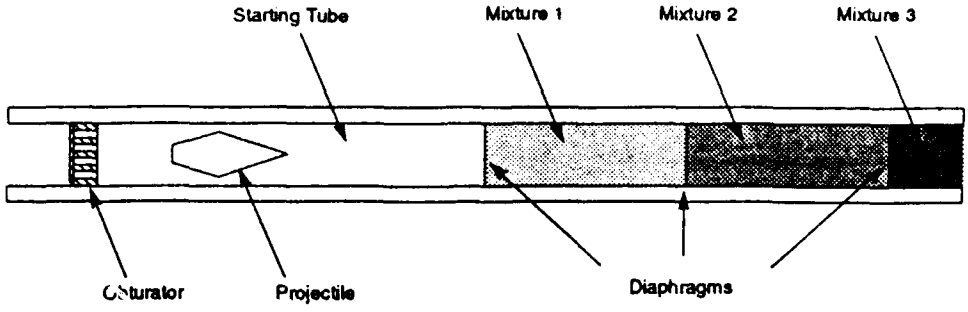

Fig. B-1 Components of a zero velocity start ram accelerator.

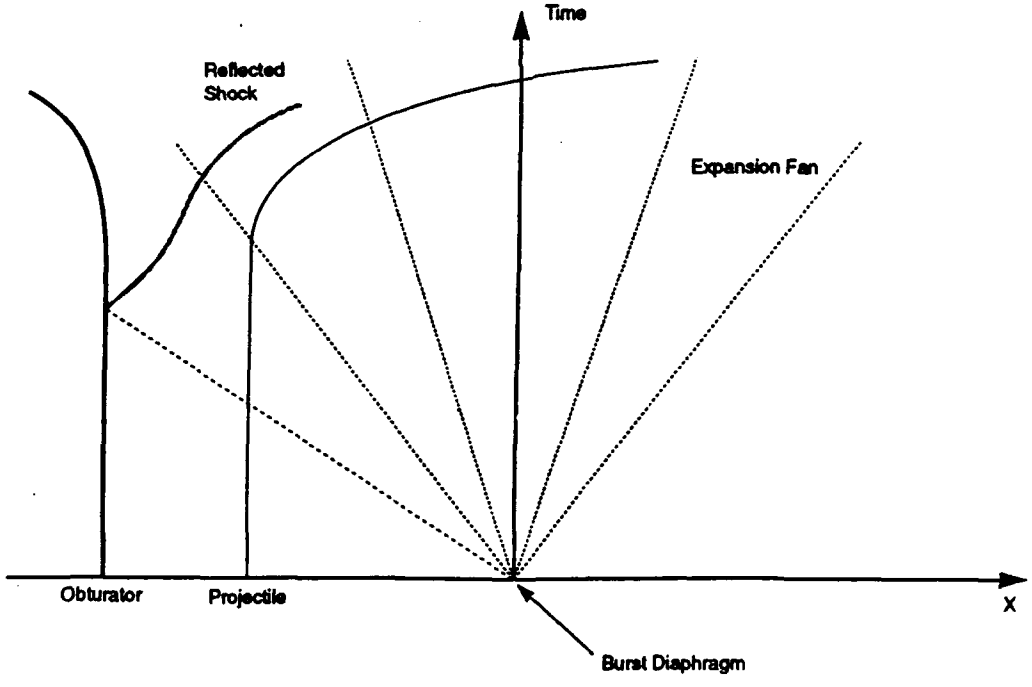

Fig. B-2 Wave diagram of a zero velocity start ram accelerator.